

STATUS OF THESIS

Title of thesis

**Investigation of Micro Bubble for the Removal of Suspended Particle and Enhancement of Dissolved Oxygen in Polluted Water**

\_\_\_\_\_  
FELIXTIANUS EKO WISMO WINARTO

hereby allow my thesis to be placed at the Information Resource Center (IRC) of Universiti Teknologi PETRONAS (UTP) with the following conditions:

1. The thesis becomes the property of UTP.
2. The IRC of UTP may make copies of the thesis for academic purposes only.
3. This thesis is classified as

Confidential

Non-confidential

If this thesis is confidential, please state the reason:

\_\_\_\_\_  
\_\_\_\_\_

The contents of the thesis will remain confidential for \_\_\_\_\_ years

Remarks on disclosure:

\_\_\_\_\_  
\_\_\_\_\_

Endorsed by

\_\_\_\_\_  
Signature of Author

Permanent Address:

Gadjah Mada University

Faculty of Technology,

Yogyakarta, Indonesia

Date: \_\_\_\_\_

\_\_\_\_\_  
Signature of Supervisor

Dr. Syed Ihtsham-Ul-Haq Gilani

Date: \_\_\_\_\_

UNIVERSITI TEKNOLOGI PETRONAS

INVESTIGATION OF MICRO BUBBLE FOR THE REMOVAL OF SUSPENDED  
PARTICLE AND ENHANCEMENT OF DISSOLVED OXYGEN  
IN POLLUTED WATER

By

FELIXTIANUS EKO WISMO WINARTO

The undersigned certify that they have read, and recommend to The Postgraduate Studies Programme for acceptance of this thesis for the fulfillment of the requirements for the degree stated.

Signature : \_\_\_\_\_

Main Supervisor : Dr. Syed Ihtsham-Ul-Haq Gilani

Date : \_\_\_\_\_

Signature : \_\_\_\_\_

Head of Department : Assoc. Prof. Dr. Ahmad Majdi bin Abdul Rani

Date : \_\_\_\_\_

INVESTIGATION OF MICRO BUBBLE FOR THE REMOVAL OF SUSPENDED  
PARTICLE AND ENHANCEMENT OF DISSOLVED OXYGEN  
IN POLLUTED WATER

by

FELIXTIANUS EKO WISMO WINARTO

A Thesis

Submitted to the Postgraduate Studies Programme

As a Requirement for the Degree of

DOCTOR OF PHILOSOPHY  
MECHANICAL ENGINEERING  
UNIVERSITI TEKNOLOGI PETRONAS  
BANDAR SERI ISKANDAR,  
PERAK

December, 2011

DECLARATION OF THESIS

Title of thesis

**Investigation of Micro Bubble for the Removal of Suspended  
Particle and Enhancement of Dissolved Oxygen  
in Polluted Water**

FELIXTIANUS EKO WISMO WINARTO

hereby declare that the thesis is based on my original work except for quotations and citations which have been duly acknowledged. I also declare that it has not been previously or concurrently submitted for any other degree at UTP or other institutions.

Witnessed by

\_\_\_\_\_  
Signature of Author

Permanent Address:

Gadjah Mada University

Faculty of Technology,

Yogyakarta, Indonesia

Date: \_\_\_\_\_

\_\_\_\_\_  
Signature of Supervisor

Dr. Syed Ihtsham-Ul-Haq Gilani

Date: \_\_\_\_\_

## **DEDICATION**

This dissertation is dedicated to:

My wife : Hartini

My two sons : Yohanes Wien Tineka and Ignasius Oktadewien Tineka

## ACKNOWLEDGEMENTS

First and foremost, I want to give all the praise and glory to my Almighty God. I confess and believe that all things I have received, and I am going to receive has come from Him. To Him always my worship is directed.

I would like specially to thank my supervisor Dr. Syed Ihtsham-ul-Hag Gilani for his advice and patient guidance in the development of this research. It has truly been a pleasure to work with you sir, and I appreciate the supervision you have given me to accomplish this work.

I would like to thank Universiti Teknologi PETRONAS for giving me the opportunity to pursue my PhD study and for the graduate assistantship.

Thanks to Dr Shamsul Rahman Mohamed Kutty for his advice and guidance in the development of this research. I appreciate the supervision he has given to me to accomplish this work.

Thanks to Zairi, Zailan, Chairul anwar, Zamil, Jani, Adam, Ridzuan and all laboratory technicians and mechanical department staff who have supported this research work. I very much appreciate their time.

A special word of appreciation is due to all postgraduate officers and my friends for their help, friendship, and support.

## ABSTRACT

Filtration and precipitation are generally used in wastewater treatment to separate pollutants. However, they are not cost effective and have problems of filter waste and time consumption. The smaller particles are left even after a filtration process, depending upon the porosity of the filter. This research proposes a new approach of using compressed air to lift up micro suspended particles in polluted water. The novelty of the approach is in its sustainability, cost effectiveness and faster solution to micro pollutant separation. Air is forced through a submerged micro diffuser to produce micro bubbles, which flow upward and entrain suspended particles to separate them from water. The study was carried experimentally and a lab test rig was designed and implemented.

Bubble size plays an important role in moving suspended particles upwards due to the buoyancy force, which in turn depends upon the vertical component of bubble velocity. Generally, the larger bubbles tend to change shape due to high buoyancy force. The bubble velocity is characterized by the Froude number and Reynolds number. The strategies to control the bubble size in monodispersed (single size) and polydispersed (multi size) cases are presented in this research. To simulate the real wastewater physiochemical characteristics (surface tension, density, viscosity, etc), Glycerin is added to distilled water in various volume fractions of 0.1% to 0.5%. The relationship between air pressure, vertical and horizontal velocities, as well as bubble size is studied. These parameters (bubble diameter, vertical velocity) lead to high effectiveness of suspended particles separation, and are validated by measuring the low concentration of pollutant (PPM), corresponding to the turbidity level. The amount of suspended particles in relation to turbidity has been studied and it is found that the turbidity level of 6.9 NTU decreases to 3.66 NTU, using 1-10 micron porous sintered glass as a submerged diffuser and at  $12 \times 10^{-3} \text{ m}^3/\text{min}$  air flow.

In most biological wastewater treatment systems, a submerged diffuser is used to provide oxygen and mixing to degrade the organic matter. In this study, the effectiveness of micro diffusers in the degradation of organic matter was investigated. The nitrification performance using both micro and macro diffusers was evaluated by measuring ammonium-nitrogen ( $\text{NH}_4\text{-N}$ ) and nitrate-nitrogen ( $\text{NO}_3\text{-N}$ ). The experimental values were compared with the theoretical values derived from the kinetic calculations. Two batch experiments were conducted for the estimation of the kinetic parameters for the degradation and the nitrification of organic matter at 1 hour, 3 hours, 6 hours, and 24 hours until 48 hours, in steps of 3 hours for each batch of experiments.

From the measurement results, the degradation kinetic COD parameter ( $k\text{COD}$ ) of the micro diffuser was found to be 1.46 times higher than the macro diffuser. Therefore the degradation kinetics of soluble COD parameter ( $k_s\text{COD}$ ) of the micro diffuser was found to be 1.5 times higher than macro diffuser. The difference between micro and millimeter diffusers in removed COD was approximately 6%, and in removed sCOD was approximately 16%. The main data parameters in Nitrification of wastewater were ammonium and nitrate. The measurement results of ammonium and nitrate using micro diffuser was achieved at 3% higher than macro diffuser.



## ABSTRAK

Penyaringan dan pengendapan secara asas selalu digunakan untuk mengasingkan bahan tercemar di dalam sesuatu proses rawatan air kumbuhan. Walau bagaimana pun, rawatan ini kurang menjimatkan terutama di dalam proses penapisan bahan buangan maupun masa yang terlalu lama untuk sesuatu proses. Butiran-butiran kecil masih lagi terperangkap walaupun setelah proses penyaringan dilakukan, gelembung angin mikro masih tertinggal akibat daripada proses aliran secara berterusan. Oleh yang demikian, kajian ini dilakukan dengan menggunakan kaedah dan pendekatan baru bagi mengasingkan butiran-butiran kecil mikro tersebut di dalam bahan kumbuhan. Udara bertekanan tinggi digunakan didalam proses ini bagi merawat butiran-butiran yang terperangkap didalam air yang tercemar tersebut. Udara bertekanan tinggi di alirkan ke arah butiran-butiran tenggelam yang diserap di bahagian bawah untuk menghasilkan buih-buih mikro bagi mengapungkan butiran yang terperangkap berkenaan dan seterusnya mengasingkannya ke udara bersama-sama dengan buih mikro tersebut. Dengan penemuan terbaru ini diharapkan dapat mengurangkan kos pemprosesan, proses penyaringan butiran yang cepat dan pantas maupun proses yang berterusan.

Merujuk kepada hukum tekanan "buoyancy", Saiz buih memainkan peranan yang penting di dalam proses pengapungan butiran-butiran kecil di dalam cecair yang mana ianya berkait rapat dengan kadar aliran buih secara menegak. Secara amnya, buih yang besar mampu mengubah sesuatu bentuk dengan merujuk kepada tekanan tinggi buoyancy, manakala kadar aliran buih pula ditentukan oleh nombor "Froude" dan nombor "Reynolds" di dalam kejuruteraan mekanik bendalir. Teori untuk kajian ini diterjemahkan dengan mengawal saiz buih sama ada secara saiz tunggal (monodispersed) atau secara saiz pelbagai (polydispersed). Untuk mendapatkan gambaran yang lebih tepat mengenai sifat-sifat atau keadaan fizikal bahan kimia (ketegangan permukaan, kadar alir, kepadatan dll) di dalam bahan kumbuhan tersebut, Glycerin di tambah ke dalam air sulingan sebanyak 0.1% hingga 0.5%. Setiap

penambahan jumlah tersebut di analisa iaitu perhubungan antara tekanan udara, keadaan kadar alir(menegak atau melintang) dan begitu juga dengan saiz buih yang terhasil. Setiap jumlah atau keputusan berkaitan(ukur lilit buih dan kadar alir) akan mempengaruhi keberkesanan penyingkiran butiran-butiran kecil di dalam cecair bahan buangan tersebut dan ianya boleh dilihat melalui jumlah amaun pencemaran(PPM) yang kecil yang dapat dikesan melalui tahap kekeruhan bahan cemar di dalam tangki. Jumlah butiran yang telah disingkirkan dan tahap kekeruhan cecair akan di analisa sekali lagi dan di dapati tahap kekeruhan cairan tersebut telah menurun daripada 6.9 NTU kepada 3.66 NTU. Untuk tujuan analisa tersebut, bikar kaca 1-10 mikron digunakan sebagai alatan untuk menyerap cairan tenggelam dengan 0.2 l/min udara bertekanan dialirkan.

Di dalam kebanyakan proses biologi untuk sistem rawatan air, alatan untuk menyerap cairan tenggelam digunakan untuk menyalurkan gas oksigen dan mencampurkannya untuk menguraikan jumlah bahan organik di dalam sesuatu cairan. Di dalam kajian ini di dapati keberkesanan bahan serapan mikro di dalam proses penguraian bahan organik terhasil . kebolehan proses pengoksidaan ammonia kepada asid nitrat yang menggunakan mikro dan ukurlilit bahan terserap tersebut boleh diukur dengan mengira ammonium- nitrogen( $\text{NH}_4\text{-N}$ ) dengan nitrate-nitrogen ( $\text{NO}_3\text{-N}$ ). Nilai yang diperolehi melalui kajian akan dibandingkan dengan nilai teori yang diperolehi secara kiraan kinetik. Kajian ini telah dilakukan dua peringkat yang mana setiap peringkat akan mengambil kira anggaran parameter kinetik untuk penguraian dan penitritan bahan organik pada setiap 2jam sehingga 48 jam.

Daripada keputusan kajian tersebut didapati bahawa perbandingan parameter penguraian kinetik (kCOD) untuk mikro dan ukurlilit bahan terserap adalah 1.46 kali lebih tinggi. Parameter penurunan kinetik (COD) untuk bahan serapan mikro juga adalah lebih tinggi iaitu sebanyak 1.5 kali. Di dalam keadaan yang berlainan, mikro dan ukurlilit bahan terserap juga menyingkirkan 6% COD dan 16% sCOD. Bagi proses pengoksidaan ammonia kepada asid nitrat , bahan asas yang digunakan adalah ammonium nitrogen dan nitrat yang mana keputusan yang diperolehi mendapati tahap penyingkirannya lebih tinggi 3% berbanding dengan milli dan ukurlilit bahan terserap.

In compliance with the terms of the Copyright Act 1987 and the IP Policy of the university, the copyright of this thesis has been reassigned by the author to the legal entity of the university,

Institute of Technology PETRONAS Sdn Bhd.

Due acknowledgement shall always be made of the use of any material contained in, or derived from, this thesis.

Felixtianus Eko Wismo Winarto, 2011

Institute of Technology PETRONAS Sdn Bhd

All rights reserved.

## TABLE OF CONTENT

STATUS OF THESIS .....	i
DECLARATION OF THESIS .....	iv
DEDICATION .....	v
ACKNOWLEDGEMENTS .....	vi
ABSTRACT .....	vii
ABSTRAK .....	ix
TABLE OF CONTENT .....	xii
LIST OF FIGURE .....	xvi
LIST OF TABLE .....	xxii
NOMENCLATURE.....	xxiii
LIST OF ABBREVIATION .....	xxv
CHAPTER 1.....	1
INTRODUCTION.....	1
1.1 Problem Statement .....	3
1.2 Research Objective.....	4
1.3 The Scope of theResearch .....	4
1.4 Methodology .....	5
1.5 Thesis Organization.....	6
CHAPTER 2.....	9
LITERATURE REVIEW.....	9
2.1 The Hydrodynamics of Upward Moving Bubble.....	10
2.1.1 The Forces Acting at the Time of Bubble Generation .....	12
2.1.2 The Bubble Size .....	16
2.1.3 The Forces Acting at the Time of Detachment of Bubble. ....	17
2.1.4 The Forces Acting on Free Moving Bubble.....	20
2.2 Coalescence and Breaking Bubble.....	22
2.3 Dimensionless Number.....	26

2.4. Suspended Particle Entrainment .....	27
2.5 DO Level.....	33
2.6 Biodegradation and Nitrification .....	37
2.7 Use of Micro Bubbles in Organic Matter Degradation.....	38
2.8 Kinetics in a Batch Reactor.....	40
2.9 Summary .....	42
 CHAPTER 3 .....	 45
METHODOLOGY .....	45
3.1 Introduction.....	45
3.2 The Experimental Set-up .....	50
3.2.1. Sub-milli Hole Diffuser .....	51
3.2.2 Micro Hole Diffuser.....	52
3.3 The Experimental Procedure.....	54
3.3.1. The Micro Bubble Size Selection for Aeration.....	55
3.3.2. Measuring Apparatus .....	59
3.3.2.1. <i>The Particle Doppler Anemometry</i> .....	59
3.3.2.2 <i>The High Speed Camera</i> .....	65
3.3.2.3 <i>Dissolved Oxygen Meter</i> .....	65
3.3.2.4 <i>Turbidimeter</i> .....	65
3.3.2.5 <i>Surface Tension Meter</i> .....	67
3.3.2.6 <i>Density Meter</i> .....	69
3.3.2.7 <i>Viscometer</i> .....	70
3.3.2.8 <i>The Pollutant</i> .....	71
3.4 The Forces Acting During Bubble Generation and Detachment.....	72
3.4.1 The Forces Acting on a Moving Bubble.....	76
3.4.2 The Forces Acting on a Bubble-particle Pair.....	78
3.4.2.1 <i>When Particle Diameter is Similar to Bubble Diameter</i> .....	79
3.4.2.2 <i>When Particle Diameter is Smaller than Bubble Diameter</i> .....	80
3.4.2.3 <i>When Particle Diameter is Larger than Bubble Diameter</i> .....	82
3.5 The Investigated Variables and Parameters.....	83
3.6 Summary .....	84

CHAPTER 4.....	87
RESULTS AND DISCUSSIONS .....	87
4.1 Dynamics of Bubbles .....	87
4.1.1 The High Speed Camera Image Results.....	88
4.1.2 PDA Graph Results .....	91
4.1.2.1 <i>The Effect of Air Inlet Pressure on Bubble Characteristics....</i>	94
4.1.2.2 <i>The Effect of the Water Level on Air Inlet Pressure and</i> <i>Bubble Diameter .....</i>	97
4.1.2.3 <i>The Effect of Buoyancy and Drag Force on Bubble Dynamics</i>	98
4.1.3 Effect of Glycerin Water Solution on Bubble Dynamics.....	100
4.1.3.1 <i>The PDA Graph of Bubble Dynamics in Glycerin Polluted</i> <i>Water .....</i>	102
4.1.3.2 <i>The Dimensionless Number of Bubble Dynamics in Glycerin</i> <i>Polluted Water.....</i>	108
4.1.3.3 <i>The Bubble Production in Variance Porosity Diffuser .....</i>	110
4.1.4 Effect of CMC Polluted on Water Turbidity.....	113
4.2. Biodegradation and Nitrification of Organic Mater .....	122
4.2.1 DO Level .....	124
4.2.2 COD Removal .....	125
4.2.3 sCOD Removal .....	127
4.2.4 Removal of Ammonia .....	129
4.2.5 Oxidation of Ammonia to Nitrate .....	131
4.3 Summary .....	133
CHAPTER 5.....	137
CONCLUSIONS AND RECOMMENDATIONS.....	137
5.1 Conclusions .....	137
5.2. Research Contributions .....	139
5.3. Research Recommendations .....	140
REFERENCES.....	141
List of Journal Publications.....	151

List of Conferences .....	151
APPENDIXES .....	152
A: Figures of Experimental Set-up .....	152
B: Tables and Figure of Measurement.....	154
C. Measurement Apparatus (Figures and Specification Tables). .....	157

## LIST OF FIGURES

Figure 2.1 Upward velocity as function of bubble diameter from Grace & Weber, .....	11
Figure 2.2 The balance of all forces acting on a growing bubble .....	13
Figure 2.3 the vortices inside a free moving air bubble in water .....	15
Figure 2.4 sketch and notation of idealized bubble shape .....	17
Figure 2.5 Growing air bubble inside the water column .....	19
Figure 2.6 Free moving milli bubbles .....	20
Figure 2.7 coalescence between two bubbles a. vertically, b. horizontally, c. inclined .....	23
Figure 2.8. Coalescence and breaking rate as function of bubble size .....	24
Figure 2.9. The bubble break-up vs gas sparge rate .....	24
Figure 2.10. A sequence of bubble images showing the process of bubble break-up at P=3.5 MPa .....	25
Figure 2.11 Breakup and coalescence process in a vertical channel .....	26
Figure 2.12 Schematic view of particles adhering to a gas bubble (a) single particle, (b) monolayer, (c) multilayer and (d) cluster of suspended particles through a single particle. ....	28
Figure 2.13 The representation of the forces acting on a particle (a) adhering to a flat gas-liquid interface, the hydrostatic pressure ( $F_p$ ) has positive effect on adhesion and (b) adhering to a spherical bubble, the bubble overpressure reduces the adhesion strength $F_g$ is gravitational force, $F_b$ is buoyancy force and $F_c$ is capillary force.....	29
Figure 2.14 The images of bubble attach the particle (a small asperity), showing that the particle rolling on the bubble surface is insignificant. The times shown are relative to the first image.....	29
Figure 2.15. The images show the particle positions on the bubble surface. The particle contacted the bubble surface at about 2 ms and left the bubble surface about 61 ms later. ....	30
Figure 2.16 The illustration of reducing the suspended solid will effect reducing the micro organism .....	31



Figure 2.17 Relationship between removal of <i>Giardia</i> and Turbidity.....	32
Figure 2.18 Relationship between removal of <i>Cryptosporidium</i> and Turbidity .....	33
Figure 2.19 Bunsen absorption coefficient of dissolved gases of interest in water .....	35
Figure 2.20. Graphical analysis for determination of first-order reaction .....	42
Figure 3.1 a Water circulation in aeration column, start with slower till faster flow .....	47
Figure 3.1 b. The air millimeter bubbles trajectory and suspended particles circulation in water column. ....	48
Figure 3.2 a Gas holdup and liquid velocity system.....	49
Figure 3.2. b. The micro air bubbles trajectory and suspended particles in vertical water column.....	49
Figure 3.3 Schematic diagram of experimental set-up to produce bubbles in a vertical column.....	51
Figure 3.4 Experimental set-up showing, (10 x 10) cm vertical column for measurements of bubble dynamics. ....	51
Figure 3.5 Perforated aluminum plat 3 mm thickness machining by EDM die sinker (a). 0.272 mm; (b). 0.103 mm.....	52
Figure 3.6 a. Sintered porous glass diffuser has 10-16 $\mu\text{m}$ pore size. b. SEM image of sintered glass diffuser showing porosities as dark points. c. The 300 magnification of the glass porous. ....	53
Figure 3.7 Schematic diagram of experimental set-up for Biodegradation and Nitrification.....	54
Figure 3.8 a. The existing aeration process, b. The proposed aeration process.....	57
Figure 3.9 Micro bubble aeration procedure.....	58
Figure 3.10 Monitor screen showing the burst when the laser meets bubble .....	60
Figure 3.11 Beams focusing point .....	63
Figure 3.12 The confidence vs scattering angle of the Dantec Dynamics A/S 2002 .....	64
Figure 3.13 The Hach 2100P portable Turbidimeter work principles.....	67
Figure 3.15 The Microscope of CMC, The particle size is 1 to 20 micron, monitored by Scanning electron microscope (SEM). ....	72
Figure 3.16 The balance of forces acting on a growing bubble, for various inclination angles of the diffuser pores.....	75

Figure 3.17 The free air bubble forces in water. ....	78
Figure 3.18. The bubble-particle pair, when their diameters are similar. Assuming the bubble and suspended particle are vertically in line.....	80
Figure 3.19 The bubble (○) is bigger than the particle (●). Assuming the bubble and suspended particle are vertically in line. ....	82
Figure 3.20 The bubble (○) is smaller than the particle (●). Assuming the bubble and suspended particle are vertically in line. ....	83
Figure 4.1 (a) monodispersed bubbles magnified 4 times (b) polydispersed bubbles magnified 2 times. ....	89
Figure 4.2 The relationship between bubble diameter and upward velocity of millimeter bubbles.....	90
Figure 4.3 The air bubbles are formed by the porous sintered glass (a) the 10-16 μm porosity generated bubble diameters in a range 30 μm to 60 μm with 20 times magnification (b) the 16-40 μm porosity, the maximum bubble diameter was 100 μm with 20 times magnification.....	91
Figure 4.4 PDA print outs for Monodispersed bubble monitored at (a) 22 kPa, (b) 24 kPa using 16-40 micro porosity sintered glass diffuser in the tap water.....	93
Figure 4.5 Polydispersed bubble was monitored at 27 kPa, used 16-40 micro porosity sintered glass diffuser in tap water medium.....	94
Figure 4.6 The effect of various inlet air pressures on the bubble size through different porosity diffusers. Error bar in y direction is ± 5%.....	97
Figure 4.7 Relationship between bubble diameters, and air pressure versus altered water level are measured at air flow 1.25 lit/min.....	98
Figure 4.8. The relationship between bubble diameter and vertical velocity using 16-40 μm porous sintered glass.....	98
Figure 4.9 The relationship between Buoyancy, Drag force and Bubble diameter .....	99
Figure 4.11 The relationship of Glycerin impurities in distilled water to viscosity, water density and surface tension.....	101
Figure 4.12 Polydispersed bubble from 1-10 μm porosity sintered glass diffuser at air pressure 25 kPa and air flow 1 l/min in 0.1% glycerin solution. ....	103

Figure 4.13. Polydispersed bubble from 1-10 $\mu\text{m}$ porosity sintered glass diffuser at air pressure 25 kPa and air flow 1 l/min in 0.3% glycerin solution.....	103
Figure 4.14. Polydispersed bubble from 1-10 $\mu\text{m}$ porosity sintered glass diffuser at air pressure 25 kPa and air flow 1 l/min in 0.5% glycerin solution.....	104
Figure 4.15 Polydispersed bubble from 1-10 $\mu\text{m}$ porosity sintered glass diffuser at air pressure 23 kPa and air flow 0.8 l/min in 0.5% glycerin solution.....	105
Figure 4.16 The relationship between inlet air pressure and bubbles diameter in varied percentage of glycerin in distilled water using 1-10 $\mu\text{m}$ sintered glass diffuser. ....	107
Figure 4.17 The relationship between bubble diameter vs bubble vertical velocity. The y error bars at distilled water, 0.2% and 0.4% glycerin are 0.03, 0.03, and 0.05 respectively. ....	108
Figure 4.18 The relationship between velocity versus Froude number in glycerin polluted water.....	109
Figure 4.19 The relationship between Reynolds number versus bubble diameter .....	110
Figure 4.20 The effect of various inlet air pressures on the bubble size through different porosity diffusers in 0.5% glycerin pollutant.....	111
Figure 4.21 Relationship between bubble diameter and vertical velocity in distilled water. Maximum error bar in y direction is $\pm 5\%$ . ....	112
Figure 4.22 Relationship between bubble diameter and vertical velocity in polluted water.....	113
Figure 4.23 Velocity ratio( $v_B / v_C$ ) versus particle diameter. ....	114
Figure 4.24 Relationship between the suspended particle diameter and combine velocity ( $v_C$ ). ....	115
Figure4.25 The linearity of PPM and Turbidity of CMC population in distilled water.....	116
Figure 4.26. The turbidity of CMC solution in distilled water versus micron bubble aeration volume using 1-10 $\mu\text{m}$ porous sintered glass.....	118
Figure 4.27 The turbidity of CMC solution in distilled water vs micron bubble aeration time using 1-10 $\mu\text{m}$ porous sintered glass.....	119

Figure 4.28 The turbidity of CMC solution in distilled water vs micron bubble aeration volume using 10-16 $\mu$ m porous sintered glass. ....	119
Figure 4.29 The turbidity of CMC solution in distilled water vs micron bubble aeration time using 10-16 $\mu$ m porous sintered glass. ....	120
Figure 4.30. The relationship between velocity ratio and particle removal rate. ....	121
Figure 4.31 The micro air bubble image captured by high speed camera at 2000 fps. ....	122
Figure 4.32 DO versus time in various water using millimeter air bubble and micro bubble aeration. ....	124
Figure 4.33 The salinity level of UTP wastewater in 24 hours measurement. IW is stand for influent wastewater and EW is effluent wastewater. ....	125
Figure 4.34 Graph of: COD value vs Sampling Time (hrs) ....	126
Figure 4.35 Degradation rate of COD. ....	127
Figure 4.36 Graph of: sCOD vs Sampling time . ....	128
Figure 4.37 Degradation of sCOD . ....	129
Figure 4.38 Ammonia removal vs sampling time . ....	130
Figure 4.39 Ammonia removal vs sampling time . ....	131
Figure 4.40 Nitrogen removal vs sampling time. ....	132
Figure 4.41 Nitrate Production vs sampling time . ....	133
Figure A.1: The Laboratory scale stagnant water column (100 mm W x 100 mm mm L x 500 mm H).....	152
Figure A.2: The experimental set-up water column (120 mm W x 120 mm L x 2 m H).....	153
Figure B.1 Turbidity decreasing of wastewater using micro bubble aeration . ....	156
Figure C.1 The Laser Doppler Anemometry (PDA) used to measure the bubble size and velocities. ....	157
Figure C.2 The Fastcam-x1280pci camera head . ....	157
Figure C.3 The DO meter. ....	158
Figure C.4 The Hach 2100P portable Turbidimeter. ....	158
Figure C.5 The interface angle and the surface tension calculation display . ....	159
Figure C.6 The IFT 700 surface tension meter. ....	159

Figure C.7 The DMA 35 N portable density meter. ....	160
Figure C.8 The model 35 viscometer.....	161

## LIST OF TABLES

Table 2.1 Dissolved oxygen concentration, mg/l (Cs) .....	36
Table 3.1. Maximum uncertainties in mean velocity. ....	62
Table 3.2 Summary of equations showing various forces exerted on a bubble at the time of generation and detachment . ....	74
Table 3.3. The variables and parameters investigated .....	84
Table 4.1 Bubbles diameter and rise-up velocity for various of diffuser holes. ....	89
Table 4.2 Bubble diameter and velocity for various pressure and air flow of 1-16 $\mu\text{m}$ porosity sintered glass diffuser in tap water. ....	95
Table 4.3 Bubble diameter and velocity for various pressure and air flow of 16-40 $\mu\text{m}$ porosity sintered glass diffuser in tap water. ....	96
Table 4.4 Physiochemical properties of distilled and polluted water. ....	101
Table 4.5 Effect of pressure and air flow on the bubbles diameter and velocities in a glycerin solution, using 1-10 $\mu\text{m}$ sintered glass diffuser.....	106
Table 4.6 The Comparison of PPM and Turbidity using CMC solution. ....	116
Table 4.7 The decreasing of turbidity level using 1-10 $\mu\text{m}$ porous sintered glass....	117
Table 4.8 The decreasing of turbidity level using 10-16 $\mu\text{m}$ porous sintered glass...	117
Table 4.9 The decreasing of turbidity level using 16-40 $\mu\text{m}$ porous sintered glass...	118
Table B.1: Comparison of DO (dissolve oxygen) in various water using millimeter air bubble and micro bubble. ....	154
Table B.2: Turbidity decreasing of wastewater using micro bubble aeration.....	155
Table C.1 The Fastcam-x1280pci Framing rate vs image resolution . ....	162
Table C.2 The Fastcam-x1280pci Camera head specification .....	163
Table C.3 The EW-35641-00 specifications .....	164
Table C.4 The specification of Turbidimeter model 2100P.....	165
Table C.5 Specification of DMA 35 N portable density meter .....	166

## NOMENCLATURE

$C_D$	<i>drag coefficient</i>
$C_L$	<i>lift coefficient</i>
$d_b$	<i>bubble diameter (mm, <math>\mu\text{m}</math>)</i>
$d_p$	<i>particle diameter (mm, <math>\mu\text{m}</math>)</i>
$D_o$	<i>diffuser hole diameter (mm, <math>\mu\text{m}</math>)</i>
$d_{32}$	<i>sauter diameter of bubble (mm, <math>\mu\text{m}</math>)</i>
$e$	<i>restitution coefficient</i>
$F_B$	<i>buoyancy force (mN)</i>
$F_{BA}$	<i>Basset force (mN)</i>
$F_{BB}$	<i>bubble buoyancy force (mN)</i>
$F_C$	<i>particle-bubble collision force (mN)</i>
$F_D$	<i>liquid drag force (mN)</i>
$F_{DB}$	<i>bubble drag force (mN)</i>
$F_{DP}$	<i>particle drag force (mN)</i>
$F_{1,g}$	<i>Bubble inertial force (mN)</i>
$F_{1,m}$	<i>liquid-solid suspension inertial force (mN)</i>
$F_M$	<i>gas momentum force (mN)</i>
$Fr$	<i>Froude number</i>
$F_\sigma$	<i>Surface tension force (mN)</i>
$g$	<i>gravity acceleration (<math>\text{ms}^{-2}</math>)</i>
$Re$	<i>bubble Reynolds number based on liquid properties</i>
$T$	<i>Temperature in Celsius.</i>
$t$	<i>time (s)</i>
$K$	<i>proportionality constant for calculating the effective viscosity of liquid-gas suspension</i>
$P$	<i>air inlet pressure (kPa)</i>
$U$	<i>rise velocity of bubble base (m/s)</i>
$U_G$	<i>superficial gas velocity (with respect to the total cross-section of column)(m/s)</i>
$u_m$	<i>suspension velocity (m/s)</i>

$u_b$	<i>bubble rise velocity relative to the liquid phase (m/s)</i>
$u_e$	<i>bubble expansion velocity (m/s)</i>
$u_m$	<i>suspension velocity (m/s)</i>
$u_o$	<i>superficial gas velocity through the diffuser (m/s)</i>
$u_g$	<i>superficial gas velocity through the orifice (m/s)</i>
$v_b$	<i>bubble velocity (m/s)</i>
$v_c$	<i>combine velocity (m/s)</i>
$v_p$	<i>particle velocity (m/s)</i>
$V$	<i>bubble volume (<math>\mu\text{m}</math>)</i>

#### *Greek letters*

$\alpha$	<i>air volume absorption in water</i>
$\gamma$	<i>contact angle</i>
$\epsilon$	<i>shear strain rate</i>
$\epsilon_s$	<i>solids holdup</i>
$\zeta$	<i>coefficient of suspension inertial force</i>
$\mu_g$	<i>air viscosity (kg/m s)</i>
$\mu_L$	<i>liquid viscosity (Pas)</i>
$\mu_n$	<i>specific growth rate of nitrifying</i>
$\mu_{nm}$	<i>Maximum specific growth rate of nitrifying</i>
$\rho_g$	<i>air density (<math>\text{kgm}^{-3}</math>)</i>
$\rho_l$	<i>liquid density (<math>\text{kgm}^{-3}</math>)</i>
$\rho_m$	<i>density of liquid-solid suspension (<math>\text{kgm}^{-3}</math>)</i>
$\rho_s$	<i>solids density (<math>\text{kgm}^{-3}</math>)</i>
$\sigma$	<i>surface tension (<math>\text{Nm}^{-1}</math>)</i>
$\tau$	<i>dimensionless form of time</i>
$\omega$	<i>rate of rotation</i>
$\theta$	<i>diffuser hole inclination angle</i>



## LIST OF ABBREVIATIONS

<i>AFM</i>	<i>Atomic Force Microscope</i>
<i>BOD</i>	<i>Biological Oxygen Demand</i>
<i>CFD</i>	<i>Computer Fluid Dynamic</i>
<i>CMC</i>	<i>Carboxy Methyl Cellulose</i>
<i>COD</i>	<i>Chemical Oxygen Demand</i>
<i>DO</i>	<i>Dissolve Oxygen</i>
<i>EDM</i>	<i>Electric Discard Machine</i>
<i>IAF</i>	<i>Induced Air Flootation</i>
<i>LDA</i>	<i>Laser Doppler Anemometry</i>
<i>MBRs</i>	<i>Membrane Bioreactors</i>
<i>MLSS</i>	<i>Mixed Liquor Suspended Solid</i>
<i>MLVSS</i>	<i>Mixed Liquor Volatile Suspended Solid</i>
<i>PDA</i>	<i>Particle Doppler Anemometry</i>
<i>PPM</i>	<i>Part Per million</i>
<i>sCOD</i>	<i>Soluble COD</i>
<i>SEM</i>	<i>Scanning Electron Microscope</i>
<i>STP</i>	<i>Sewage Treatment Plan</i>
<i>TSS</i>	<i>Total Suspended Solid</i>
<i>UTP</i>	<i>Universiti Teknologi PETRONAS</i>



## CHAPTER 1

### INTRODUCTION

Liquid and solid wastes as well as air emissions continue to be produced by every community. The liquid waste is essentially the water supply of the community after it has been used in a variety of applications. From the sources of generation, wastewater may be defined as a combination of the liquid or water-carried wastes removed from residences, institutions, and commercial and industrial establishments, together with such ground water, surface water, and storm water [1].

When untreated wastewater accumulates and is allowed to go septic, the decomposition of the organic matter it contains will lead to nuisance conditions including the production of malodorous gases. In addition, untreated wastewater contains numerous pathogenic microorganisms that dwell in the human intestinal tract [2]. Wastewater also contains nutrient, which can stimulate the growth of aquatic plants, and may contain toxic compounds or compounds that potentially may be mutagenic or carcinogenic. For these reasons, the immediate and nuisance-free removal of wastewater from its sources of generation, followed by treatment, reuse, or disposal into the environment is necessary to protect public health and the environment [1].

In the early regulation, the treatment objectives were concerned primarily with (1) the removal of colloidal, suspended and floatable material, (2) the treatment of biodegradable organics and (3) the elimination of pathogenic organism. Later, the wastewater objectives were based primarily on aesthetic and environmental concerns. The earlier objectives involving the reduction of biological oxygen demand (BOD), total suspended solid (TSS), and pathogenic organisms continued but at higher levels. Removal of nutrients, such as nitrogen and phosphorus, also began to be addressed. Now the water-quality improvement objectives have continued, but the emphasis has shifted to the definition and removal of constituents that may cause long-term health effects and environmental impacts. Consequently, the early treatment objective remain

valid today, the required degree of treatment has increased significantly, and additional treatment objectives and goals have been added [3].

Removal of colloidal, suspended, and floatable materials can be carried out using filtration or precipitation. However, they are not cost effective and have problems of filter waste and time consumption. The treatment of biodegradable organics needs sufficient oxygen supply; the submerged diffuser aerobic aeration that produces milli air bubbles, is used to increase the dissolved oxygen (DO) level. However, the milli bubbles cause turbulence and they are quicker to reach the top water surface, therefore the oxygen absorption (reaction time) is inadequate.

A submerged diffuser aerobic aeration is one of the known water purification processes. The movement of air bubbles in a water body increases the dissolved oxygen level (DO), and accelerate the biodegradation of organic matter. In addition, it involves suspended particles entrainment and/or stirring effect. One of the procedures to generate air bubbles is using compressed air through submerged diffuser at the base of the water column.

Controlling the size of air bubbles is one of the main requirements of aerobic aeration, i.e., there will be better oxygen transfer when there is larger contact surface area and sufficient time. Better suspended particle entrainment is achieved when the bubble has a suitable upward velocity. Stirrer effect is required for better mass and energy transfer. The bubbles can be classified on the basis of their size, i.e., millimeter bubble and micrometer bubble. The generation of air bubble is mostly determined by the diffuser hole, and adjustment of air pressure-flow, where the holes size is much smaller compared to bubble size. To produce a millimeter size bubbles, a diffuser with minute or sub-millimeter size holes is required. It is difficult to drill sub-millimeter holes in a diffuser plate. One of the possible solutions to make smaller holes is wire cutting or laser machining, which are extremely expensive and not very common. For the suspended particle separation needs micro hole to produce micro air bubbles. One of the options to produce micro bubble is used the porosity of sintered glass as micro diffuser holes. Porous sintered glass can generate micro size bubbles, due to the fine porosities of the sintered glass. The porosity is formed by the glass

crystal cavities, therefore the holes are varied in size and irregular shape. Due to that condition, it is very difficult to produce the uniform holes and uniform air bubbles. The porosity of sintered glass available is limited in range of 1 to 100  $\mu\text{m}$ . Experimentally for producing air bubbles less than 100  $\mu\text{m}$ , the maximum glass porosity 40  $\mu\text{m}$  is applied.

### **1.1 Problem Statement**

In wastewater treatment, aeration is the process where air is introduced to the wastewater to provide an aerobic condition for the bacteria to degrade the organic matter. The purposes of the aeration are to supply the oxygen required for the metabolization of the microorganisms and to provide mixing which results in sufficient contact between the microorganisms and the dissolved or suspended organic matter.

Two functions of the aeration are suspended particle separation and DO level enhancement. To improve the performance of aeration in suspended particle separation and DO level enhancement need to decrease the bubble size. The aeration process should be done in proper way and shorter time. One possibility is using micro bubble aeration, due to the small bubble size the smaller will be the vertical and horizontal velocities. Hence, for similar volume of input air flow, the smaller bubble size improves surface area and smaller velocity those are suitable for long air-water contact. Hence the suspended particle separation and the increasing DO level can be achieved in shorter periods of time.

In the peak time of wastewater production at UTP due to the increasing of resident population, the wastewater treatment (especially for Biodegradation and Nitrification using activated sludge) time is inadequate. Covering this problem need to improve the DO level increasing in other that the process can be done in a proper time. One of the solutions is to improve the aeration system and change the millimeter with the micro bubble aeration. The micro bubble aeration has advantages not only significantly DO level enhancement but also the entrainment of suspended particle, with the result that

the effluent of cleaner wastewater can be achieved. The particle disposal can be collected as by product.

## **1.2 Research Objective**

The main objective of this research is to study the effectiveness of micro bubbles in removing suspended particles and enhancing the aeration process in a vertical wastewater treatment reactor. This objective is achieved to:

- Study the suspended particle entrainment by enforcing bubble flow in the polluted water.
- Study the effect of micro bubbles in enhancing the DO level in biodegradation and nitrification process.

## **1.3 The Scope of the Research**

To achieve the objectives, this research has been divided into the following main activities: development of millimeter and micrometer submerged diffusers in an aeration system and evaluate the diffusers' performances. The measuring techniques are High Speed Camera and Particle Doppler Anemometry (PDA). This evaluation was done in distilled water and polluted water.

The separation/lifting of suspended particles need a linear upward movement of bubbles to reject or minimize the turbulence effect, which can be attained by smaller air bubbles. Due to the turbidity of real wastewater, it is not possible to use PDA to monitor the bubble upward motion inside the reactor, one needs to imitate wastewater into transparent that the PDA measurement can be done. Actual wastewater has been simulated by the addition of glycerin in distilled water to get similar physiochemical characteristics (density, viscosity and surface tension) as that of the wastewater. The suspended particle separation by micro bubbles aeration is studied by adding carboxy methyl cellulose (CMC) into the polluted water. The addition increases the turbidity

level and by measuring the decrease in the turbidity level, the process effectiveness can be studied.

The dynamics of the micro bubbles' upward movement is observed by using PDA. These hydrodynamic behaviors are controlled by the physical depth of the column. By assuming that the bubbles are fully and uniformly distributed in the stagnant water column, the hydrodynamics of the micro air bubble can be explored.

The CMC pollutant addition in the water represents suspended particles that increase the water turbidity. The particle entrain process can be studied by the measure of turbidity level decrease in period of time along the aeration process.

The effective DO level enhancement can be achieved by the larger interface area and sufficient time. This condition is fulfilled by decreasing the bubble size (millimeter to micro). The DO supports microorganism to degrade the organic matter in the wastewater, therefore the micro bubbles aeration system should be developed in wastewater treatment. The performance, the DO level increasing rate, the experimental and the kinetic results are discussed in both the millimeter and micro bubbles aeration system.

The experiment was carried out to find the effectiveness difference between micro and milli bubbles aeration in degradation and nitrification of municipal wastewater. The degradation measured the COD and sCOD, whereas the nitrification measured the Ammonia removal and nitrate production.

#### **1.4 Methodology**

To achieve the main objective of this research some serial experimental works should be followed:

- Develop a submerged perforated aluminium diffuser for producing millimeter bubbles and a sintered porous glass diffuser for producing the micro bubble in a vertical water column.

- Equip the vertical water column with several transducers (flow meter, control valve and pressure gauge).
- Study the free flowing bubbles using High speed camera.
- Study the diameter and velocity of the bubble using the PDA (Particle Doppler Anemometry).
- Simulate the wastewater physiochemical by using glycerin for studying the bubble parameter (size and velocity).
- Add CMC (Carboxy Methyl cellulose) for studying the correlation between turbidity and PPM (part per million) of pollutant and measuring the turbidity decrease after aeration.
- Measure the DO (Dissolved Oxygen) enhancement.
- Study the biodegradation and nitrification using UTP's domestic wastewater.
- Study the surface condition of sintered glass for measuring the pore size and condition using SEM (Scanning Electron Microscope).

## **1.5 Thesis Organization**

The thesis is divided into 6 different chapters:

Chapter 1 contains introduction, problem statement, objectives, scope and methodology of the research work.

The literature reviews are presented in chapter 2. The dynamics of bubbles include their velocity, diameter, the time of generation and detachment and the acting forces on it. The DO level is naturally in the open ordinary water, and the level would be influenced by many factors. The suspended particle entrain can be achieved when suitable forces are applied. The suitable forces are produced by micro bubbles.

The research methodology, the experimental set-up, the method of bubble generation and the material of water pollutant are detailed in the chapter 3. The millimeter and micro bubbles are produced by submerged diffuser that is situated at the base of water column. The perforated aluminium diffuser produces millimeter



bubbles while sintered porous glass produces micro bubbles. The inlet air is flowed through the transducers and diffuser to generate bubbles in the base of the water column. The distilled water, tap water and polluted water are used in this research. The water pollutants are glycerin and CMC for to simulate similar physiochemical of wastewater and to represent of suspended particle respectively.

The research results and the data analysis on bubble dynamics are presented in chapter 4. The results are high speed camera images, PDA print out of bubble diameter and velocities in monodispersed and polydispersed cases, the relationships between bubble diameter versus air inlet pressure and flow, the bubble diameter and velocities characterized by Reynolds number and Froude number respectively and the effect of pollutant (glycerin and CMC). The hydrodynamics of bubble-particle pair versus velocities ratio and their combined velocities respectively are studied. The validation in entrain the suspended particles process by turbidity level decreasing and PPM (pollutant level decreasing) also are observed. The influence of increase of pollutants percentage and elevated air inlet pressure on bubbles diameter and its velocities are investigated. The entire phenomena exist due to the change in the physiochemical characteristics and surface tension of the water.

The biodegradation and nitrification results are discussed in detail in chapter 5. The comparison of milli and micro bubbles' effectiveness in biodegradation and nitrification process of wastewater are studied. The UTP's domestic wastewater is used for the application of the system with measuring DO level, COD, sCOD, removal of ammonia and oxidation of ammonia to nitrate.

Chapter 6 contains the conclusion, that different bubbles' sizes have different applications. Micro bubbles can be effectively used for entrainment of suspended particles and increased oxygen transfer.



## CHAPTER 2

### LITERATURE REVIEW

Today the degree of water treatment has been significantly increased and additional treatment objectives and goals have been added [3]. Especially for aerobic biodegradation treatment has been much improved by effectively in DO enhancement. One of the DO level enhancements is aeration process [4]. Previously aeration process use millimeter air bubbles. The DO level can be increased effectively using micro bubbles due to the larger surface contact area between air and water and sufficient oxygen transfer time [5]. One needs to study the micro air bubbles' characteristics.

The DO level increasing is depending on the surface area of contact between air and water. The larger the contact the higher of DO increasing would be. The same volume of air flow in aeration process, the decreasing size of bubbles would determine the contact surface area. The smaller the bubbles the larger the contact area would be. The micro bubbles characteristics have been studied by many researchers [6]. The performance of micro bubbles in lifting-up suspended particles and DO level enhancement has been studied in this research.

Pollutants in the wastewater are detergent, soap, shampoo and anything that can be flushed down to toilet, drain or sewer [1]. The contaminants can be classified as organic or inorganic. Biodegradation is one of the known methods to treat wastewater [7]. The biodegradation can be classified by aerobic or anaerobic, depending upon the oxygen level in the process. To increase the water Dissolved oxygen (DO) level, aeration process is used. By using micro air bubbles the high level of DO can be achieved [5]. Air is forced through submerged micro diffuser holes to generate micro bubbles inside the water. The bubbles are not only to degrade the organic matter but also to lift-up the suspended particles, in the wastewater [8].

Generally wastewater is not transparent, therefore the air bubbles' characteristics can not be studied using the PDA because it depends on light refraction. Most of the

detergents use glycerin as a solvent [3], therefore it makes a major component of wastewater and eventually it effects the physiochemical characteristics of wastewater. Hence, glycerin in various volume fractions ranging from 0.1 to 0.5 % is used to pollute the water to a level of raw wastewater in term of physiochemical characteristic to study the dynamics of micro bubble [9].

## **2.1 The Hydrodynamics of Upward Moving Bubble**

The pollutant effect the water physiochemical characteristics i.e. viscosity, surface tension and density etc[10, 11]. The viscosity of a liquid is a measure of the fluid's resistance to flow when acted upon by an external force such as a pressure differential or gravity. An increase in liquid viscosity generally increases the required net inlet pressure. Viscosity affects the size of liquid particles. The same intermolecular forces that determine viscosity create surface tension. Surface tension is a measure of the internal forces generated by molecules due to their position in the surface of a liquid or the interface between two liquids (water and air bubble). All these conditions would affect the bubbles and suspended particles hydrodynamics. Suspended solids settle more quickly in liquids with lower viscosities than with higher viscosities [12]. Milli bubbles' characteristics (size and velocities) in the water column have significant alteration between pure water and contaminated water as shown in Figure 2.1. Especially for the ellipsoidal regime it altered much due to different water physiochemical characteristics and bigger size bubble. [13-15]. In this research, micro size bubbles' characteristic in the distilled and pollutant water has been studied. The spherical shape of micro bubbles is maintained along their upward movement and their velocity never reaches beyond 2 cm/s.

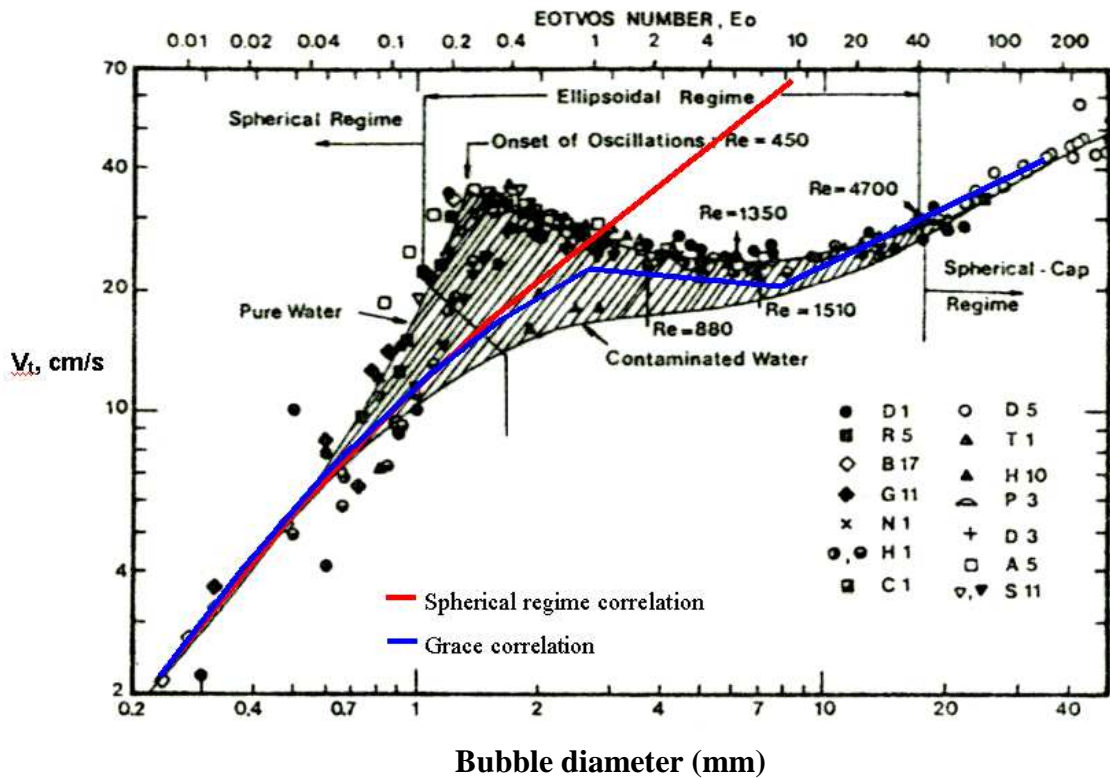


Figure 2.1 Upward velocity as function of bubble diameter from Grace & Weber, 1982 as cited in [14].

The water viscosity changes with the pollutant concentration and the chemistry of the pollutant type [1]. Most of the pollutant contains surfactants [16]. Surfactants are molecules that have an affinity for molecule interfaces: common examples include soap and oil. Owing to their molecular structure, they find it energetically favorable to reside at the free surface, and to increase the viscosity with increasing the solution concentration [17]. The change in viscosity leads to increase the drag force, where the drag force is skin friction between moving bubble and water molecules, resulting in an opposites force to buoyancy.

The surfactant contaminant in the water also reduces the surface tension [17, 18]. In general, surfactants with smaller (lighter) molecules, diffuse more rapidly to the interface than that with larger (heavier) molecules [17]. The existence of pollutant in the water decrease the surface tension [17, 19].

The density of polluted water does not vary too much, due to the existence of pollutant [1]. Therefore, the influence of water density changing the bubble

hydrodynamics is small. Usually the addition of pollutant in the water increases the water density.

The vertical and horizontal velocities of air bubble are influenced by many forces that can be classified into pull-up and pull-down forces. The pull-up forces are buoyancy and gas momentum forces. Buoyancy depends on bubble volume, gravitation and liquid-gas density differences[12], while gas momentum force depends upon air velocity through diffuser (air pressure and flow)[13]. These forces work from bubble detachment point until a position where the bubble is moving freely in the water column. The Buoyancy force works on the bubble unless it is inside the water column. The pull-down forces are liquid drag, surface tension, bubble inertial particle-bubble collision and liquid-solid suspension inertial forces [20]. This pull-down forces increase gradually along the depth of water column where the air bubble was positioned.

### **2.1.1 The Forces Acting at the Time of Bubble Generation**

Fig 2.2 shows the acting forces at the time of bubble generation while air is continuously forced through diffuser. The bubble adheres on the diffuser surface when the pull-up is less than the pull-down forces. The air inlet flow increases the bubble size.

The generated bubble size does not depend on the diffuser hole but also depends on the wetting surface characteristic. The degree of wetting of a solid surface by water is determined by their relative surface energies. Common solids can be wetted by water, because of the hydrogen bonding in the interface [6]. The water-air interface produces higher hydrogen bonding force than water-solid surface interface. The hydrogen bonding forces generate the surface tension force. In aqueous systems, the wetted surface has a high surface energy which is referred as hydrophilic whereas the low surface energy is referred as hydrophobic [6]. The hydrophobic diffuser surface generates big bubbles, whereas the hydrophilic diffuser surface generates small bubbles[6].

The two directions of acting forces on the bubble can be definite as vertically upward and vertically downward. The vertically upward forces are buoyancy ( $F_B$ ) and momentum forces ( $F_M$ ), while vertically downward forces are drag ( $F_D$ ), surface tension ( $F_\sigma$ ), Basset ( $F_{BA}$ ), inertial ( $F_{l,g}$ ), particle bubble collision ( $F_C$ ) and liquid-solid suspension inertial ( $F_{l,m}$ ) forces. The balance of these forces determines the growing bubble and its detachment as shown in Figure 2.2.

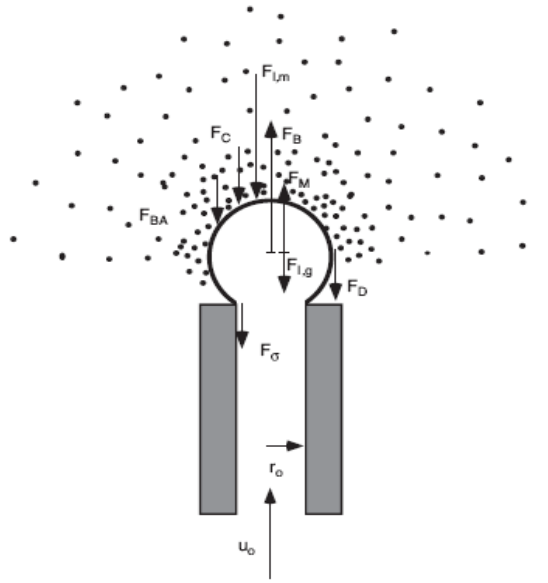


Figure 2.2 The balance of all forces acting on a growing bubble [13].

In general the forces acting on a bubble at the time of generation, through a diffuser hole, are described by Yang et al. [13] :

$$F_B + F_M = F_D + F_\sigma + F_{BA} + F_{l,g} + F_C + F_{l,m} \dots \dots \dots (2.1)$$

$$F_B = \frac{\pi}{6} d_b^3 (\rho_l - \rho_g) g \dots \dots \dots (2.2)$$

$$F_M = \frac{\pi}{4} D_o^2 \rho_g u_o^2 \dots \dots \dots (2.3)$$

$$F_D = C_D \left( \frac{\pi}{4} d_b^2 \right) \frac{\rho_l u_b^2}{2} \dots \dots \dots \left( C_D = \frac{24}{Re} \right) \dots \dots \dots (2.4)$$

$$F_\sigma = \pi D_o \sigma \cos \gamma \dots \dots \dots (2.5)$$

$$F_{BA} = \frac{3}{2} d_b^2 \sqrt{\pi \rho_l \mu_l} \int_0^\tau \frac{du/d\tau}{\sqrt{1-\tau}} d\tau \dots \dots \dots (2.6)$$

$$F_{l,g} = \frac{d}{dt} [\rho_g (\frac{\pi}{6} d_b^3) u_b] \dots\dots\dots(2.7)$$

$$F_C = \frac{\pi}{4} D_o^2 (1 + e) \epsilon_s \rho_s \mu_e^2 \dots\dots\dots(2.8)$$

$$F_{l,m} = \frac{d(\iiint \rho_m u_m \delta V)}{dt} = \zeta \frac{d}{dt} [\rho_m (\frac{\pi}{6} d_b^3) u_b] \dots\dots\dots(2.9)$$

The buoyancy force depends on air bubble diameter and the differences in water and air densities. After detachment of bubble from diffuser, two main forces acting on it are buoyancy and drag force. The resultant of these two forces would be responsible for bubble movement. The bigger bubble has higher buoyancy as well as higher drag force, due to its size. Generally the higher forces acting on the bubble produce higher pressure. This pressure would change the bubbles' shape if the inner tension (surface tension) is smaller. Therefore the bigger bubble continuously changes its shape [21, 22]. Ever changing shape of the bubble produces the vortex inside the bubble as shown in Figure 2.3. Reduction of the bubble size can decrease the buoyancy force, drag force and shape changing as well as the limitation of vortex [23].

Kulkarni [24] classified the acting forces into the lift force and drag force. He found different lift coefficients ( $C_L$ ) for the same depths at different instances. The correlation of air bubble drag force and fluid flow in a venturi is investigated by Soubiran et al. [25], with the assumption that the oscillations would not occur. The drag and virtual mass forces acting on a single air bubble are numerically investigated by Dijkhuizen et al. [26].



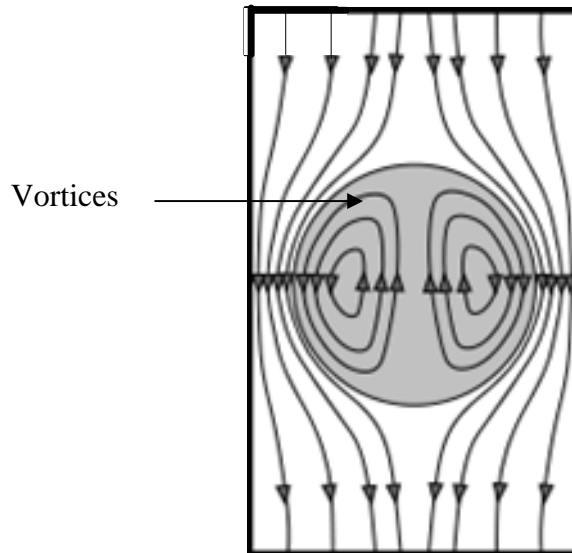


Figure 2.3 the vortices inside a free moving air bubble in water [23].

The gas momentum force depends on gas density ( $\rho_g$ ) and velocity ( $u_g$ ). The air velocity depends on the air inlet pressure and flow that have controlled through adjustable valve. The more inlet pressure the more bubbles produced and it would shorten the vertical distance between bubbles. The phenomena of the collisions and merging bubbles frequently happens in vertical path, therefore bigger bubbles are generated. The air pressure needs to be controlled minutely, as well as limitation of gas momentum force, to produce micro bubbles [13].

The air bubble and suspended particle in water suffer the frictional force. The frictional force is the drag force that depends on the bubble/particle vertical velocity, fluid density, fluid viscosity, wet area and the drag coefficient  $C_d$  [25] The drag force always resists the movement, therefore the direction is downward when bubble/particle is moving upward and vice versa [12]. In general the air bubbles move upward, whereas the suspended particles has two movements, upward (generate scum on the top surface) and downward (generate sediment in the base of water column).

Surface tension force depends on the diffuser hole circumference and the air-liquid interface surface tension [18]. Most pollutants in the water decrease the interface surface tension, therefore the smaller surface tension would decrease the vertically downward forces. Finally this situation results in smaller bubbles'

production, due to bubble detach when the smaller vertically upward forces is maintain [18].

The Basset force is described as the force due to the lagging boundary layer development with changing relative velocity (acceleration) of air bubbles moving through a fluid [13]. The Basset force is counted with viscous effect due to the temporal delay in boundary layer development as the relative velocity change with time. The basset force is difficult to implement and commonly neglected for practical reasons, however, it can be substantially large when the air bubble is accelerated at a high rate [13].

Another force acting on the bubble inside water is the inertial force ( $F_{l,g}$ ) and it is a result of the acceleration of moving bubble in the water. The quantity is equal to the moving bubble mass time its' acceleration The sum of external forces is equal to the inertial force of the particle, as it is "resisting" the change in motion imposed by external forces [12].

The bubble-particle collision force exist when the air bubble colliding the suspended particle. After the collision, the air bubble and the particle move upward together when the vertically upward forces of bubble is bigger than downward forces of bubble-particle pair. The other possibility situation is the bubble-particle remains in the colliding location, if the overall upward and downward forces are in balance [13].

The liquid-solid suspension inertial force ( $F_{l,m}$ ) is created by the compressibility of air that always changes in density against time. The change can be in three dimensions, and expressed in the three directions: abscissa, ordinate and depth integrations [13].

### **2.1.2 The Bubble Size**

Since the water psychochemical characteristics have strong influence to the generation of bubble, therefore the bubble diameter is related to the fluid density, viscosity, surface tension and air inlet velocity [27, 28]. They used acetaldehyde,

acetone, cyclohexane, n-heptane isopropanol, methanol and toluene to study the average sauter bubble diameter and gave the following relationship:

$$d_{32} = 0.289\rho_L^{-0.552}\mu_L^{-0.048}\sigma^{0.442}U_G^{-0.124} \dots\dots\dots(2.10)$$

However, the bubble diameter is linked to a dimensionless number, Froude number by [12] using following equation:

$$Fr = U_G^2 d_{32}^{-1} g^{-1} \dots\dots\dots(2.11)$$

Figure 2.4 shows the bubble growing from orifices. The size of bubble can be expressed from its volume. The idealized bubble volume is determined by orifice radius. Tange and Sheu et al. [29], [20] use orifice radius as the dominant factor to formulate the idealized bubble volume, and expressed as:

$$V_i(r_i) = \frac{4\pi r_i^3}{3}(\cos^3 \theta_i - 3\cos \theta_i + 2) \dots\dots\dots(2.12)$$

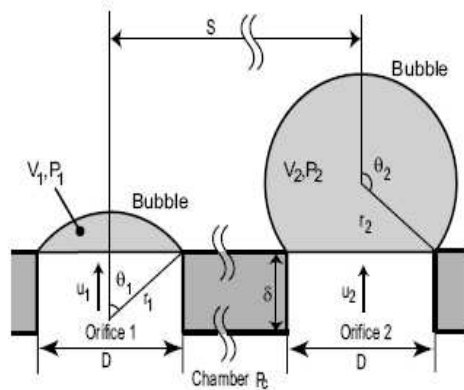


Figure 2.4 sketch and notation of idealized bubble shape [29].

### 2.1.3 The Forces Acting at the Time of Detachment of Bubble.

Figure 2.5 shows a growing bubble. When the bubble continues to grow, the upward forces increase significantly. The momentum force remains constant, whereas the buoyancy increases as fast as volume growing, due to buoyancy force proportionally depend on bubble volume. Before detachment the vertically downward forces are

dominant, but when the bubble detach from the diffuser, the upward forces dominate the downward forces. Yang et. al [13] suggest a balance forces equation as follows:

$$F_B + F_M \geq F_D + F_\sigma + F_{1,g} + F_C + F_{1,m} \dots\dots\dots(2.13)$$

The forces acting at the time of detachment were investigated by Kracht and Katz [30, 31]. Their studies have shown that shape stabilization is not instantaneous during the first 10-15 ms due to detachment force. This detachment force also produces bubble collision, excitation, and coalescence. The dynamic behaviour of equal-sized spherical bubbles interaction (merger, separation, pairing-off, re-pairing and oscillation) were investigated by Ruzicka [32]. He reduced the air inlet pressure to control the period of bubble generation, and ensured that the vertical distance between bubbles was long enough to decrease the influence of the detachment force.

One of the reasons for bubble shape change is the amount of pollution in water. Pollutions change the physiochemical characteristics of water (surface tension, viscosity and density). The decreasing of surface tension and the increasing density and liquid viscosity are subjected to reduce the bubble size, reported by Scafer [33]. Idogawa et al. [34] found that an increase of the surface tension would generate bigger bubble. The application of different gases and variable pressure, and found that the bubble size decreased when there was an increase of the gas density [35]. Hong et al. [36] used glycerine as a pollutant to study the bubble-particle collision forces. The concentration level and the types of pollutant influencing the velocity and bubble shapes were studied by Kracht, Paimanakul and Paruchuri et al. [30, 37, 38]. The relationship between pollutant concentration level and bubble size, as well as velocity is characterized by Froude Number and Reynolds Number. These relationships are studied in detail in this research.

The turbulence effect and coalescence always exist due to bubble horizontal velocity as discovered by Shawkat and Zahradnik et al. [39, 40], who detailed the turbulence characteristics. While Yang et al. [41] discovered that for the stability of bubble flow, turbulence need to be eliminated.

When the bubble detaches from diffuser, the Basset force starts to act, due to the upward acceleration of bubble. This acceleration develops lagging boundary layer and decrease the pull-up forces [21]. The force balance equation becomes:

$$F_B + F_M \geq F_D + F_{BA} + F_{1,g} + F_C + F_{1,m} \dots\dots\dots(2.14)$$

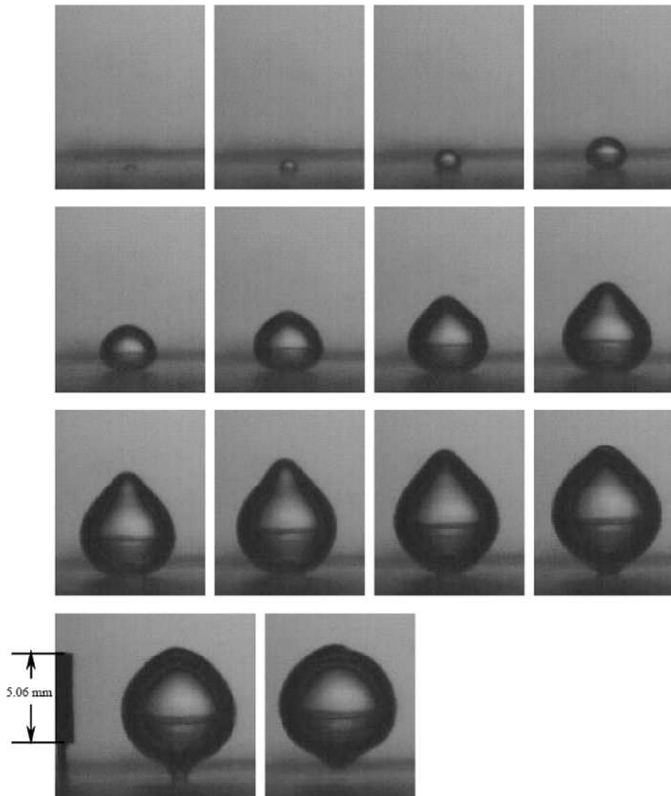


Figure 2.5 Growing air bubble inside the water column [20]

After the bubble detaches itself from its source, the main forces that act on it are buoyancy and drag. The buoyancy force mainly depends on the volume of the bubble and the drag force depends on the contact surface area of the bubble. Bigger bubble has higher buoyancy and drag force, both acting in opposite directions, this causes shape deformation. As the bubble becomes more deformed in the horizontal direction, the drag force would increase [42]. The drag force appears as horizontal velocity and moves in a zig-zag pattern upward.

On the other hand, small bubble has a small buoyancy and drag force. There is almost no shape deformation, the bubble shape remains in a sphere form. The spherical bubble has the lowest velocity, and it has strong relationship between

bubble shape and bubble velocity [30]. Compared to the bigger bubble, a smaller bubble has a more linear vertical movement due to negligible horizontal velocity. The other bubble shape is spheroidal or elliptical as studied by Zaruba and Tomiyama et al. [21, 42]. They found that the spheroidal bubbles have high Reynolds number. In comparison to spheroidal bubbles, spherical bubbles have low Reynolds number, i.e. laminar flow and negligible stirring effect. In this research this fine bubble has been found suitable for suspended particle separation.

**2.1.4 The Forces Acting on Free Moving Bubble**

When the bubble moves upward, the momentum force starts diminishing with the decreasing depth [13]. The Basset force will remain unchanged with uniform velocity and the surface tension force works to maintain the bubble shape. Therefore the equation 2.14 becomes:

$$F_B > F_D + F_{BA} + F_{1,g} + F_C + F_{1,m} \dots\dots\dots(2.15)$$

Fig 2.6 shows free moving bubbles. Their shapes are not in circular, due to high drag force and less surface tension. This phenomena is frequently found in the milli size bubbles. However, the micro size bubbles maintain their circularity along the upward motion.

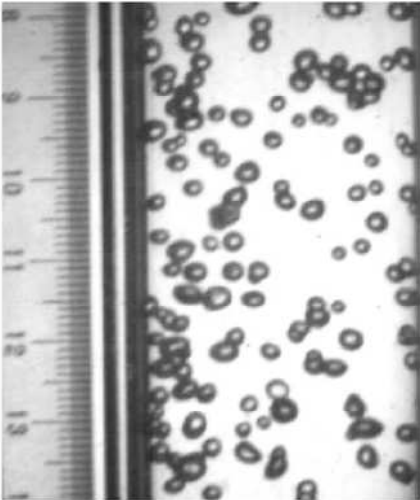


Figure 2.6 Free moving milli bubbles [43]

The free bubble moving forces would play a role in the suspended particle separation. The main principal of suspended particle lift-up depends on bubble forces and particle-water interaction. Hong et al. [36] investigated the bubble forces using micro force balance. The diameter of the bubble and particle was approximately 1 mm. A simulation of collision between the bubble and a stationary particle revealed that the force on the particle oscillated: first increased, then decreased, and increased again. The oscillation of the measured force showed a discontinued particle lift-up process. By using Atomic Force Microscope (AFM) [44] studied the hydrodynamic drag force of the collision between 20  $\mu\text{m}$  hydrophilic silica particle and 230  $\mu\text{m}$  air bubble. The hydrodynamic interaction forces between a solid sphere attached to an AFM cantilever and air bubble were studied by Nguyen et al. [45]. Previously they found that hydrophobic particle has adhesion force to air bubble that makes it easier to separate from water, while hydrophilic particle has adhesion force to water, which makes it harder to attach to air bubbles and remains suspended in water [46]. Due to the preference of hydrophilic particles to remain in water, a certain size of bubble is therefore required to produce a sufficient lifting force to separate the suspended particles from water. The surface force between hydrophobic surfaces causes an “adhesion” as reported by Pushkarova [47]. The changes of air bubble shape continuously change the buoyancy and drag forces on the bubble. To reduce the adhesion forces between suspended particles and water some researcher added surfactant in the water. The particles’ interaction to air, is studied by John Ralston et al. [48] and Vamsi [38] and produced repulsion between air and water surfaces [49]. The attraction forces between AFM probe and a flat hydrophobic surface in water is also studied by Nguyen et al. [50]. The study of the adhesion between suspended particle and bubble is done by Omatta [51] and it is reported that adhesion force influences gas-liquid mass transfer, bubble coalescence and particle agglomeration. According to Nguyen et al. [52], once the suspended particle is attached on the air bubble, it slides down along the bubble surface and remains attached to the underside of the air bubble. The bubble-particle interaction during bubble upward movement consists of collision, attachment and detachment [53]. The other force that influences air bubble movement is wake-induced force, studied by Katz [31]. The stirring effect of air bubble upward movement is induced by force oscillation due to bubble shape

deformation and wake-induced force. These forces need to be decreased by controlling the bubble size and velocity. Millimetre air bubbles (3-6 mm) always produce turbulent flow [39] due to shape deformation and oscillation [54]. Finally, the bubbles coalesce and produce sufficient kinetic energy to create the turbulence effect in the water column [55]. The relationship of bubble shape (spherical or non spherical) and upward velocity was investigated by Kracht[30]. The primary cause of widely scattered velocity is more influenced by bubble deformation; low deformation results in low velocity and large deformation results in high velocity [42], and fine bubbles can stabilize the flow to become laminar [21].

Even though the addition of surfactants increases the adhesion force between air bubbles and suspended particles, nevertheless in some circumstances, the existence of surfactant is unwanted, for example in drinking water. Surfactants exist in wastewater due to detergent, oil, and other surfactant materials. The separation of suspended particles in oily wastewater using induced air floatation (IAF) has been done by Paimanakul [37]. The success of suspended particles removal from water is indicated by the water turbidity level decreasing has been done. A correlation between turbidity level and rate of removal of suspended particles is discussed in this research.

## **2.2 Coalescence and Breaking Bubble.**

Coalescence and breaking between bubbles are influenced by many factors like surface tension, inlet pressure, distance between bubbles, etc. Tange [29] reported coalescence between bubbles can be vertically, horizontally and decline, therefore coalescence depend on the distance and position between two bubbles as shown in Figure 2.7.



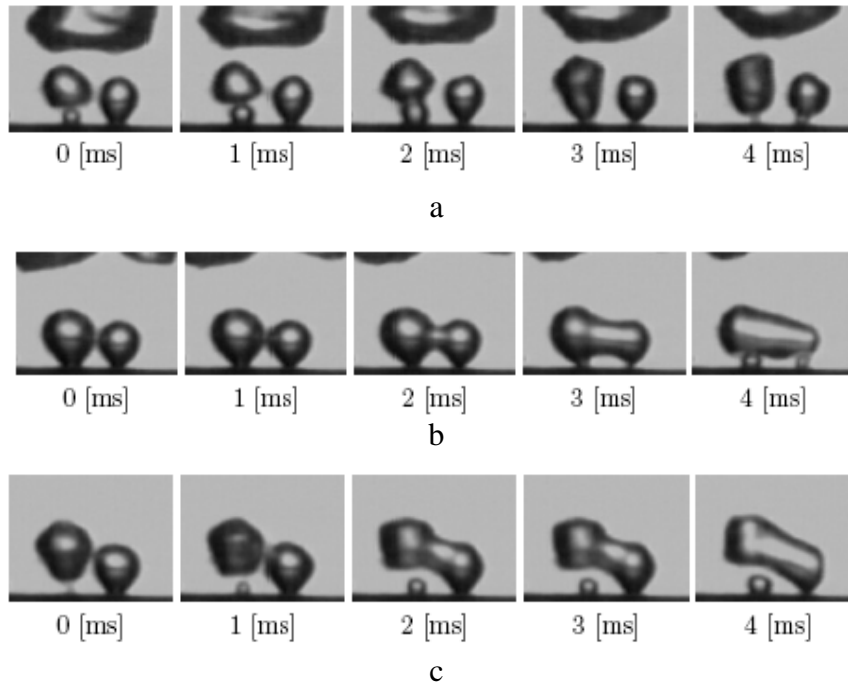


Figure 2.7 coalescence between two bubbles a. vertically, b. horizontally, c. inclined [29].

Coalescence and breaking is influenced by bubble size in both conditions pure water and salinities water [56]. Coalescence rate is nearly constant or weaker size dependence, whereas breaking rate increase when the bubble size increases, as shown in Figure 2.8. The result are calculated using the physical dimensions of the column employed, and the gas velocity is taken 3.5 cm/s. Large bubbles is higher breakage rate due to higher collision efficiencies. This collision is influenced by higher velocity and cross section area of larger bubble. The increase the gas superficial velocity the increase bubbles break-up would be, due to increase bubble collision as shown in Figure 2.9. There is a maximum in the bubble size as a function of gas rate due to the competing effects of coalescence and break-up. The collision among bubbles vertically and/or horizontally that creates bigger bubbles. This phenomenon prevents small bubbles production. However, some researchers i.e. Huilin and Shuyan [57],[58] found that bubble could be separated, so the result is smaller bubbles.

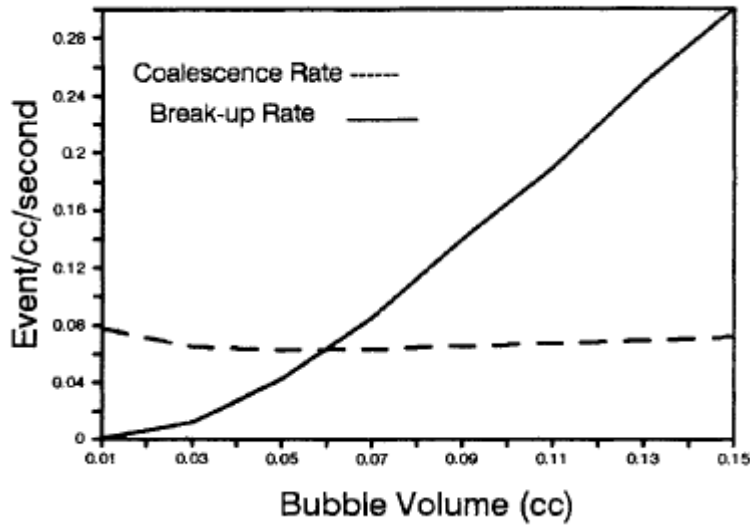


Figure 2.8. Coalescence and breaking rate as function of bubble size [56].

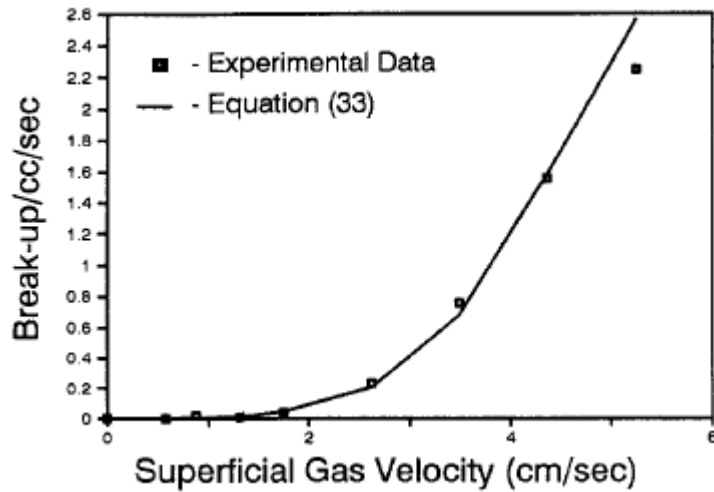


Figure 2.9. The bubble break-up vs gas sparge rate [56]

Hua et al. [59] investigate the relation between Reynolds number and breaking bubble, and found breaking bubble start at Reynolds number 200. The visualization of bubble breaking is reported by Fan et al. [22] as shown in Figure 2.10.

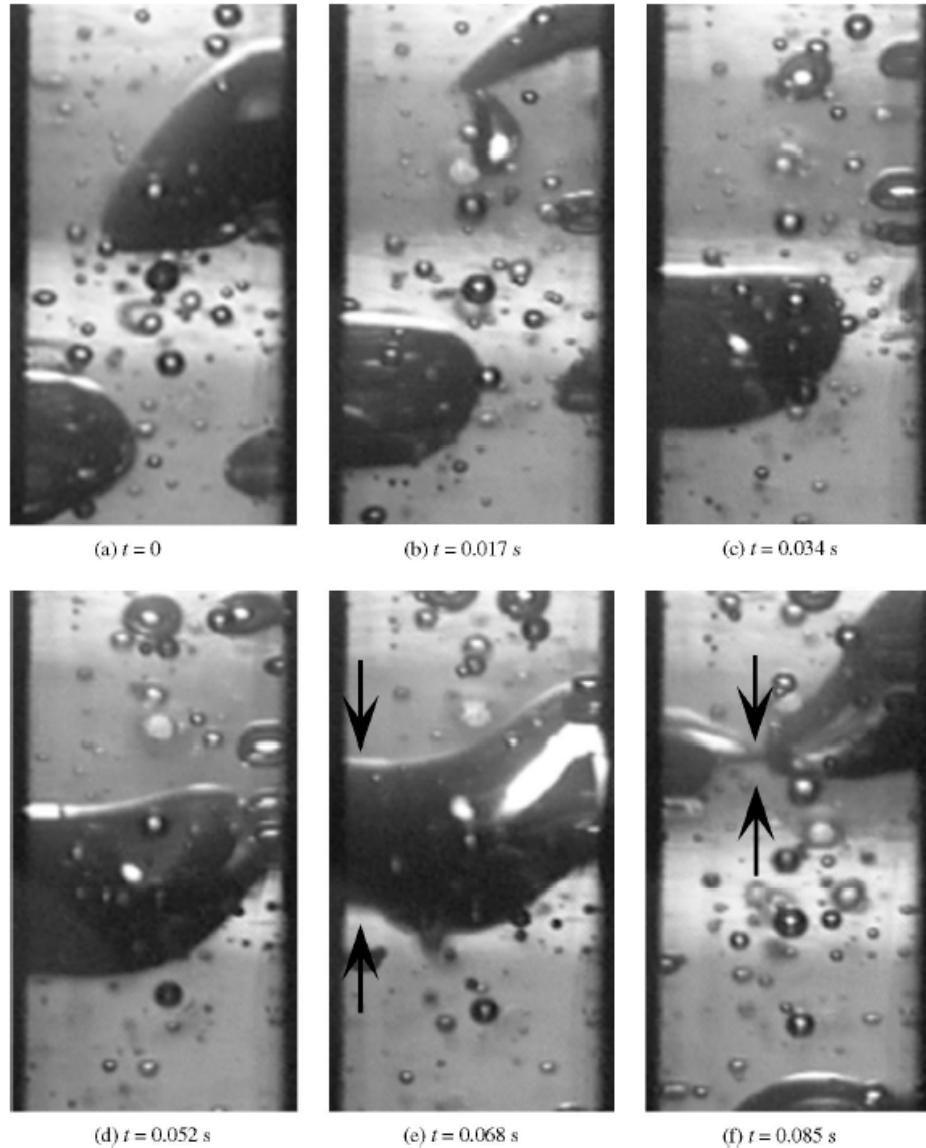


Figure 2.10. A sequence of bubble images showing the process of bubble break-up at  $P=3.5$  MPa [22].

An equilibrium of bubble breakup and coalescence that result in a given bubble size distribution is shown schematically in Figure 2.11. Close to the wall, the high gas volume fraction due to the accumulation of small bubble would tend to coalesce forming larger bubble. The larger bubble would travel to the center of the water column cause of highest upward velocity exist in the center of water column. At the center of the water column, larger bubble can breakup due to the high shear stress and turbulence intensity. The resulting small bubbles would tend to migrate to the wall.

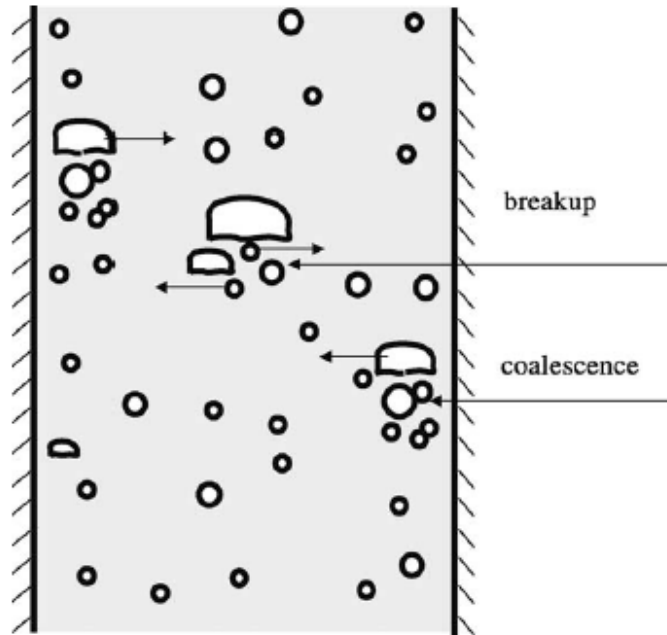


Figure 2.11 Breakup and coalescence process in a vertical channel [60].

### 2.3 Dimensionless Number.

Dimensionless numbers play a key role in bubbles' flows, due to the indication of the relative importance of forces, energies, or time scales in presence and lead the way to simplification of complex problems. Besides, the use of dimensionless parameters and variables in bubbles' flows brings a universal character to the system of equations governing the physical phenomena, transforming an individual situation into a generic case [61]. In this research the bubbles' flows has been characterized by Reynolds number and Froude number.

Reynolds number define as the ratio of inertial forces ( $\rho v^2 / D$ ) to viscous forces ( $\mu v / D^2$ ). The ratio represents the flow condition and is formulated as bellow:

$$\text{Re} = \frac{\rho v D}{\mu} \dots\dots\dots(2.16)$$

The bubble is a moving object in the water, therefore the density ( $\rho$ ) and the viscosity ( $\mu$ ) represent of water properties, whereas the velocity ( $v$ ) and length of chord/bubble diameter ( $D$ ) are bubble properties. The water properties are remain constant, whereas the air properties are continuously changing due to the change of its

velocities (vertical and horizontal velocity) and the change of length of chord cause the bubble shape change. In the millimeter bubbles case, the velocities are high due to the higher buoyancy and the length of chord is continuously changed due to the change of the bubble's shape. The result is higher Reynolds number and can be classified as turbulent flow. While in the micro bubbles case, the velocities are low, due to the lower buoyancy and the length of chord is small, due to the smaller size (micron size), hence this Reynolds is very low.

Froude number defined as the ratio of a characteristic velocity to a gravitational wave velocity, or equivalently be defined as the ratio of a body's inertia to gravitational forces. The Froude number equation is formulated as:

$$Fr = \frac{v}{\sqrt{gD}} \dots\dots\dots(2.17)$$

Where in the bubbles flows case, Velocity ( $v$ ) is represent the bubble's velocity in the water,  $g$  is gravitational acceleration and the length of chord ( $D$ ) is the diameter of bubble. The Froude number has three characteristics of flow, there are[12]:

1.  $Fr < 1$ , the flow is defined as tranquil flow or sub critical flow, where the velocity is low.
2.  $Fr=1$ , the flow is defined as critical flow.
3.  $Fr>1$ , the flow is defined as rapid or super critical flow.

#### **2.4. Suspended Particle Entrainment**

Study the reducing suspended particle has been done by measuring the water turbidity. The relation of contamination (part per millions/PPM) in the water have a linear relation with turbidity number. The correlation factor of PPM and turbidity relationship is found equal to 1 ( $R^2=1$ ), it shows that the turbidity decreasing will represent the decreasing of the PPM [9]. Finally the PPM decreasing will sense of the lift up suspended particle.

Omaata et al. [51] study the lift-up suspended particle is determined by the adhesion force of the particle to a gas bubble under stagnant conditions. The particles has hydrophobic behaviour therefore they subject to competitive adhesion and

agglomeration. For small cohesive forces, particles adhere to a bubble individually or as a monolayer as shown in Figure 2.12 a,b. For cohesive forces exceeding a certain limit, a second layer can be attached to the first one (Figure 2.12 c). When the cohesion forces are higher than adhesion forces, the particles agglomerate in a rigid cluster that can adhere to a gas bubble through a single or only few particles (Figure 2.12 d) thus, the strength of cohesion forces affects the fraction of bubble coverage. The balance of forces of cohesive forces play into account is shown in Figure 2.13 [51, 53].

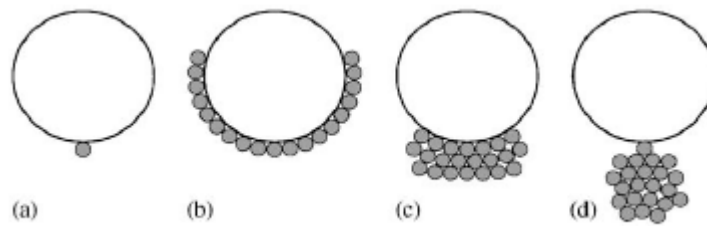


Figure 2.12 Schematic view of particles adhering to a gas bubble (a) single particle, (b) monolayer, (c) multilayer and (d) cluster of suspended particles through a single particle[51].

The visualization of the lift-up of suspended particle is reported by Nguyen et al. [52] as shown in Figure 2.14. Nguyen experiments focused on the visualization of the particle motion over the bubble surface. A high-speed image on the order of milliseconds is used to capture the events of the bubble–particle approach and the rupture of a water film. The images taken during the bubble–particle approach showed rapid change in the bubble–particle intercenter distance. However, during the particle sliding, the change in the bubble–particle intercenter distance is significantly small since the film thickness was relatively smaller than the bubble and particle radii, but the polar coordinate of the particle changed significantly.

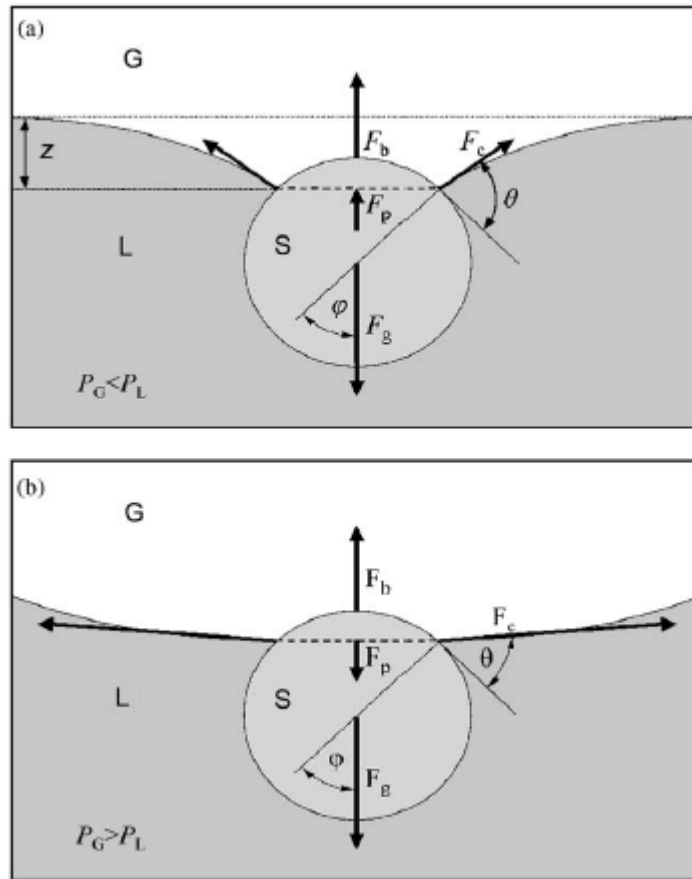


Figure 2.13 The representation of the forces acting on a particle (a) adhering to a flat gas-liquid interface, the hydrostatic pressure ( $F_p$ ) has positive effect on adhesion and (b) adhering to a spherical bubble, the bubble overpressure reduces the adhesion strength [51].  $F_g$  is gravitational force,  $F_b$  is buoyancy force and  $F_c$  is capillary force

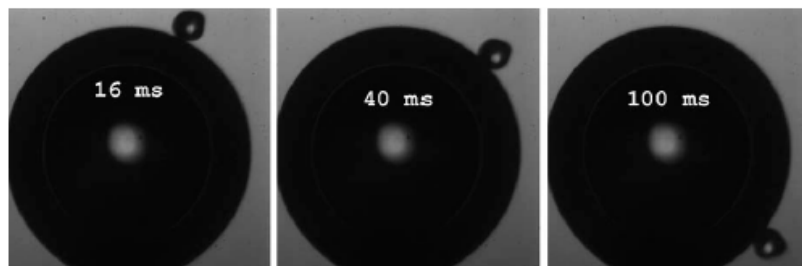


Figure 2.14 The images of bubble attach the particle (a small asperity), showing that the particle rolling on the bubble surface is insignificant. The times shown are relative to the first image.[52]

A series of images of the particle motion over the bubble surface is shown in Figure 2.15. The camera is focused on the plane of the bubble equator. The particle trajectory slightly shifts from in the front of the focus plane. Hence the shown 2D images do not directly give the real radial and polar positions on the bubble surface.

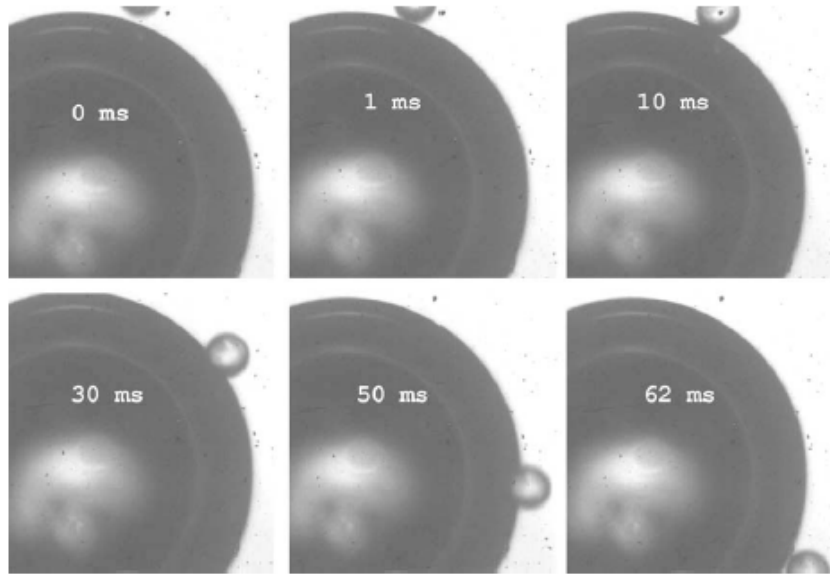


Figure 2.15. The images show the particle positions on the bubble surface. The particle contacted the bubble surface at about 2 ms and left the bubble surface about 61 ms later.[52]

The reduction of suspended particle, the reduction of microorganism would be due to the microorganism generally nested in the suspended particle, as shown in Figure 2.16. The microorganism would reduce as their nest (suspended particles) eliminated.



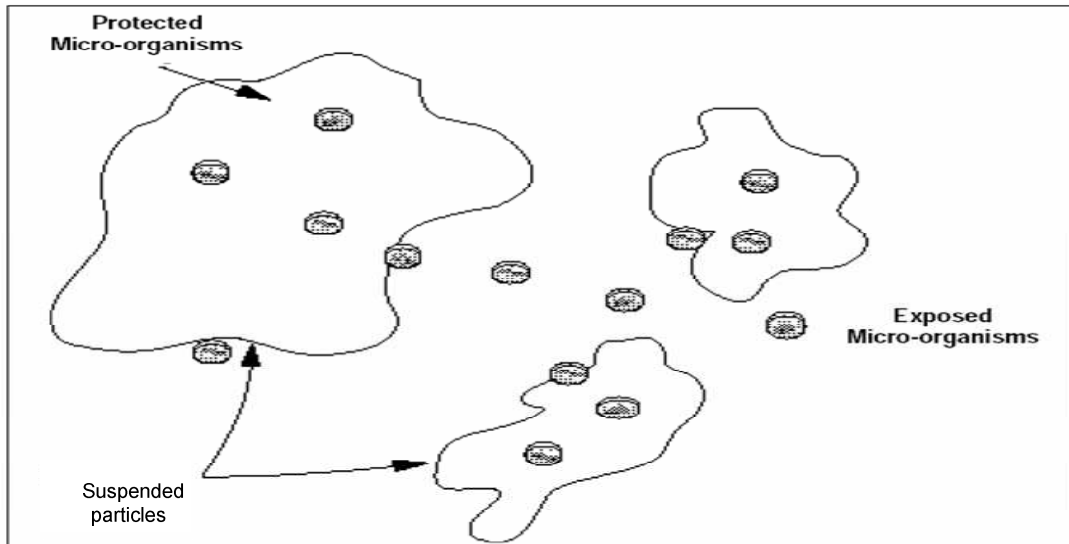


Figure 2.16 The illustration of reducing the suspended solid will effect reducing the micro organism [7].

Figure 2.17 shows the relationship between the turbidity reduction and pathogen/protozoa removal, have been discovered by some researchers as cited in [7]. Patania et al (1995) concluded effective cyst removal up to 2 log when a median turbidity decreasing is 1.4 log using rapid granular titration. The source water turbidity average 6.5 NTU in level decreasing 0.1 to 0.2 NTU can remove 2.25 log of *Cryptosporidium* and 2.8 log of *Giardia* for conventional treatment direct filtration in full scale study were investigated by Nieminski and Ongerth (1995). In the same year Ongerth and Pecararo (1995) resumed that the very low turbidity level source (0.35 to 0.58 NTU) 3 log of cyst can be removed with optimal coagulation, while with intentionally suboptimal coagulation 1.5 log of *cryptosporidium* and 1.3 log of *Giardia* can be removed. Figure 2.17 shows the *Giardia* removal by decreasing the turbidity level.

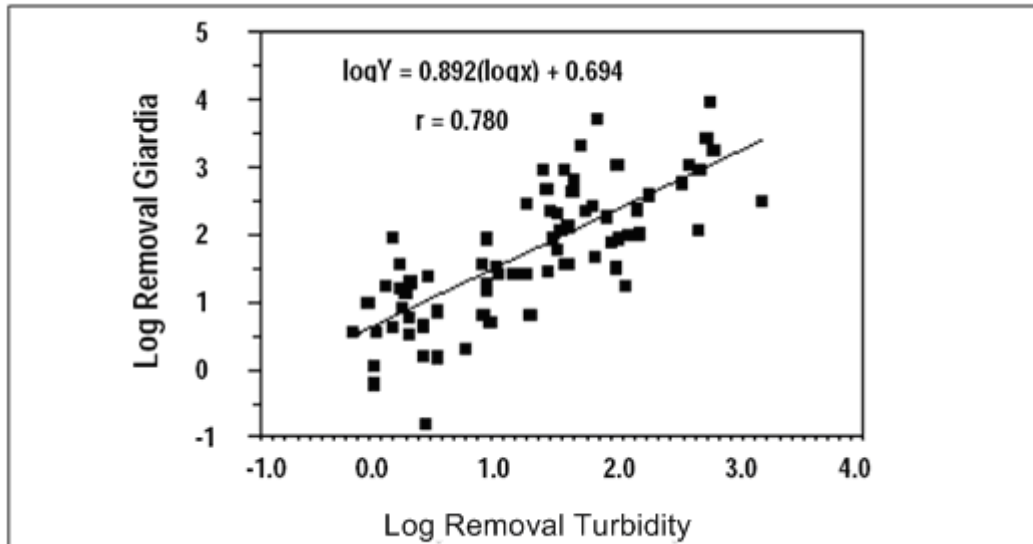


Figure 2.17 Relationship between removal of *Giardia* and Turbidity[7].

Le Chavallier and Norton 1991 discovered from three drinking water treatment plants using different watersheds for every log removal of turbidity can be removed 0.89 log of *Cryptosporidium* and *Giardia*. A high correlation ( $R^2 = 0.91$ ) exists between overall turbidity removal and both *Cryptosporidium* and *Giardia* removal, through conventional water treatment, Nieminski and Ongeth (1992) published that *Giardia* cyst removal by filtration of well-conditioned water results in 90% or better turbidity reduction, which produces effective cyst removal of 2 log (99%) or more. Le chavallier et. al. (1996) studied 66 surface water treatment plant using conventional treatment, most of the utilities achieved between 2 and 2.5 log removals for both *Cryptosporidium* and *Gardia* and a significant correlation ( $PPM=0.01$ ) between removal of turbidity and *Cryptosporidium* existed. Maintaining the overall low level of particulate impurities (turbidity) in treated water mightbe an effective safeguard against the presence of oocys and pathogens, Gregory (1994). Anderson et.al (1996) proclaimed that in a pilot plant study, the removal of particles  $>2\mu^3$  was significantly related to turbidity reduction  $R^2=0.97$  ( $PPM<0.0001$ ): the reduction of turbidity would relate to the removal of *Giardia* cyst,  $R^2=0.67$ ( $PPM=0.13$ ) and *Cryptosporidium* oocysts ( $p<0.08$ ). Figure 2.18 shows the decreasing of turbidity level would effect the *Cryptosporidium* removal.

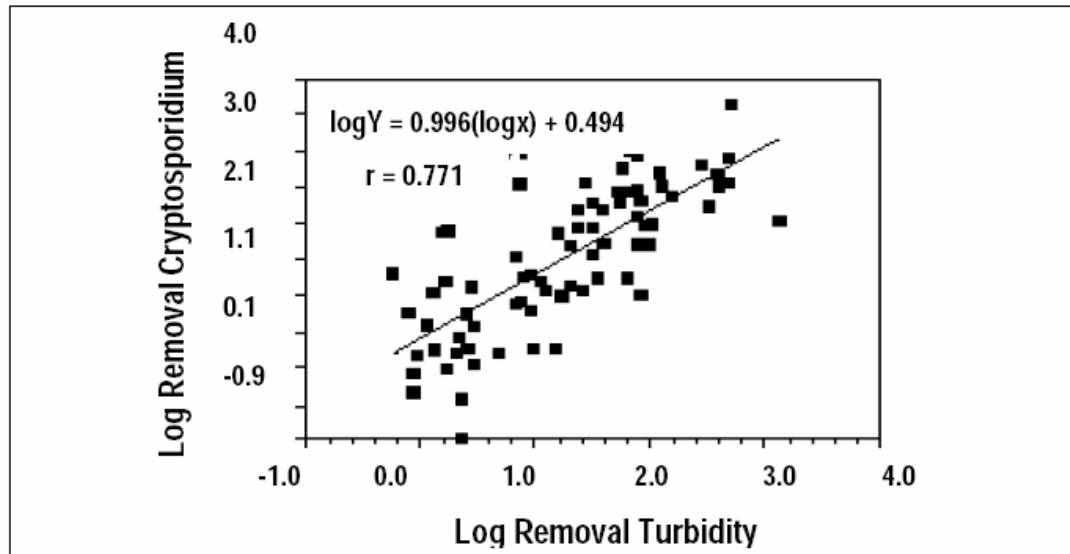


Figure 2.18 Relationship between removal of *Cryptosporidium* and Turbidity [7].

## 2.5 DO Level

In the previous sections, three processes (DO level control, suspended particle lift-up, and micro organism biodegradation) can not be explicitly separated. Pohorecki et al. [28] reported four different regions may be distinguished in a bubble column. .

1. The region of primary bubbles (produced by the gas distributor),
2. The region of secondary bubbles (produced by break-up of the primary ones),
3. The region of dynamic equilibrium between coalescence and disruption of the bubbles,
4. The separation region, at the top of the liquid layer.

Michaud [62] found that for clean water aeration, the oxygen transfer efficiency provided by fine bubbles usually exceeds that of coarse bubbles. In wastewater, contaminants would be influent by a factor called alpha to adjust the clean water transfer efficiency. Alpha is the ratio of oxygen transfer in a generic wastewater to oxygen transfer in clean water. The clean water transfer efficiency multiplied by alpha yields the wastewater transfer efficiency. The following issues consider and understand when evaluating aeration systems:

1. The bubbles size affects the oxygen transfer efficiency. Smaller bubbles have more surface area per unit volume. This provides more area through which oxygen can diffuse and thereby increase overall transfer efficiency, but small bubbles creates more friction and rise slower than the big one. The combination of more transfer area and greater contact time enhance transfer efficiency.
2. Surface active agents (surfactants), such as detergents, lower alpha and the oxygen transfer efficiency. By changing the surface tension, surfactant cause fine bubbles to coalesce into fewer, larger bubbles. In addition, the thin film of detergent molecules between the air bubbles and the wastewater can act as barrier, increasing resistance to oxygen transfer.
3. Fouling is another phenomenon that decreases oxygen transfer efficiency. Most fine bubble systems being installed use a diffuser made of flexible synthetic membrane with many small slits or a ceramic disk with very fine holes. Both provide attractive sites for microbial growth and precipitation of inorganic compounds. This type of fouling can cause bubbles to coalesce, thereby decreasing the overall transfer efficiency[62].
4. Finally, aeration basin and aerator layout geometry can dramatically shift oxygen transfer efficiency. Standard clean water transfer efficiency tests are usually based on full floor coverage. This creates a nearly ideal situation for oxygen transfer. A turbulent counter-current flow regime is established with a volume of water being dragged upward with rising bubbles, being opposed by an equal flow of water traveling downward. As a result of incomplete coverage, large scale currents can form a spiral roll in the basins. The air bubbles flow with the water, and significantly reduces the oxygen transfer efficiency.

The absorption of air in the water can be calculated from the equation [63].

$$\alpha = \frac{V_{gas}(STP)}{V_{solvent}(STP)} * \frac{1}{P_A} \dots\dots\dots(2.18)$$

Figure 2.19 shows the Bunsen absorption coefficient ( $\alpha$ ) of gases in water. The oxygen by air is the lowest absorption coefficient, whereas the pure oxygen is the highest.

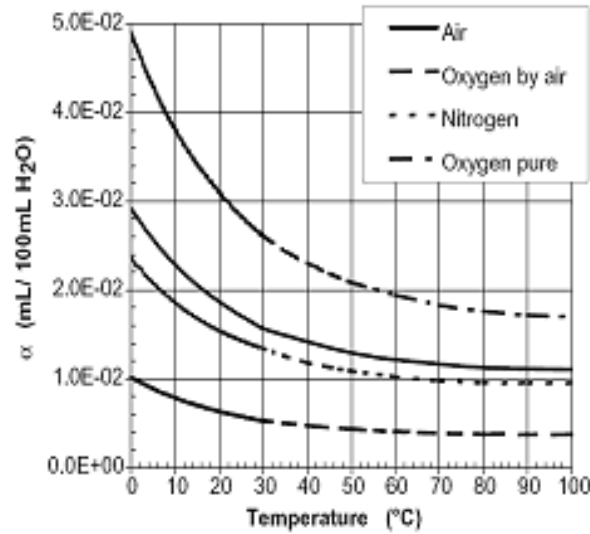


Figure 2.19 Bunsen absorption coefficient of dissolved gases of interest in water [64].

Some of researchers reported that the particles inside the water will move upward because of the kinetic energy of the air bubbles floatation substitute to potential energy of particle (collision mechanisms) [22, 57, 58, 65, 66]. Mechanism for particles smaller than 10- $\mu$ m, Brownian diffusion and colloidal forces strongly influence the collection of such particles by air bubbles in floatation. The suspended particles diameter in the range of 40-160 nm, were removed using fine bubbles of typical average diameter of 150  $\mu$ m. Nguyen et. al [67] reported that the experimental results show the collection efficiency to have minimum suspended particle size in the order of 100 nm. Fan et al [22] reported the stirrer process using the principle of the air bubble dynamics.

DO level also has constraint by salinity, more salty will reduce the water ability to dissolve oxygen [1]. Salinity was originally conceived as a measure of the mass of dissolve salts in a given mass of solution. The experimental determination of the salt content by drying and weighing presents some difficulties due to the loss of some components [3]. The only reliable way to determine the true or absolute salinity of natural water is to make a complete chemical analysis. However, this method is time-consuming and cannot yield the precision necessary for accurate work. Thus, to determine salinity, one normally uses indirect methods involving the measurement of physical property such as conductivity, density and sound speed [3]. Table 2.1 shows the DO level in the range of 20 to 30°C, and 0 to 5 PPM of the water salinity.

Table 2.1 Dissolved oxygen concentration, mg/l (Cs) [1].

Temperature. °C	Salinity, part per thousand	
	0	5
20	9.08	8.81
21	8.9	8.64
22	8.73	8.48
23	8.56	8.32
24	8.40	8.16
25	8.24	8.01
26	8.09	7.87
27	7.95	7.73
28	7.81	7.59
29	7.67	7.46
30	7.54	7.33

Many processes in the industries produce wastewater that contain of organic toxic compounds, and organic matter can be degraded by microorganisms. Betancur [68] proposes a mathematical model for acclimation process of bioreactor treating toxic wastewater, and he found that only microorganism is one key parameter in biomass growth. To maintain Oxygen concentration in the wastewater, some researchers used a submerged membrane bioreactors (MBRs) [69, 70]. Smidt [71] used aerobic aeration as a post-aeration, anaerobic digester. All previous work show that it is essential to control oxygen concentration in a biodegradation and a chemical process.

Micro air bubbles have a larger surface contact between air and water than milli bubbles, and effect significantly, the DO level increase. For example at the same air flow rate, decreasing the bubble diameters from 2.5 mm to 500 micron would increase the interfacial contact area between the air and water by a factor of five for spherical bubbles [6]. The oxygen is needed for aerobic microorganism to degrade the organic matter that remains in wastewater. This phenomenon can be used to support microorganism life effectively.

Micro bubbles have small buoyancy that gives a slow vertical velocity. It needs more time to reach top surface of water column. This phenomenon gives sufficient time to transfer oxygen from air bubble to water. Hence, time required to achieve maximum DO level in shorter for the smaller bubbles.

The presence of the impurities in the water significantly reduces the alpha factors in the gas bubble zone, and the result of saturation DO concentration and volumetric oxygen mass-transfer in the water will reduce. Chern [72] using Silica, Soybean oil and surfactant impurities in water study the DO concentration and oxygen transfer rate mg/L-h.

## **2.6 Biodegradation and Nitrification**

Biodegradation and nitrification of wastewater can be achieved effectively when the dissolve oxygen (DO) level in the water is sufficient. Aerobic wastewater treatment uses microorganism (bacteria) to feed on waste in the water and convert them to carbon dioxide and water. The purpose of aeration of water is to provide oxygen to the microorganism in the degradation [7, 73, 74]. The aerobic biological decomposition of an organic waste continues until all of the waste is consumed. Nitrification is two steps biological process, from ammonium nitrogen oxidized to nitrite and nitrite oxidized to nitrate [1].

The contaminations in the wastewater influence the water physiochemical i.e. surface tension, viscosity and density, also acting forces in the wastewater like: Van Der Waals, Brownian, colloid and frictional shear stress [75]. The forces acting on the air bubble like: buoyancy, drag, momentum, surface tension, Basset, particle bubble collision and liquid-solid suspension inertial forces [13], is also influenced by the existence of the contaminant. The balance of these forces act in the time of generation, detachment and floating upward motion of bubble are studied. They bubble diameter (size), velocities (vertical and horizontal) are determined, and hence its influence DO level for biodegradation and nitrification process.

Aerobic purification of dairy water was studied by Escobar [76]. The delaying of aeration on pre-storage during 30 hours leads to higher degradation rates than delaying the air intake for longer times. When the aeration apply in the beginning (influent), the maximum substrate consumption rate is obtained, the maximum ammonium uptake rates varied between 0.505 and 0.972 mg N/l per day, being a bit higher than in ordinary municipal wastewaters treatment plants.

## 2.7 Use of Micro Bubbles in Organic Matter Degradation

In wastewater treatment systems, the standard aerator is used in the secondary treatment process to support the biological growth of the organisms in the aeration tank. However, these standard aerators produce turbulent air flow that leads to high transport coefficients. The micro-porous diffuser also requires large horsepower. Therefore the fine bubble diffusers are commonly used in biological treatment plants [7]. The use of these fine bubble diffusers is due to its durability; sustainability and cost effectiveness.

Submerged air diffusers are used in wastewater treatment facilities to increase dissolved oxygen (DO) levels and promote water circulation. Submerged diffusers release air or pure oxygen bubbles at depth, producing a free, turbulent bubble-plume that rises to the water surface through buoyant forces at roughly an  $11^\circ$  angle of spreading [77]. The ascending bubble plume entrains water, causing vertical circulation and lateral surface spreading. Oxygen transfers to the water across the bubble interface as the bubbles rise from the diffuser to the water surface.

When a submerged diffuser is operated, there are two main interfaces over which oxygen transfer occurs. Oxygen transfer occurs across the bubble interface as the bubbles rise through the water column. Oxygen transfer also occurs across the water surface at the air–water interface. The bubble-transfer rate involves some additional considerations. The liquid-phase equilibrium concentration of a given bubble is not only a function of temperature and atmospheric pressure, but also hydrostatic pressure and gas-phase oxygen composition[1]. As bubbles rise, bubble–water gas transfer of oxygen, nitrogen, argon, carbon dioxide, and trace gases occurs due to a concentration gradient between the equilibrium bubble concentration and the ambient water concentration. Over depth, the bubble–water transfer of all gases affects the gas-phase oxygen composition and the equilibrium oxygen concentration. The equilibrium oxygen concentration inside a bubble also depends on gas flow rate and the changing bubble–water transfer coefficient over depth.

The functioning of aerobic processes, such as activated sludge, biological filtration, and aerobic digestion, depends on the availability of sufficient quantities of

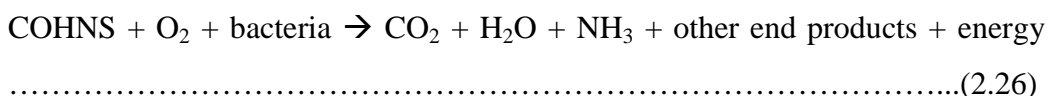


oxygen. The most common application of oxygen transfer is in the biological treatment of wastewater.

Aerobic wastewater treatment uses microorganisms to feed on the waste in the water and convert them to carbon dioxide and water. To keep the process going, the wastewater needs to be aerated with oxygen. The purpose of aeration of water is the improvement of their physical and chemical characteristics, the removal or reduction of taste and odor and precipitation of inorganic contaminants such as iron and manganese. In water treatment, the purpose of aeration is to ensure continued aerobic conditions for the microorganism to degrade the organic matters [7] [63].

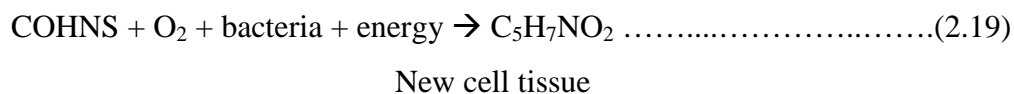
If sufficient oxygen is available, the aerobic biological decomposition of an organic waste will continue until all of the waste is consumed. Three more or less distinct activities occur. First, a portion of the waste is oxidized to end products to obtain energy for cell maintenance and the synthesis of new cell tissue [1, 63, 78].

*Oxidation:*



Simultaneously, some of the waste is converted into new cell tissue using part of the energy released during oxidation.

*Synthesis:*



Finally, when the organic matter is used up, the new cells begin to consume their own cell tissue to obtain energy for cell maintenance. This third process is called endogenous respiration [74].

*Endogenous respiration:*

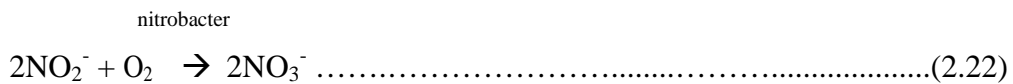
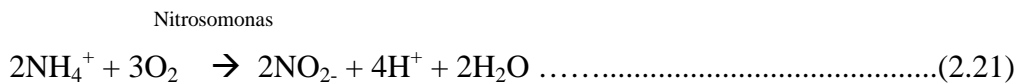


Using the term COHNS (which represents the elements carbon, oxygen, hydrogen, nitrogen, and sulfur) to represent the organic waste and the term C<sub>5</sub>H<sub>7</sub>NO<sub>2</sub>

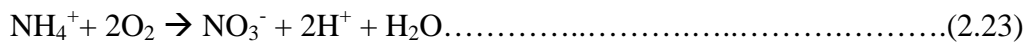
[first proposed by Hoover and Porges (1952)] to represent cell tissue, the three processes are defined by the following generalized chemical reactions [1]

Nitrification is the term used to describe the two-step biological process in which ammonium nitrogen (NH<sub>4</sub>-N) is oxidized to nitrite (NO<sub>2</sub>-N) and nitrite is oxidized to nitrate (NO<sub>3</sub>-N). The need for nitrification in wastewater treatment concerns over the effect of ammonia on receiving water with respect to dissolved oxygen (DO) concentrations [78-80].

Aerobic autotrophic bacteria which are *Nitrosomonas* and *Nitrobacter* are responsible for nitrification in activated sludge process which oxidize ammonia to nitrite and then to nitrate, respectively. Two-step oxidation from ammonium nitrogen to nitrate can be described as follows:



Total oxidation reaction



Based on the total oxidation reaction above, oxygen required for complete nitrification (oxidation of ammonium) is 4.57 g O<sub>2</sub> per g N oxidized with 3.43 g O<sub>2</sub>/g used for nitrite production and 1.14g O<sub>2</sub>/g NO<sub>2</sub> oxidized [1, 63].

## 2.8 Kinetics in a Batch Reactor

Treatment process kinetics in the batch reactor was calculated in first order to determine the performance of the degradation and nitrification. The derivation of the material balance equation for batch reactor (Figure 2.20) for a reactive constituent is written as follows:

Accumulation = inflow – outflow + generation

$$\frac{dC}{dt}V = QC_0 - QC + r_cV \dots\dots\dots(2.24)$$

In a batch reactor there is no inflow or outflow from the control volume, therefore the Q is 0, the equation for batch reactor is:

$$\frac{dC}{dt} = r_c \dots\dots\dots(2.25)$$

When flow is not occurring, the concentration per unit volume is changing according to the applicable rate expression. The rate of reaction in first order is formulated:

$$r_c = -kC \dots\dots\dots(2.26)$$

The integration in limits between  $C = C_0$  and  $C = C$  and  $t = 0$  and  $t = t$  yields.

$$\int_{C=C_0}^{C=C} \frac{dC}{C} = -k \int_{t=0}^{t=t} dt = -kt \dots\dots\dots(2.27)$$

The final result is:

$$\frac{C}{C_0} = e^{-kt} \dots\dots\dots(2.28)$$

This formula is similar to the BOD equation

$$BOD_r = UBOD(e^{-k_1t}) \dots\dots\dots(2.29)$$

Where  $BOD_r$  = amount of waste remaining at the time t(days) expressed in oxygen equivalents, mg/l.

$k_1$  = first order reaction rate constant, 1/d

UBOD = total or ultimate carbonaceous BOD, mg/l

t = time, d

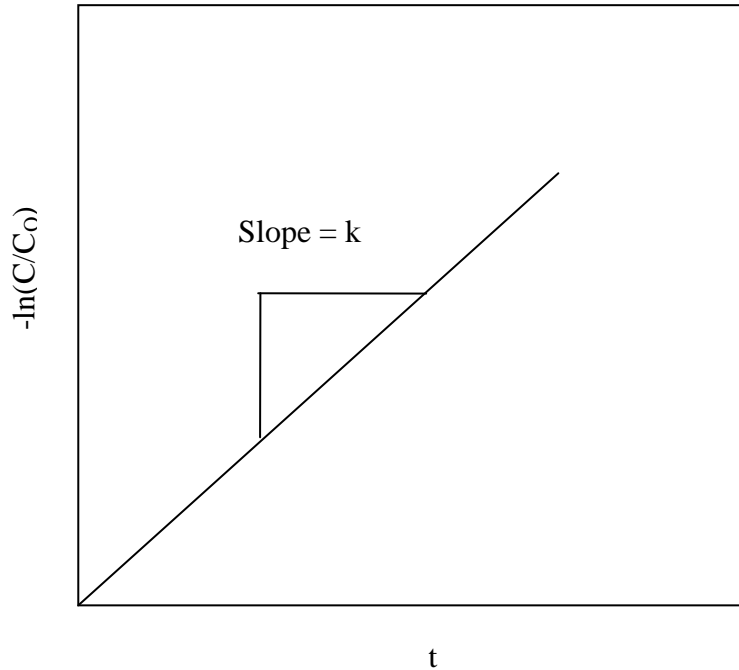


Figure 2.20. Graphical analysis for determination of first-order reaction [1].

## 2.9 Summary

This chapter covered; investigation of the micro bubbles movement in the transparent water, and the possibilities of micro bubbles performance, which is DO level and pathogen removal. The researchers before never study the significances of increasing DO level when the micro bubble was used in aeration process and the other effect of the micro bubble aeration in suspended particle entrainment, therefore the result is the clearer water. The performances of micro bubble aeration subject to suspended particles separations and high DO level increasing. For this research is proposed a novelty of water purification system that of using micro bubbles better separation suspended particle, and better DO level increasing in the same time, therefore optimum biodegradation and nitrification also clearer effluent water can be achieved. The millimeter bubble in aeration (as in ordinary wastewater treatment) can be replaced into micro bubble aeration. The aeration system needs to be designed and applied in the water treatment plant. This research deals with experimental set-up and experimental procedure. The experimental set-up is followed by bubble dynamics and suspended particle entrainment, whereas the experiment procedure is followed by

Biodegradation and Nitrification process. The activated sludge technique is used in Biodegradation and Nitrification of UTP resident wastewater equipped with submerged millimeter and micro bubble aeration. The suspended particle entrainment is simulated using CMC polluted water.



## CHAPTER 3

### METHODOLOGY

Two experimental set-ups equipped with flow and pressure transducers are used to study the bubble dynamics and biodegradation process. Some measurement devices like the LDA/PDA, high speed camera, DO-meter, turbidimeter, surface tension-meter, density-meter and viscometer are used to monitor the required variables and parameters. The polluted water is simulated to the closer similarity of wastewater physiochemical characteristic. The acting forces calculations of suspended particles entrain in air bubbles rise motion using proposed equations are represented. The relation graphs of velocity ratio and bubble size are plotted to represent the rate of separation process. Finally the suspended particle entrainment and DO level enhancement in wastewater treatment need the suitable bubble size and velocity. The sub-millimeter holes in aluminium plate and micro porous of sintered glass plate submerged diffusers are used to generate the milli and micro air bubble respectively in the aeration system.

#### **3.1 Introduction**

In millimetre bubble aeration, the perforated aluminium plate is used as diffuser. The diameter of varied holes range between 0.103 to 0.272 mm where the pressurized air goes through and air bubbles emerge from the aluminium plate surface. Figure 3.1.a. shows the water circulation in aeration system using millimetre air bubble. The diffuser is located in the bottom side of water column where the pressured air is injected. The swirls exist stronger when the faster air flow is applied, whereas the swirls exist weakness when micro bubbles flow is slower due to its smaller buoyancy. Figure 3.1.b. shows the expression of millimetre bubbles and suspended particles circulating within the vertical water column. The bubbles motions push water and suspended particles upward. On reaching the top level of water, the bubbles are

floating on the water surface and breaks released the trapped air into the atmosphere. When the bubbles break, they leave wave towards the walls of the container. This small wave would help suspended particle to move to the edge of the vertical water column. Some of the particles close to the wall of the container would move down with the passage of water and return back to move upward after reach the base of water column. This circulation last longer as the aeration process. The settled particles would form scum on the water surface close to the container wall.

In micro bubble aeration, the porosity of sintered porous glass has been used as diffuser holes to produce micro size bubbles. Different porosities of sintered glass is used to produce different size of micro bubbles. The diffuser holes are formed due to the void fraction among glass crystals. Small crystals produce small porosity and hence smaller diffuser hole [81-83]. These porosities works as diffuser holes where the pressurized air goes through sintered glass, the air bubble emerges from the surface of the diffuser. Since all the spaces between variation glass crystals are not equal, therefore they always produce air bubble in a range of size. Using sintered glass, the production of same size holes is very difficult. The pressurized air is adjusted minutely to produce micro bubbles. This suitable pressure can not be increased anymore, due to increase inlet air pressure will also increase the inlet air flow. The increasing air inlet flow will generate bigger bubbles (millimeter size bubble), due to emerges between bubbles vertically. Experimentally the maximum pressure is 33 kPa, where the maximum air flow is 0.012 m<sup>3</sup>/s.



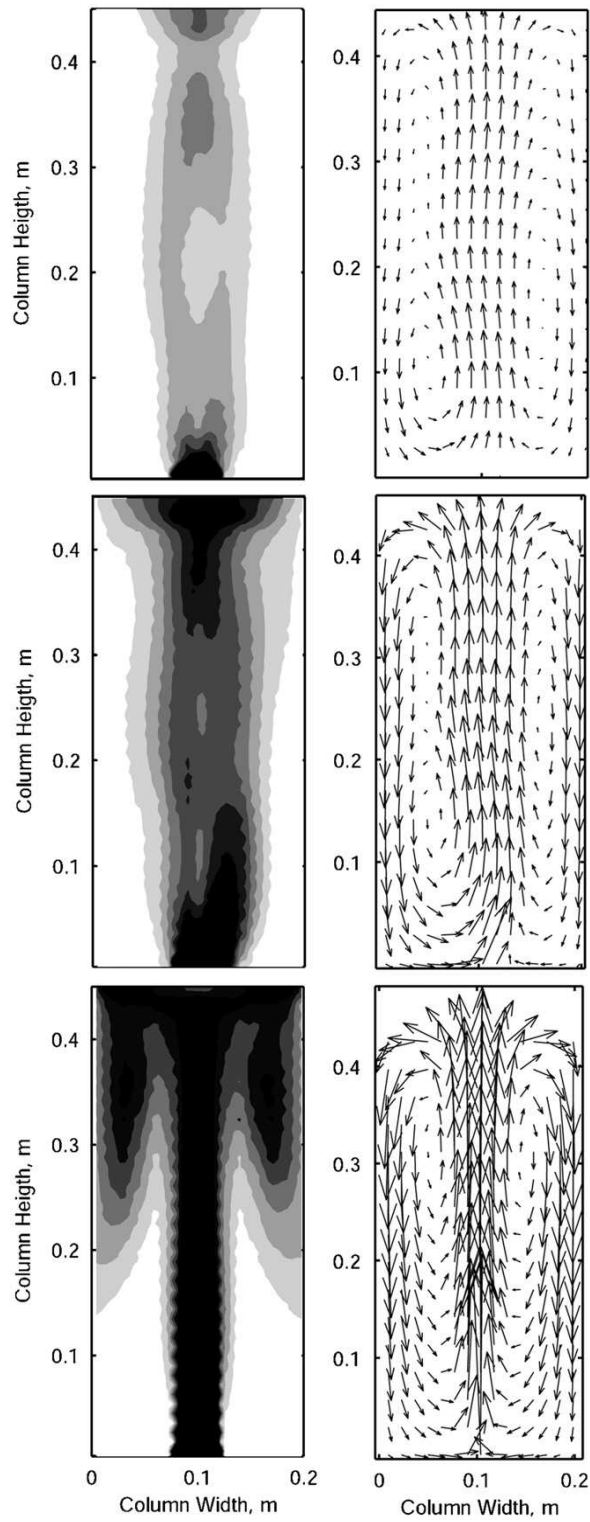


Figure 3.1 a Water circulation in aeration column, start with slower till faster flow[84]

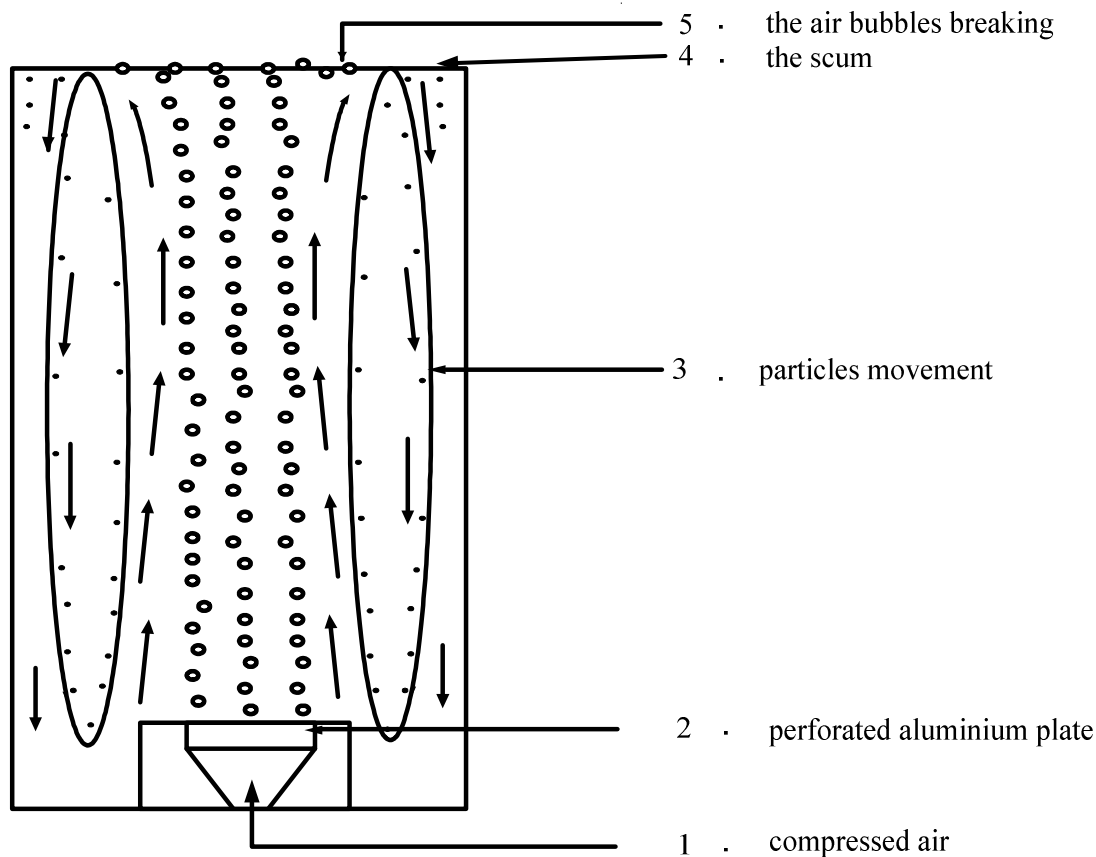


Figure 3.1 b. The air millimeter bubbles trajectory and suspended particles circulation in water column.

Figure 3.2.a. shows the gas holdup and liquid velocity. The micro bubbles have longer distance in horizontal than vertical due to the longer distance between its porous holes of sintered glass. Therefore every bubble has its gas holdup and liquid velocity. Fig 3.2.b. shows the expression of micro bubbles and suspended particles circulating within the vertical water column. The bubbles push the suspended particles upward, therefore they slip among water molecule. While the water stands still at its place. The bubble-particle pairs move slowly. When the micro bubble breaks on the water surface the particle is left behind. The settled particles would form scum on the water surface close to the container wall. The water would be clearer than before aeration process.

The process of removing the suspended particles is continued for a certain period of time, but not all the suspended particles can be removed from the water; however, a significant reduction of water turbidity indicates the effectiveness of this system.

The bubble characteristics, such as diameter and velocity are investigated for their relationship with air pressure and flow through the diffuser.

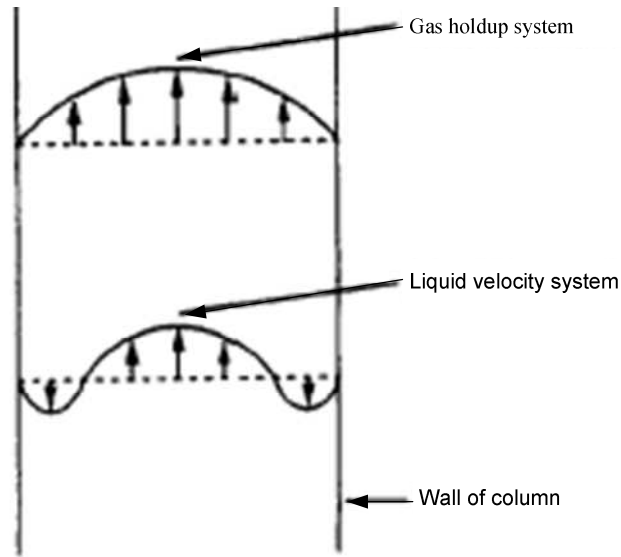


Figure 3.2 a Gas holdup and liquid velocity system[85]

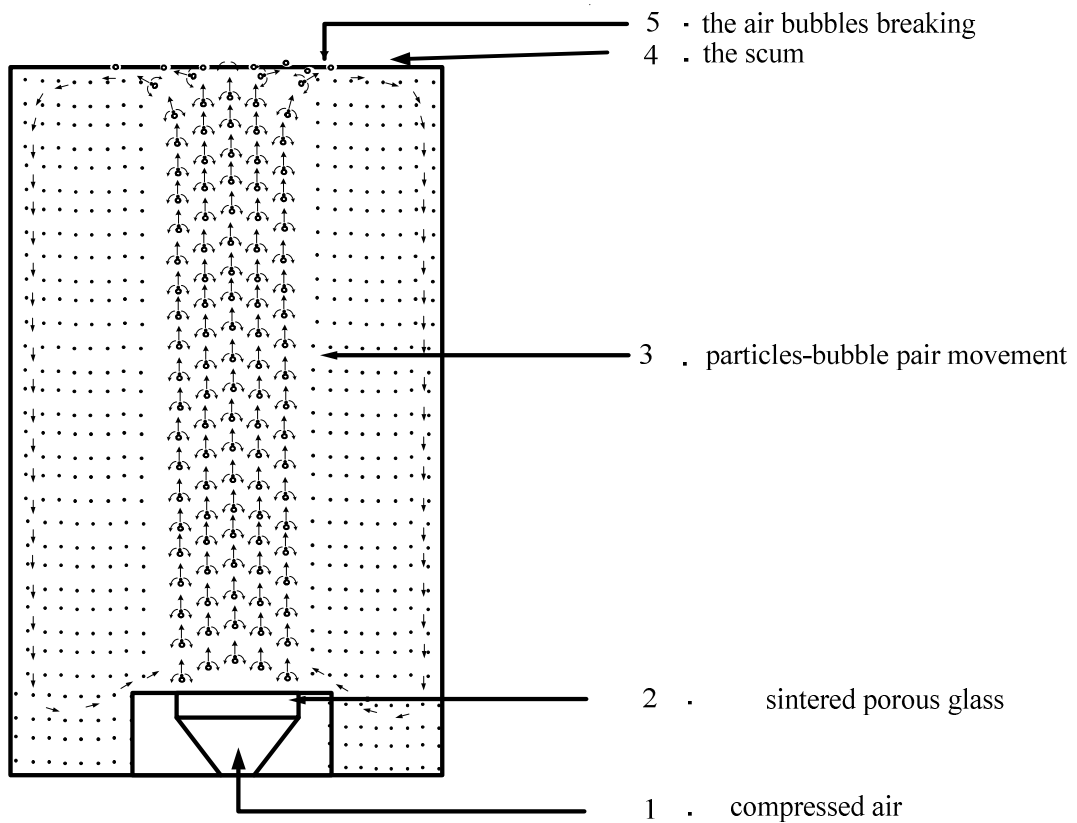


Figure 3.2. b. The micro air bubbles trajectory and suspended particles in vertical water column.

### 3.2 The Experimental Set-up

The experimental set up is a square water column, having a cross-sectional area of 100 cm<sup>2</sup>, with submerged diffuser at the bottom of the column as shown in Figure 3.3. and Figure 3.4. The diffusers are a perforated aluminum and porous sintered glass. Perforated Aluminium diffuser is a circular disc of 50 mm diameter, 3 mm thickness and having holes in it in the range of 0.1mm to 0.4 mm. It use for produce millimeter bubbles. The porous sintered glass with porosities of 1-40 μm is used to produce air micro size bubbles. The air was forced through the diffuser to produce air bubbles through the holes at the diffuser surface. The bubbles released from the diffuser surface would move upward due to buoyancy force and the horizontal and vertical components of their velocity would depend upon the size of the bubble. The vertical would help in moving upward, whereas horizontal component of velocity would force the bubble to move left or right. The horizontal motion of bubble is considered to be as a stirring action, i.e. it would mix the suspended particles into water. The Bubbles will act as function as stirrer, dissolve oxygen, suspended particles lift-up, transfer mass and transfer heat. The transducers are fixed between compressed air source and the diffuser. The transducers are monitoring the characteristics of air before entering into the water column. The parameters those are monitored as pressure, air flow and temperature. The max pressure gauge range is 40 kPa and flow meter is measure between 0 to 5 lit/min. The range of the millimeter bubble is 1 to 50 mm, whereas the micro bubble is 1 to 100 micron.

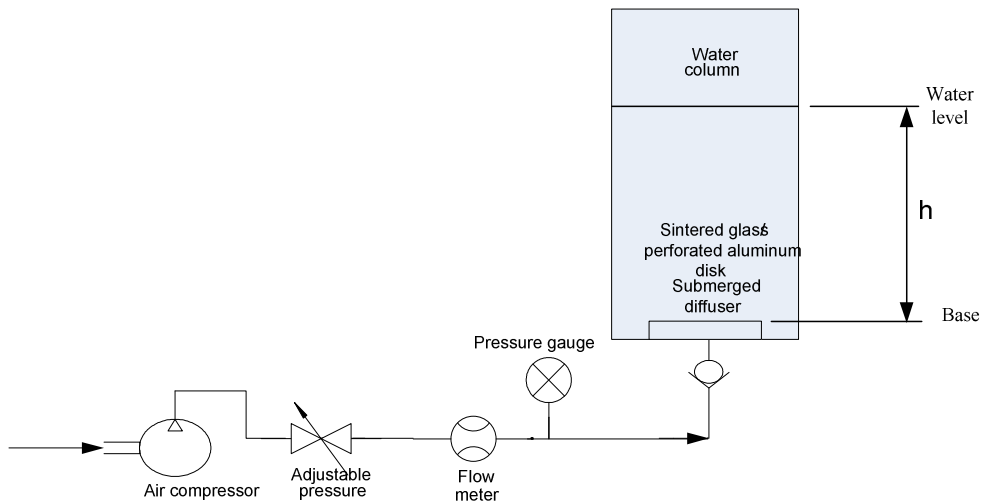


Figure 3.3 Schematic diagram of experimental set-up to produce bubbles in a vertical column.

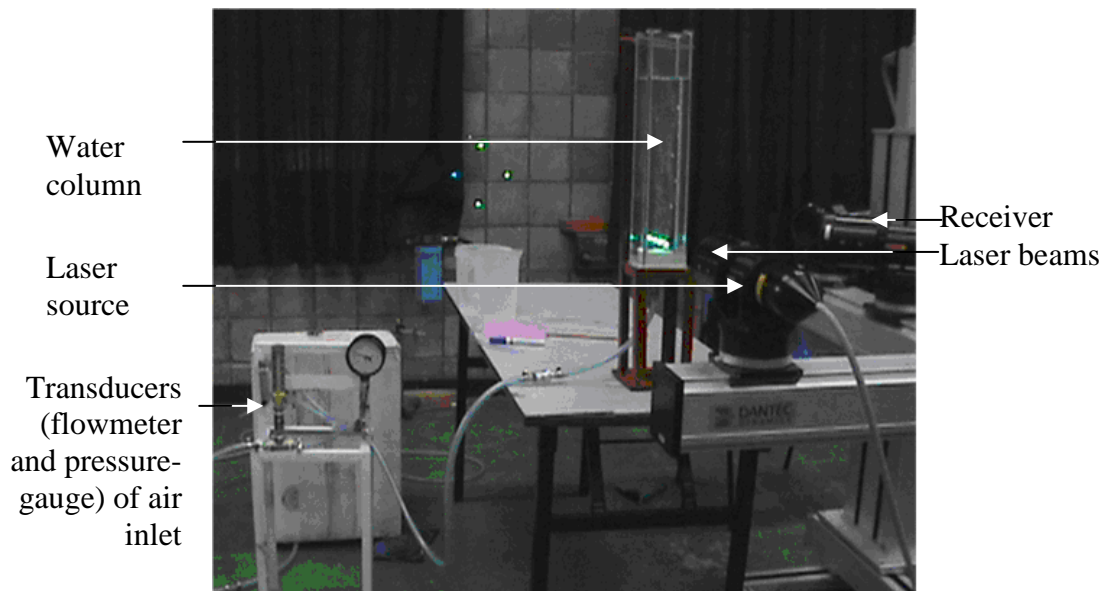


Figure 3.4 Experimental set-up showing, (10 x 10) cm vertical column for measurements of bubble dynamics.

### 3.2.1. Sub-milli Hole Diffuser

The capability of conventional drilling machines is limited by the drill size, therefore they may not be used for very fine holes. Another way of drilling micron holes is (Electric Discard Machine) EDM machine, which has again the limitation of cutting thread, but is capable of drilling sub-milli size holes as shown in Figure 3.5. Additionally, the holes drilled by EDM are not circular because of electric spark

uncertainties. However, a diffuser was prepared having holes in the range of 0.103 mm to 0.272 mm

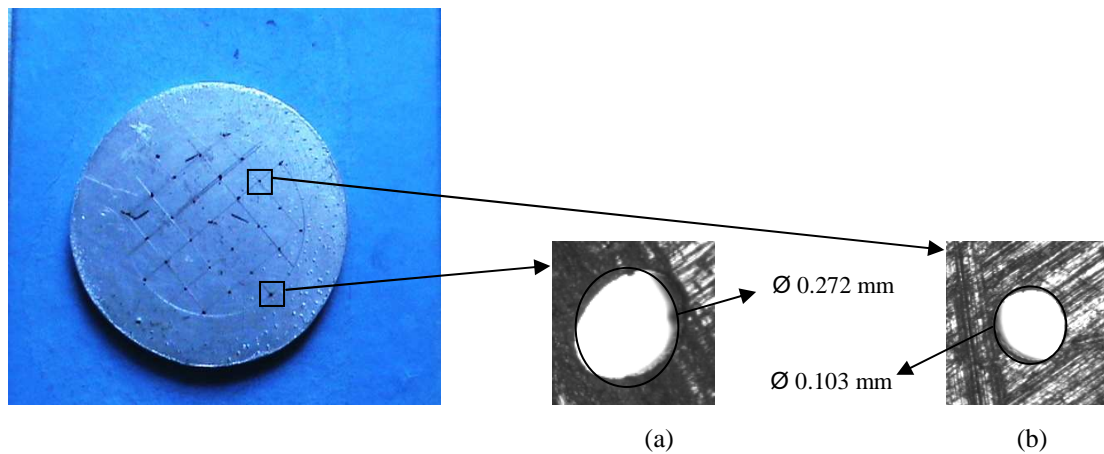


Figure 3.5 Perforated aluminum plat 3 mm thickness, 50 mm diameter machining by EDM die sinker (a). 0.272 mm; (b). 0.103 mm

### 3.2.2 Micro Hole Diffuser

The sintered porous glass has micro porosity that can function as a diffuser to produce micro bubbles. The three sizes (1-10, 10-16 and 16-40  $\mu\text{m}$ ) of sintered porous glass were used in this research as shown in Figure 3.6.

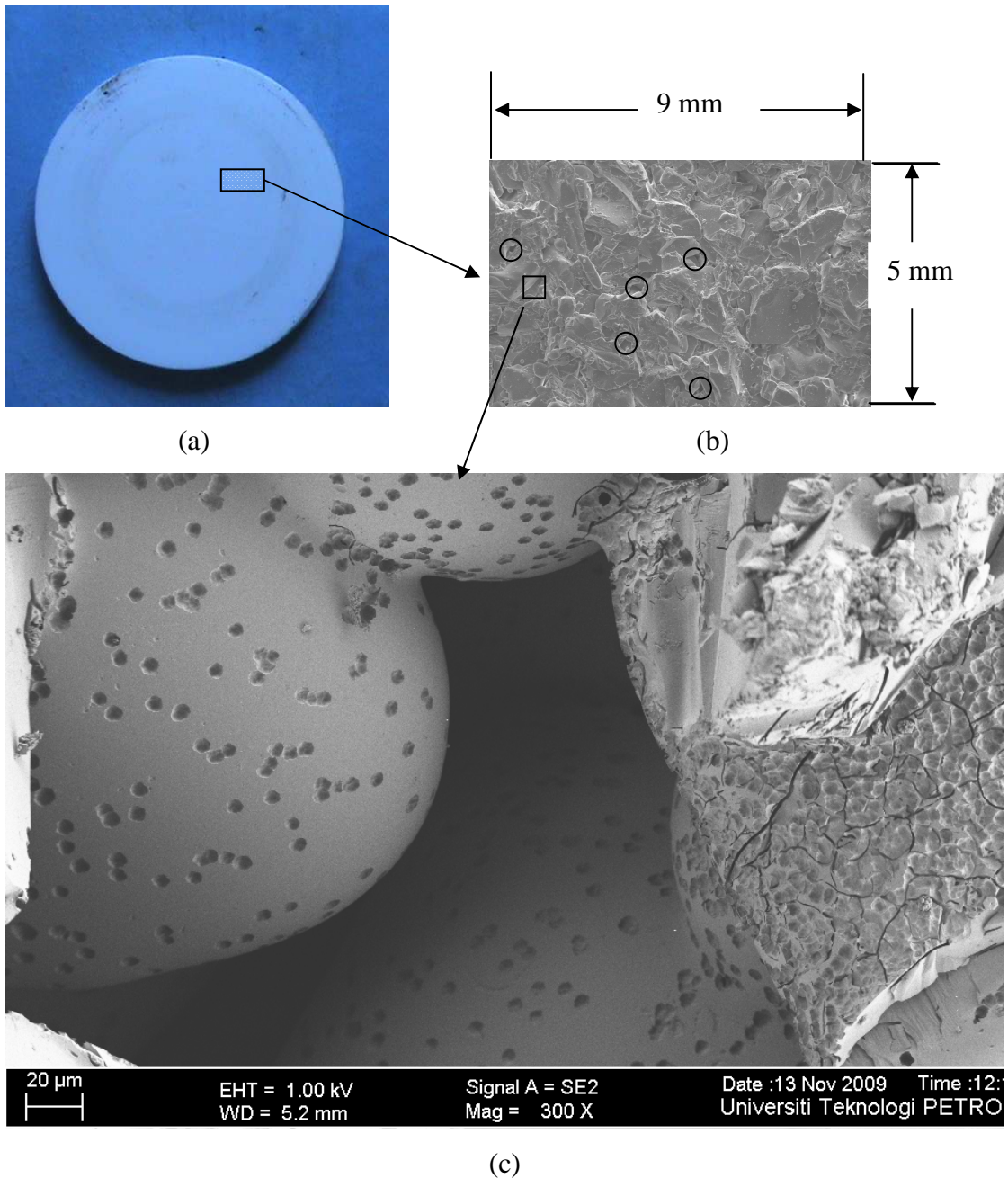


Figure 3.6 a. 5 mm diameter of Sintered porous glass diffuser has 10-16  $\mu$ m pore size. b. SEM image of sintered glass diffuser showing porosities as dark points. c. The 300 magnification of the glass porous.

The surface is not in a plain due to the roughness. The porosity locate in among of the glass crystals, therefore the porosity holes in general have inclination and very rare in vertical position. Different glass crystal size distribution and their porous position at the surface tend to vary the bubbles production. In micro bubble production the

horizontally merging between bubbles is rare, due to the horizontal distance between porosity holes is longer than the diameter of porous hole.

### 3.3 The Experimental Procedure

To study the effectiveness of biodegradation and nitrification process, the comparison between millimeter and micrometer diffuser were done. An experimental setup using two vertical reactors A and B, each of 140 mm length, 140 mm width and 500 mm height were used. Perforated aluminum was used to produce millimeter size air bubbles in reactor A. Porous sintered glass with porosities in the range of 10-16 micron was used to produce the micro bubbles in reactor B. Compressed air at a pressure of 63 kPa at a flow rate of 2.5 L/min was forced through the diffusers at the bottom side of both reactors. Figure 3.7 showed the schematic diagram of experimental apparatus.

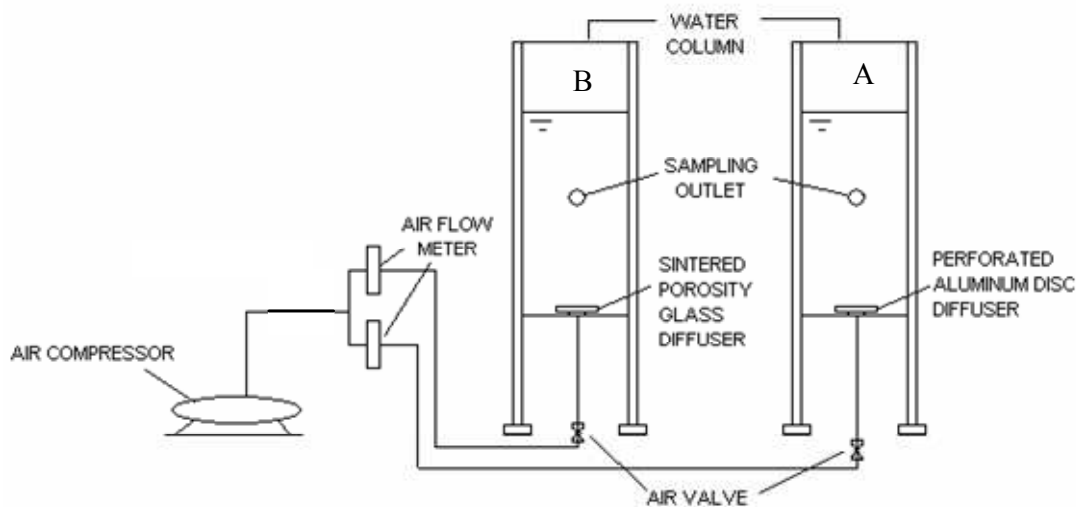


Figure 3.7 Schematic diagram of experimental set-up for Biodegradation and Nitrification.

Biomass for the degradation of organic matter was taken from a municipal activated sludge plant and placed in both reactors. The biomass was acclimatized for 2 weeks prior to experimentation. The 5 liters of raw wastewater sample was treated in both reactors. Aeration was then provided through the perforated aluminium disc diffuser and the micro sintered glass bubble diffuser in reactors A and B, respectively.



Aeration was continuously provided throughout the study. Sampling was taken at regular intervals of time; 1, 3, 6, 24 hours until 48 hours and then every 3 hours after. The samples were settled, filtered, diluted (1:20) and tested for COD, sCOD degradation rate, ammonia-nitrogen ( $\text{NH}_4\text{-N}$ ) removal and nitrate-nitrogen ( $\text{NO}_3\text{-N}$ ) production.

### **3.3.1. The Micro Bubble Size Selection for Aeration.**

The wastewater aeration is one of the processes done before discharging the wastewater into the river. The purpose of aeration is to supply oxygen to the microorganism in the wastewater. Generally the aeration process use millimeter air bubbles, whereas the micro bubbles aeration increase the DO level significantly due to increased interface area between air and water. The millimeter bubbles have faster upward motion, whereas the micro bubbles have slow upward motion and give sufficient time for transferring oxygen. Figure 3.8 shows the existing and new proposed aeration process. The micro bubbles aeration is an effective and efficient process, due to high DO level increment, short time of aeration and savings in energy, whereas the millimeter bubble aeration needs additional process to separate the suspended particles that remain in it. The proper selection of porous sintered glass should be started according to suitable micro bubble size. This micro bubble size is determined by the existing suspended particles. In case of varied range of suspended particles size contaminant water, this aeration need to be redone several times to reach the require turbidity level.

Figure 3.9 shows micro bubble size selection for aeration process. The bubble characteristics are determined by the type and concentration of pollutant. The pollutant influences the water physicochemical characteristic like viscosity, density and surface tension. These physicochemical characteristics are playing a role in generation, detachment and motion of micro bubbles. Since the availability of sintered glass in the bubble production is limited, therefore the selection is taken in three ranges (1-10, 10-16 and 16-40 micron porosity). In this research the bubble size is categorized in three range; fine, medium and large bubble to select the 1-10, 10-16

and 16-40 micron of porosity sintered glass. The different particle size and concentration of pollutant, the different bubble size and different porosity of sintered glass is needed. This micro bubble aeration process results with the particle disposal (solid waste) and clearer water (liquid outcome).

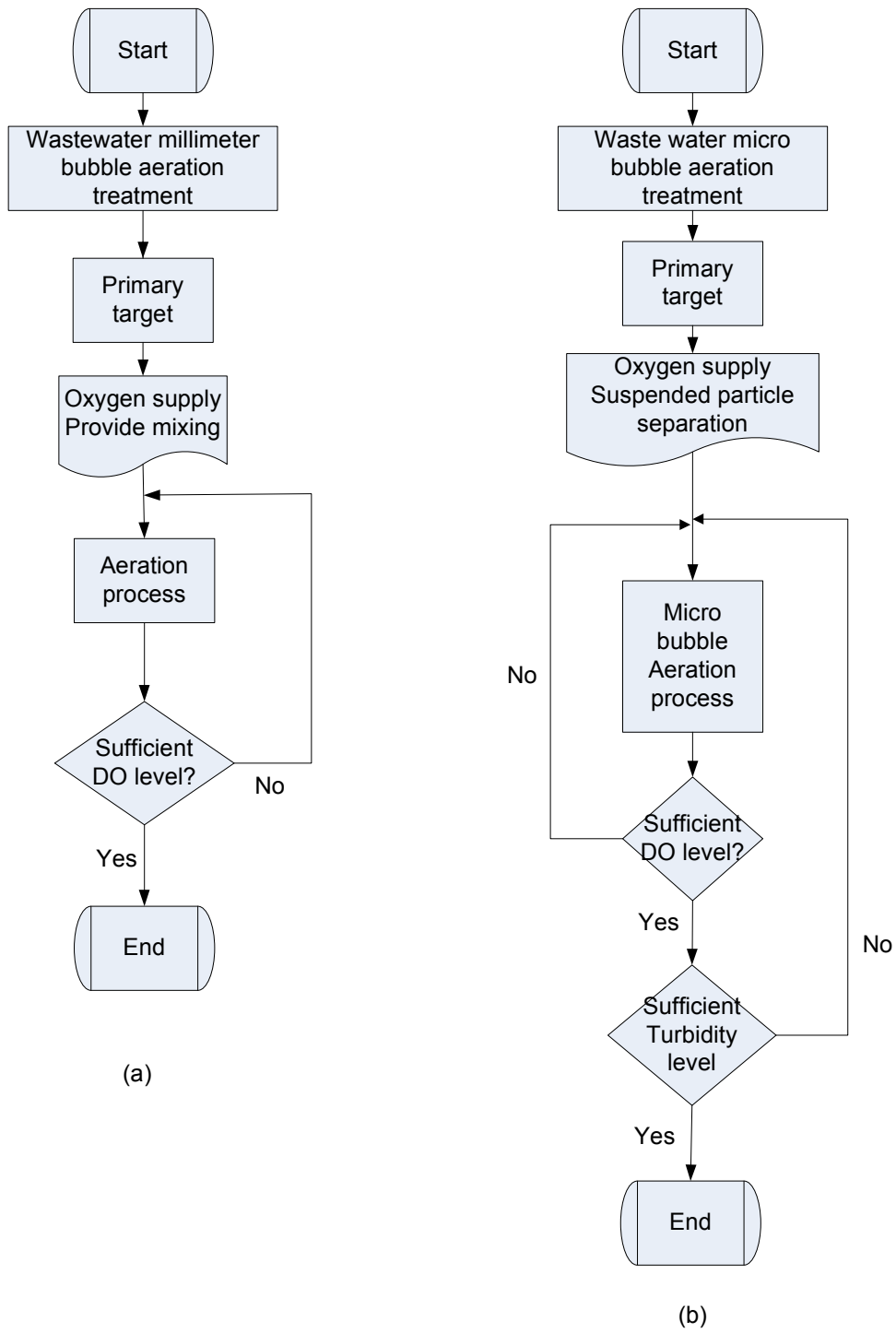


Figure 3.8 a. The existing aeration process, b. The proposed aeration process.

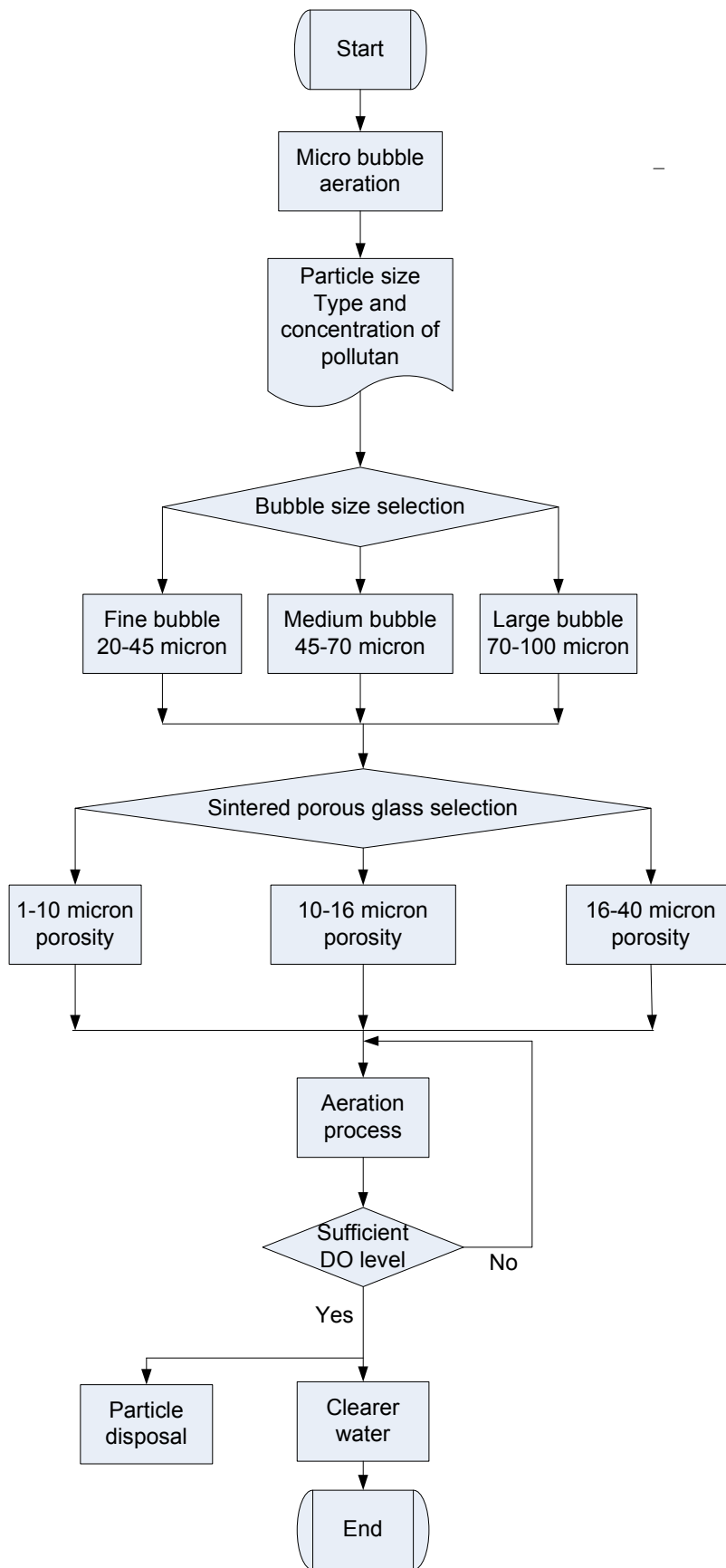


Figure 3.9 Micro bubble aeration procedure.

### **3.3.2. Measuring Apparatus**

The experiments were carried out by using the measuring devices to investigate the results. The measuring devices used were i.e: PDA, high speed camera, Turbidimeter, DO meter, Surface tension meter, density meter and viscometer. The working procedure, the use in this experiment and the specification are discussed in detail below.

#### **3.3.2.1. *The Particle Doppler Anemometry***

The bubbles movement was investigated by using the PDA. The main principal of PDA is to measure the movement of the bubbles in the water column using the laser beam. Four laser beams having a diameter of 1 mm, are shot from a laser source. Two laser beams were horizontal (blue, at the right and left position), and other two beams were vertical (green, at the top and the bottom). The light made a cross junction at a certain point. The refraction of light (when light met bubbles) was accepted by a receiver and detected as a burst shown on a monitor. Each burst was detected and noted as a data sample. The number of samples is 1 up to 2000 and the sampling duration is 30 seconds. The source voltage is 1000 volts and the anode current for the receiver is 10 mA. The data presented contain of; Bubble diameter (should less than 1 mm), and bubbles velocities (vertical and horizontal). The vertical movement is only in one direction (upward), whereas the horizontal movement is in multiple direction due to the bubbles have freedom movement in horizontal plain. Figure 3.10 shows the monitor screen of PDA.

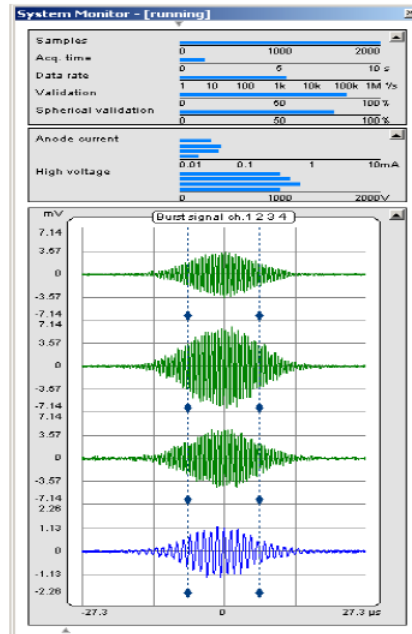


Figure 3.10 Monitor screen showing the burst when the laser meets bubble [86].

Focusing of the four laser beams, the alignment should be done before the measuring process. The alignment is done by placing a pin hole adjuster at the focusing point where these four beams would pass through it. Unless the beams are assured to be aligned in a high precision, the measurement can be taken. Figure 3.11 shows the beams focusing. The obstruction in between the traveling of the beam will result in a fluctuation in the measurement values, due to the beams are measured by a back scatter mode. The back scatter is a mode of data gathering. When the bubble hits the focusing point it will reflect a wave traveling back in the same path where it traveled come from. This wave will be interrupted any time as an obstruction.

The lens focal length was 500 mm and the measured half angle between the laser beams was  $2.2^\circ$  which produced a measuring volume with a diameter of  $63 \mu\text{m}$  and a length of 1.64 mm in air. The data measurement is taken at 5 cm from the base and 2.5 cm from the center of water column.

The error and uncertainties are produced from the bias laser beam, where the reflections beam at zero velocity of air flow in the water interference to the refraction. The total Doppler variance  $\sigma_D^2$  equals the sum of the velocity variance and broadening effects, assuming total independence and randomness of its constitutive term is given by:

$$\sigma_D^2 = \sigma_{velocity}^2 + \sigma_{broadening}^2 \dots\dots\dots(3.1)$$

$$\sigma_{broadening}^2 = \sigma_F^2 + \sigma_T^2 + \sigma_g^2 + \sigma_{Ib}^2 + \sigma_{Laser}^2 + \sigma_{others}^2 \dots\dots\dots(3.2)$$

Where the subscripts F, T, g and Ib stand for finite transit time, turbulence, mean velocity gradient and instrument broadening. The finite transit time broadening occurs when more than one bubble is within the measuring volume, but is limited in frequency counting system to the resolution of the counter. It provides that only one particle is within the scattering volume at any one time. A guarantee given by its validation circuitry, hence it is zero and the counter resolution ambiguity comes under  $\sigma_{Ib}^2$ . The turbulence variance doesn't occur due to the laminar flow of air bubble is applied, proved by the result that the Reynolds number of bubbles is maximally 70. The mean velocity gradients lead to a broadening of the probability density function across the measuring volume and to a mean velocity bias which. Instrument broadening is produced by the different electronic components. For time domain signal processing systems, the broadening due to transit time effects is zero. It provides the validation circuit prevent information influenced by the presence of more than one bubble in the scattering volume to be measured. The inherent noise becomes the main source of error consequently due to  $\pm 1$  clock pulse error of the counter.

$$\frac{\Delta v_D}{v_D} = \frac{v_D}{Nf_{clock}} \dots\dots\dots(3.3)$$

Where N is the number of cycles counted by the processor and  $f_{clock}$  is the clock frequency which for the present case is 250 MHz. The measured maximum Doppler frequency never exceeded 16 MHz and, with the frequency validation performed by comparing 10 to 16 cycles of the same burst, the accuracy of the counter is within 0.4%. The resolution of the floating point format of the data is another source of uncertainty which less than 0.1 % of the total Doppler frequency. The coprocessor used in the statistical calculations (BSA software) has an uncertainty limited by the use of 6 significant digits which is negligible. Counter and computer errors are relative to the total Doppler frequency and the may be important when the frequency shift is high relative to the velocities being measured. For the present air bubble flow measurements, the frequency shift represented at least half of the total frequency but never exceeded three quarters (for low Reynolds number bubble flows) so that, the

values given above in this paragraph have to be multiplied at most by four if they are to represent uncertainties of the velocities. Therefore, the maximum uncertainties of the velocities introduced by the counter and data format are 1.6 and 0.4% respectively at low Reynolds number bubble flows.

Finally, under the broadening due to other effects ( $\sigma_{others}^2$ ), is included a diffraction of beams according to the manufacturers of water column glass. For flows which are strongly unidirectional such as bubbles rise-up flow, the accuracy in positioning the laser beams in a plane parallel to the flow can affect the measurement of transverse components. In this case, the perpendicularity between water column axis and laser beams plane was within  $0.3^\circ$ , hence contributing to the uncertainty of the vertical velocity component with 0.5% of the axial component.

Positional error is introduced by the method used to locate the control volume inside the water column. This relies on visual observation of the beam crossing at the internal wall and leads to an uncertainty of about half the measuring volume length, i.e, 200  $\mu\text{m}$ .

From the description of uncertainties and with the formulas above, the uncertainties in mean of the fluctuating velocities and positioning the measuring volume are listed in table 3.1 follow. The corrections for velocity gradient effects were applied to the mean velocity data. The velocity gradient correction relative to the measured value was for the mean velocities less than + 1% in regions of high shear rate.

Table 3.1. Maximum uncertainties in mean velocity.

Source of uncertainty	Systematic	Random
Averaging and amplitude effect	2%	0
statistical	-	1% (sample size<50)
Perpendicularity of beams	-	0.5 % U
Velocity gradient	+ 1% (correction)	-

In conclusion, the maximum overall relative uncertainty of axial mean velocity is estimated to have a random of less than 1.5%. In the bubble flow the uncertainties are



even lower because of the laminar flow. The maximum uncertainty in the position of control volume is 200 μm for the transverse directions.

The Overall mean data sample is formulated as follow:

$$\bar{X} = \frac{\bar{x}_1 + \bar{x}_2 + \bar{x}_3 + \dots + \bar{x}_n}{n} \dots\dots\dots(3.4)$$

The range average is the average of maximum and minimum deference data captured:

$$\bar{R} = \frac{R_1 + R_2 + R_3 + \dots + R_n}{n} \dots\dots\dots(3.5)$$

The population standard deviation is noted below:

$$\sigma = d\bar{R}, \dots\dots\dots(3.6)$$

Where  $d$  is depend on sample size,  $d=1$  when the sample size is less than 50 in this research sample data size is 20.

The uncertainty of data sample is calculated as follow:

$$U = \frac{3\sigma / \sqrt{n}}{\bar{X}} \cdot 100\% \dots\dots\dots(3.7)$$

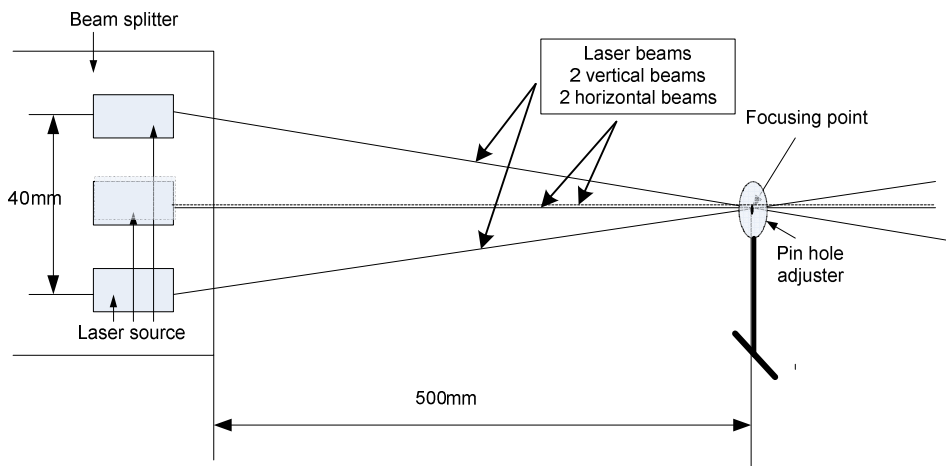


Figure 3.11 Beams focusing point [84].

Since the working principle of laser beam is refraction, scattering and polarization, the Dantec Dynamics A/S 2002 has a specification as follows. The input relative refraction index is valid in the range between 0.6° to 2° and the scattering angle between 2° to 180°. The confidence of linearity of output in parallel polarization is 98%. The dominant scattering order is first order refraction. Figure 3.12 shows the

confidence vs scattering angle. It indicates the confidence of linearity for a particular particle type. In that Figure the best scattering angle is 68°.

The calibration method of the Dantec Dynamics A/S 2002 is followed. The probe fringe spacing ( $d_{cal}$ ) is calibrated against a flywheel which known as a peripheral velocity ( $U_{ref}$ ). The flywheel velocity is calculated from number of revolutions and wheel radius ( $r$ ). The nominal velocity conversion factor  $k_{nom} = d_{nom}$  is calculated from nominal fringe spacing as formulated

$$d_{nom} = W / (2 \sin(\arctan(S_{nom} / 2L))) \text{ mm} \dots\dots\dots(3.8)$$

Where:  $W$  = laser wavelength in nm

$L$  = focal length in mm of front lens

$S_{nom}$  = nominal beam spacing in mm.

The calibrated velocity conversion factor  $k_{cal}$  is calculated as flywheel velocity  $U_{ref}$  divided by frequency  $f_{BSA}$  measured using BSA software. The calibration is performed in a number of sectors across the measuring volume at one flywheel velocity. The average of the velocity conversion factors is weighted with respect to expected sensitivity distribution  $W_z$  across the measuring volume.  $W_z$  is defined by the number of samples  $N$  in each sector. A sector is only included, when  $N_{sector} > 10\%$  of  $N_{max}$ .

[86]

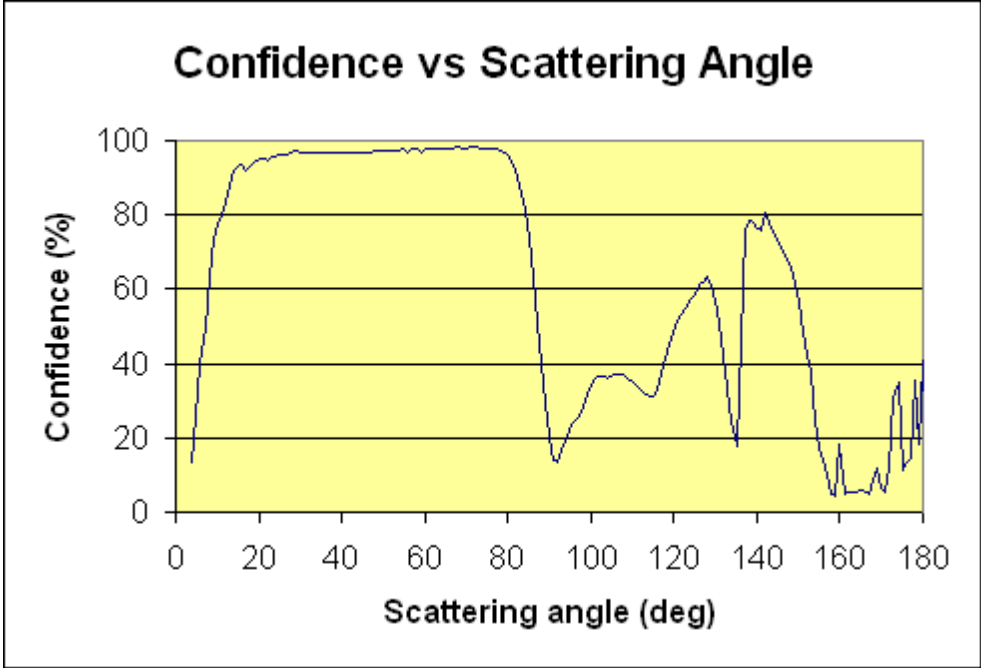


Figure 3.12 The confidence vs scattering angle of the Dantec Dynamics A/S 2002

[86].

### **3.3.2.2 *The High Speed Camera***

The Fastcam-x1280pci high speed camera was used in this research for capturing the bubble upward motion. The slow motion bubble can be captured, the bubble upward velocity and the size can be measured. This camera has framing rate in two modes i.e: full frame and partial frame. In full frame, the capturing figure rate is provided in four rates; 60, 125, 250, 500 FPS, whereas in the partial frame the rate is available in five rates; 100, 2000, 4000, 8000, 16000 FPS [87]. In this research has been chosen the partial framing in 2000 rate. This reason of the choosing is partial captured can be focused in a small area with adequate framing rate. The bubble velocity and size can be calculated from the slow motion by putting a length scale inside the captured area. The resolution (pixels) in image framing rate are available in many choices. In this research has been chosen the 640x256 resolution with 2000 framing rate.

### **3.3.2.3 *Dissolved Oxygen Meter***

The EW-35641-00 DO meter is used to measure the DO level in the water. The readings are displayed in mg/l, ppm or % saturation simultaneously with temperature value, Calibration can be done independently 100% and 0% calibration point to achieve high accuracy over the entire range. Set the DO number using the real sample with known DO level (100%) and set the DO level at zero for a relative measurement (0%). Increase reading accuracy by entering barometric pressure and salinity, the meter automatically calculate offset. Setup function displays electrode slope, zero offset and mill volt. The real time clock stamps stored reading and calibration data with date and time[88].

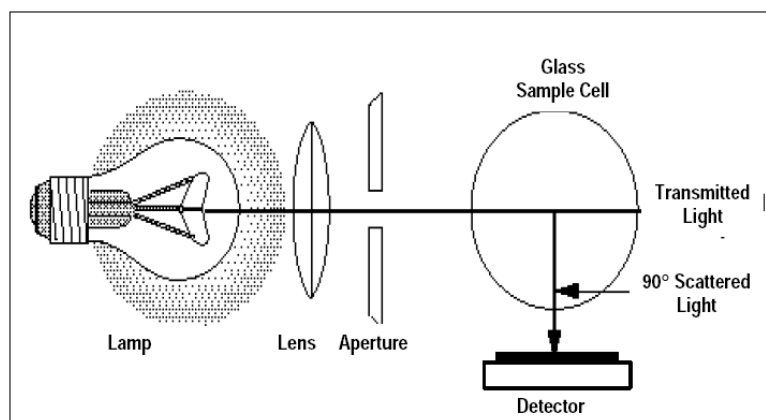
### **3.3.2.4 *Turbidimeter***

The Hach portable turbidimeter model 2100P is used to measure the water turbidity. The 2100P combines microprocessor-controlled operation and Hach's patented Ratio optics to bring greater accuracy, sensitivity, and reliability to field testing. Its two-detector optical system compensates for color in the sample, light fluctuation, and

stray light, enabling analysts to achieve laboratory-grade performance on a wide range of samples. The direct digital readout in nephelometric turbidity units, the need for calculations or interpolation of calibration charts is completely eliminated. The measurement method is Ratio Nephelometric signal (90°) scatter light ratio to transmitted light. The 2100P Portable turbidimeter is calibrated with Formazin Primary Standard at the factory and does not require recalibration before use. Hach recommends recalibration with formazin once every three month, or more often as experience dictates. Measurements may be made with the signal average mode on or off and in manual or automatic range selection mode. Using automatic range selection is recommended. Signal averaging uses more power and should be used only when the sample causes an unstable reading. Signal averaging measures and averages ten measurements while displaying intermediate results. The initial value is displayed after about 11 seconds and the display is updated every 1.2 seconds until all ten measurements are taken (about 20 seconds). After this, the lamp turns off, but the final measured turbidity value continues to be displayed until another key is pressed. When it does not in signal average mode, the final value is displayed after about 13 seconds. Accurate turbidity measurement depends on good measurement technique, such as using clean sample cells on good condition and removing air bubbles (degassing).

The sample water data is pour into clean sample cells before inserting into the instrument cell compartment. The cell needs to be wiped to remove water spots and fingerprints. The measurement can be started immediately after the lid to be closed to prevent temperature changes and settling. The instrument should place on a flat and steady surface during measurement. The optical system includes a tungsten-filament lamp, a 90° detector to monitor scattered light and a transmitted light detector. The instrument's microprocessor calculates the ratio of the signals from the 90° and transmitted light detectors. This ratio technique corrects for interferences from color and/or light absorbing material (such as activated carbon) and compensates for fluctuations in lamp intensity, providing long- term calibration stability. The optical design also minimizes stray light, increasing measurement accuracy. Along micro bubble aeration is running in 0.25% volume of CMC in distilled water, data sample is taken every 15 minutes from the water column and measured the turbidity. The data collection from three types of porosity of sintered glass are continued until 5 ours with

constant air pressure and flow. This experiment is repeated 10 times before the average of turbidity data is calculated [89]. Figure 3.13 shows the 2100P portable Turbidimeter working principles.



Source: Sadar, 1996; photo revised by SAIC, 1998.

Figure 3.13 The Hach 2100P portable Turbidimeter work principles[89].

### 3.3.2.5 Surface Tension Meter

The IFT 700 is designed to determine interfacial tension and contact angle. Basically a pendant drop or standing bubble/drop (drop fluid) may be generated in a second immiscible fluid (pressure Fluid). The drop shape image is computed, and then the interfacial tension is computed from solving algorithm of the Laplace transform equation. The bulk fluid refers to the fluid where the droplet is released, for example; water droplet release in the atmosphere, hence air is the bulk fluid, whereas the drop fluid refers to nature of the fluid of the droplet, for example; water droplet release in the atmosphere, therefore water is the drop fluid.

The calculation of surface tension starts from the angle and size of the droplet that has been captured. Assume a droplet shape is spherical, pressure inside the droplet ( $P_{int}$ ) and pressure outside ( $P_{ext}$ ), when equilibrium state is reached, the energy required to increase or decrease the droplet volume is positive. In the other words, this state matches to the minimum energy level. To increase the droplet volume ( $-P \cdot \delta v \dots$ ), energy required as follow:

$$\delta W_{volume} = -(P_{int} - P_{ext}) \delta V \dots \dots \dots (3.9)$$

The increasing the energy of surface area induces:

$$\delta W_{area} = \gamma \delta A \dots\dots\dots(3.10)$$

The  $\gamma$  is the interfacial tension. To modify the radius of a spherical droplet, the infinitesimal energy variation is:

$$\delta W = -(P_{int} - P_{ext})\delta\left(\frac{4\pi R^3}{3}\right) + \gamma\delta(4\pi R^2) \dots\dots\dots(3.11)$$

$$\frac{\delta W}{\delta R} = -(P_{int} - P_{ext})4\pi R^2 + \gamma.8\pi R \dots\dots\dots(3.12)$$

The optimum value when  $\frac{\delta W}{\delta R} = 0$

$$\text{Or } (P_{int} - P_{ext}) = \frac{2\gamma}{R} \dots\dots\dots(3.13)$$

The internal pressure is higher than the external pressure, more exactly the pressure on convex side is bigger than the concave one. Therefore, the argument does not depend on the phase nature of the droplet (liquid droplet inside a gas or gas inside the liquid). This relation can be extended to the shape of a real droplet. Curve radius  $R_i$  at each point of the surface area can be defined. Let S is a surface (separation fluid A/fluid B), which the curves  $dl_1$  and  $dl_2$  with radius  $R_1$  and  $R_2$  (Figure 3.14). The force  $f$  counterbalances the vertical resultant force from interfacial tension can be defined:

$$\Delta P.S = \Delta P.dl_1.dl_2 \dots\dots\dots(3.14)$$

$$f_i = \sigma.dl_i \dots\dots\dots(3.15)$$

$$\Delta P = 2\sigma\left(\frac{\cos \alpha_1}{dl_1} + \frac{\cos \alpha_2}{dl_2}\right) \dots\dots\dots(3.16)$$

$$(P_{int} - P_{ext}) = \gamma\left(\frac{1}{R_1} + \frac{1}{R_2}\right) \dots\dots\dots(3.17)$$

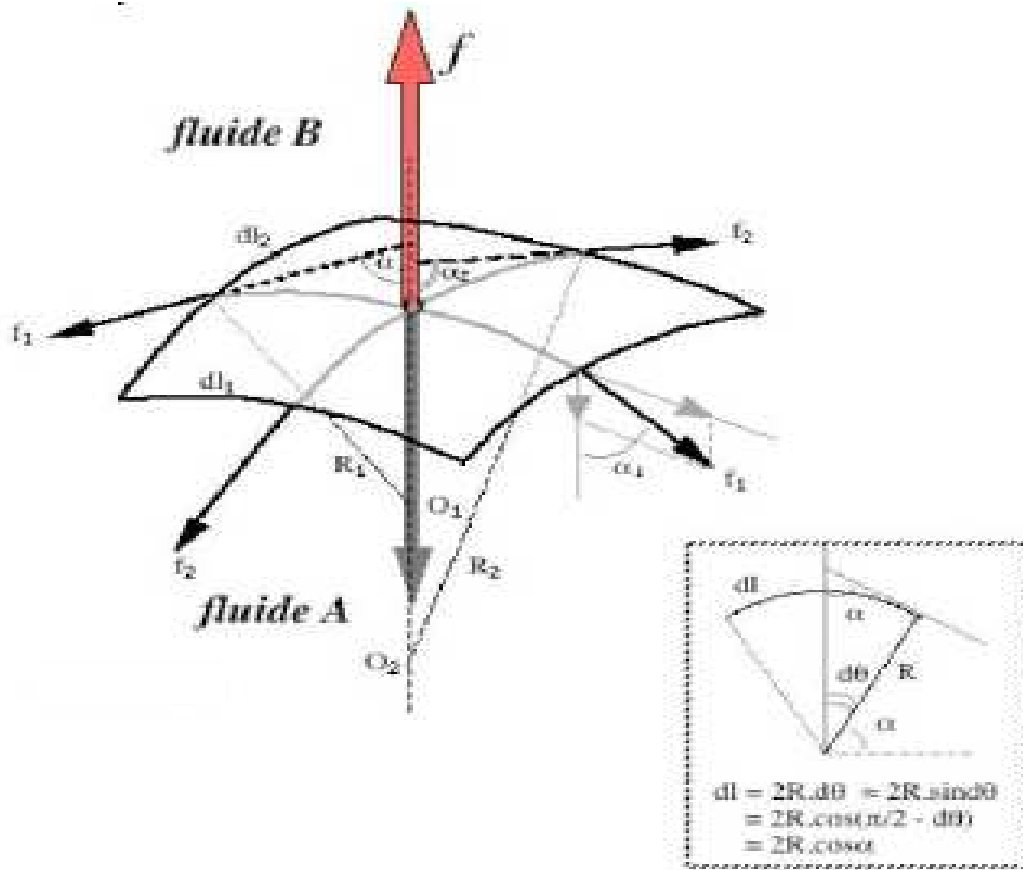


Figure 3.14 The convex layer between air bubble and water.

Moreover, taking into account the fundamental equation of the equilibrium of the forces at a point of the drop, ( $\Delta P \cdot S = mg$ ), interfacial tension can be computed after some mathematical Taylor's development and differential formulations. The IFT 700 software enables to determine the interfacial tension from the Laplace-Young equation based on the shape of the droplet [90]. The surface tension measurement is based on the drop image captured. After the angle of interface is measured, the surface tension force can be calculated.

### 3.3.2.6 Density Meter

The DMA 35 N portable density meter measures the density of liquids. Two types of unit are available in  $\text{g/cm}^3$  or  $\text{kg/m}^3$ . The sample is filled into the measuring cell using the built-in pipette-style pump or a syringe. The temperature is displayed after the

temperature sensor measures the sample temperature, this temperature can be used internally for automatic temperature compensation of the density reading. The temperature coefficient can be calculated according to the formula [91]:

$$\text{Temperature coefficient} = \left| \frac{\rho_1 - \rho_2}{t_1 - t_2} \right| \dots\dots\dots(3.18)$$

Using the DMA 35 N portable, the density of glycerin solution in the distilled water is measured, and found the density of 0.4% volume glycerin is similar with the UTP resident wastewater. Before performing any measurements, prepare suitable cleaning agent or solvents to clean the PTFE (pump piston, filling tube) and borosilicate glass (measuring cell, pump cylinder). The resistant of all material contact (PTFE and Borosilicate glass) should be eliminated. The resistant could be air bubbles or other particles that stick on the material contact, therefore every measurement should be continued with cleaning the measuring cell to avoid deposit of coating.

**3.3.2.7 Viscometer**

The Fann Model 35 viscometer is used to measure the glycerin solution in volume fraction 0.1%, 0.2%, 0.3%, 0.4% and 0.5% in this research. This model is direct reading instrument which available in six speeds and 12 speeds designs for use on either 50 Hz or 60 Hz and 115 volts electric power. These are true couette coaxial cylinder rotational viscometer since the test fluid is contained in the annular space (shear gap) between an outer cylinder and the bob. Viscosity measurements are made when the outer cylinder, rotating at a known velocity, causes a viscous drag to be exerted by the fluid. This drag creates a torque on the bob, which is transmitted to a precision spring where its deflection is measured and then compared with the test conditions and the instruments' constants. Viscosity is a measure of the shear stress caused by a given shear rate. The relationship between shear stress and the shear rate is a linear function for Newtonian fluids. Therefore the model 35 is recommended calibration for Newtonian fluid. The measurement is indicated on the dial with the standard rotor, bob, and torsion spring operating at 300 rpm and in centipoises unit.



The calibration is checked by applying known torques to the bob shaft. For any applied torque, within the torque range of the spring, there should be a specific dial reading plus or minus a small tolerance. The two methods of calibration are recommended, that are dead weight calibration and fluid calibration check. The dead weight calibration is easier to perform and if the spring requires adjustment, the proper setting can easily be verified. The standard fluid calibration check verifies the complete instrument is operating properly. It will determine problems of bent bob shaft, rotor eccentricity, and/or run out of the rotor or bob more effectively than the dead weight method. The standard fluid calibration procedure should be used for calibration using only Newtonian certified calibration fluids [92].

### **3.3.2.8** *The Pollutant*

Carboxy Methyl Cellulose (CMC) is used as a suspended particle pollutant in distilled water. The microscopic image of CMC particle is shown in Figure 3.15. The carbon molecules are white color while the dark color is the cellulose. The carbon particles produce turbidity in the water. Using air bubble aeration through submerged diffuser, the carbon particles are lifted to the top of water column, where they can be separated from water body. Hence the turbidity level would decrease.

The 0.25 % of a food grade moisture retention agent Carboxy Methyl Cellulose HP-8A is added in distilled water to imitate suspended particle pollutant as in the real wastewater. This CMC grade HP-8A increase water viscosity up to 25 cps in 2% solution [93], therefore the 0.25 % CMC polluted water does not increase its viscosity. Hence the suspended particle pollutant in the distilled water can be represented.

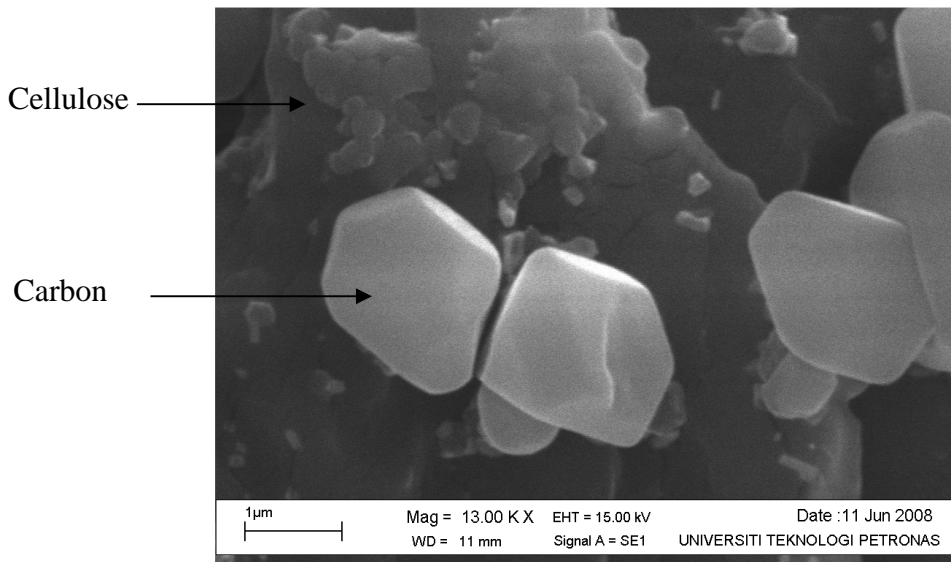


Figure 3.15 The Microscope of CMC, The particle size is 1 to 20 micron, monitored by Scanning electron microscope (SEM).

The behaviour of aeration through micro bubbles could not be understood properly unless, the physiochemical characteristics of water are close to the real wastewater. Moreover, due to the limitations of this research, the PDA can only read the motion of micro bubbles, if the solution is transparent, therefore, Glycerin impurities are used as a colloid solution to study the bubble characteristic in the water. By adding glycerin in volume fraction of 0.1%, 0.2%, 0.3%, 0.4% and 0.5% in distilled water, the physiochemical characteristic of wastewater can be imitated. The physiochemical characteristics of 0.4 % volume glycerin in the distilled water is close to UTP resident wastewater, therefore the volume fraction of 0.4% glycerin is used for further experiment.

### 3.4 The Forces Acting During Bubble Generation and Detachment

There are two situations when the bubble is extremely influenced by various forces and they are at the time of;

1. Bubble generation,
2. Bubble detachment.

Both conditions have their own force balance and different force compositions. The forces are influenced by gas momentum force, surface tension, viscosity of liquid, and air-water density differences, when a bubble is generated. Meanwhile, after detachment from the diffuser, two forces act on the bubble, which are buoyancy and viscous drag. These two forces are dependent on the liquid viscosity and air-water density differences, whereas, inviscid inertia force and bubble interaction forces are neglected.

The bubble diameter and velocity are the main factors for controlling the movement of the bubbles. Painmanakul et al. [37] found that hydrodynamic parameters (bubble size, bubble rising velocity, bubble formation frequency) are important parameters for controlling the floatation process in oily wastewater. Buoyancy and gas momentum force are in the upward direction, the others are downward. Any inclined diffuser hole position would affect the bubble magnification. The detailed forces acting before detachment are listed in Table 3.2.

Some porous diffusers have a rough surface, therefore a small part of the surface would be flat and the rest of the surface would be inclined as shown in Figure 3.16. This condition will influence the surface energy, due to a decrease in bubble pull-out force ( $F_M$  and  $F_B$ ). These acting forces will change slightly when the position of the diffuser hole is not in the plain, eventually increasing the size of the bubble (Figure 3.16. b and c).

Table 3.2 Summary of equations showing various forces exerted on a bubble at the time of generation and detachment.

Symbol	Description	Eq. when pore is in a vertical Position (Figure 1.a.) $\theta = 90^\circ$	Eq when pore is in horizontal position (Figure 1.c.) $\theta = 0^\circ$	Eq when pore is at $\theta^\circ$ inclination (Figure 1.b.) $0^\circ < \theta < 90^\circ$	Eq when the bubble detach from the diffuser
$F_B$	buoyancy force	$F_B = \frac{\pi}{6} d_b^3 (\rho_l - \rho_g) g$	$F_B = \frac{\pi}{6} d_b^3 (\rho_l - \rho_g) g$	$F_B = \frac{\pi}{6} d_b^3 (\rho_l - \rho_g) g \sin \theta$	$F_B = \frac{\pi}{6} d_b^3 (\rho_l - \rho_g) g$
$F_M$	gas momentum force	$F_M = \frac{\pi}{4} D_o^2 \rho_g u_g^2$	$F_M = \frac{\pi}{4} D_o^2 \rho_g u_g^2$	$F_M = \frac{\pi}{4} D_o^2 \rho_g u_g^2 \sin \theta$	$F_M = \frac{\pi}{4} D_o^2 \rho_g u_g^2$
$F_D$	Liquid drag force	$F_D = C_D^* (\frac{\pi}{4} d_b^2) \frac{\rho_l u_b^2}{2}$	$F_D = C_D (\frac{\pi}{4} d_b^2) \frac{\rho_l u_b^2}{2}$	$F_D = C_D (\frac{\pi}{4} d_b^2) \frac{\rho_l u_b^2}{2} \cos \theta$	$F_D = C_D (\frac{\pi}{4} d_b^2) \frac{\rho_l u_b^2}{2}$
$F_\sigma$	Surface tension force	$F_\sigma = \pi D_o \sigma \cos \gamma$	$F_\sigma = \pi D_o \sigma \cos \gamma$	$F_\sigma = \pi D_o \sigma \cos \gamma \cos \theta$	$F_\sigma = \pi D_o \sigma \cos \gamma$
$F_{BA}$	Basset force	$F_{BA} = 0$	$F_{BA} = 0$	$F_{BA} = 0$	$F_{BA} = \frac{3}{2} d_b^2 \sqrt{\pi \rho_l \mu_l} \int_0^\tau \frac{du/d\tau}{\sqrt{1-\tau}} d\tau$
$F_{l,g}$	bubble inertial force	$F_{l,g} = \frac{d}{dt} [\rho_g (\frac{\pi}{6} d_b^3) u_b]$	$F_{l,g} = \frac{d}{dt} [\rho_g (\frac{\pi}{6} d_b^3) u_b]$	$F_{l,g} = \frac{d}{dt} [\rho_g (\frac{\pi}{6} d_b^3) u_b]$	$F_{l,g} = \frac{d}{dt} [\rho_g (\frac{\pi}{6} d_b^3) u_b]$
$F_C$	particle-bubble collision force	$F_C = \frac{\pi}{4} D_o^2 (1+e) \varepsilon_s \rho_s u_e^2$	$F_C = \frac{\pi}{4} D_o^2 (1+e) \varepsilon_s \rho_s u_e^2$	$F_C = \frac{\pi}{4} D_o^2 (1+e) \varepsilon_s \rho_s u_e^2$	$F_C = \frac{\pi}{4} d_b^2 \varepsilon_s \rho_s u^2$
$F_{l,m}$	liquid-solid suspension inertial force	$F_{l,m} = \frac{d(\iiint \rho_m u_m \delta V)}{dt}$ $= \zeta \frac{d}{dt} [\rho_m (\frac{\pi}{6} d_b^3) u_b]$	$F_{l,m} = \frac{d(\iiint \rho_m u_m \delta V)}{dt}$ $= \zeta \frac{d}{dt} [\rho_m (\frac{\pi}{6} d_b^3) u_b]$	$F_{l,m} = \frac{d(\iiint \rho_m u_m \delta V)}{dt}$ $= \zeta \frac{d}{dt} [\rho_m (\frac{\pi}{6} d_b^3) u_b]$	$F_{l,m} = \frac{d(\iiint \rho_m u_m \delta V)}{dt}$ $= \zeta \frac{d}{dt} [\rho_m (\frac{\pi}{6} d_b^3) u_b]$

$$* C_D = \frac{24}{\text{Re}}$$

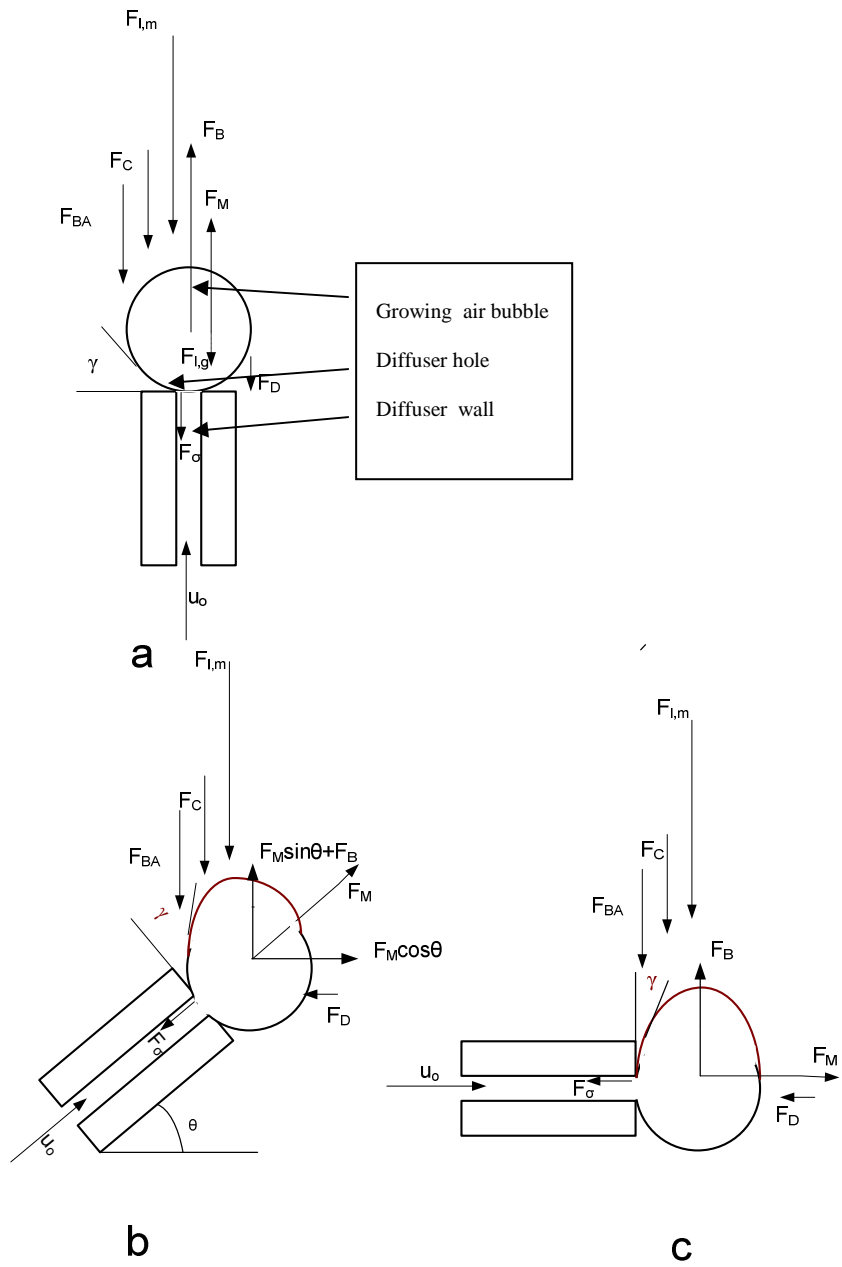


Figure 3.16 The balance of forces acting on a growing bubble, for various inclination angles of the diffuser pores.

a. Vertical diffuser pore: The forces acting on the bubble at the time of generation in a vertical position pore diffuser can be formulated as below:

$$\sum F_{vertical} = F_M + F_B - F_C - F_D \dots\dots\dots(3.19)$$

Where  $F_M$  is momentum force and  $F_B$  is buoyancy force.

The momentum force of air inlet ( $F_M$ ) would help to generate the bubble, and is dependent on cross sectional area of diffuser hole, density of air and velocity of air entering the diffuser. The relationship is:

$$F_M = \frac{\pi}{4} D_o^2 \rho_g u_o^2 \dots\dots\dots (3.20)$$

The buoyancy force is dependent on volume of bubble, density differences between water and air and gravitation acceleration. Its can be formulated as:

$$F_B = \frac{\pi}{6} d_b^3 (\rho_l - \rho_g) g \dots\dots\dots (3.21)$$

At the time of detachment, the force acting on the bubble would be:

$$\sum F_{detachment} = F_B + F_M - (F_D + F_\sigma + F_{BA} + F_{l,g} + F_C + F_{l,m}) \dots\dots\dots (3.22)$$

b. Incline diffuser pore ( $\theta^\circ$ ): The forces acting on the bubble at the time of generation can be described into two directions (vertical and horizontal): The horizontal force acting as an enlarge bubble size force.

$$\sum F_{vertical} = F_M \sin \theta + F_B \dots\dots\dots (3.23)$$

$$\sum F_{horizontal} = F_M \cos \theta \dots\dots\dots (3.24)$$

The effective bubble generation forces are:

$$F_{pull-out} = F_M \sin \theta + F_B - F_\sigma - F_D \dots\dots\dots (3.25)$$

At the time of detachment, the force acting on the bubble would be:

$$\sum F_{detachment} = F_B + F_M \sin \theta - (F_D + F_\sigma + F_{BA} + F_{l,g} + F_C + F_{l,m}) \dots\dots\dots (3.26)$$

Incline diffuser pores always generate bigger bubbles due to smaller bubble pull-out force and detachment force ( equation (3.18) and (3.20)) and the enlarge bubble force (equation (3. 21)).

### 3.4.1 The Forces Acting on a Moving Bubble

The details of forces acting on bubbles are reported by Fan, Vazquez, and Yeoh [22, 94, 95]. They detailed all acting forces on a bubble. Ruzicka et al. [32] studied the forces at Reynolds number 50 to 200. Kulkarni [24] studied the bubble lift force by balancing the upward and downward forces acting on the bubble. The buoyancy force

depends on the density differences between water and air, while the drag force depends on CD (drag coefficient), length of chord (effective bubble diameter) and velocity. Fan [22] described the CD equal to 24/Re when the value of Re=1 and for value of Re in the range of 1 to 500 Rivikind and Ryskind suggested the following equation which is cited by Xu at el. [14]:

$$CD = \frac{1}{\kappa + 1} \left[ \kappa \left( \frac{24}{Re} + \frac{4}{Re^{1/3}} \right) + \frac{14.9}{Re^{0.78}} \right] \dots\dots\dots (3.27)$$

$$\text{Where, } \kappa = \frac{\mu_g}{\mu_l}$$

As K depends on air and water viscosity therefore, the CD equation becomes:

$$CD = \frac{0.484}{Re} + \frac{0.081}{Re^{1/3}} + \frac{14.6}{Re^{0.78}} \dots\dots\dots(3.28)$$

$$\text{Where Reynolds number is : } Re = \frac{\rho v D_b}{\mu_l} \dots\dots\dots(3.29)$$

Figure 3.17 shows the buoyancy and drag force on the free bubble and the vorticity inside the bubble due to the friction between air and water. The drag force on a bubble is formulated:

$$F_{DB} = CD \left( \frac{\pi}{4} d_B^2 \right) \frac{\rho_l v_B^2}{2} [12] \dots\dots\dots(3.30)$$

$$= \left( \frac{0.484\mu}{\rho_l v_B d_B} + \frac{0.081\mu^{1/3}}{(\rho_l v_B d_B)^{1/3}} + \frac{14.6\mu^{0.78}}{(\rho_l v_B d_B)^{0.78}} \right) \left( \frac{\pi}{4} d_B^2 \right) \frac{\rho_l v_B^2}{2}$$

$$= 0.06\mu\pi d_B v_B + 0.01\mu^{1/3}\pi d_B^{1/3} v_B^{2/3} + 1.9\mu^{0.78}\pi d_B^{1.22} v_B \dots\dots\dots (3.31)$$

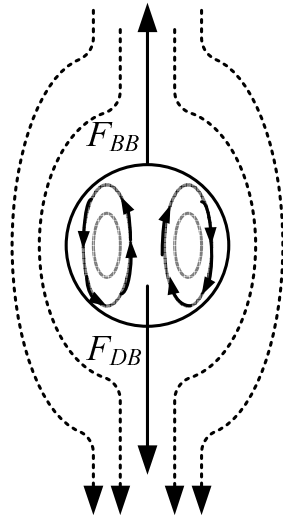


Figure 3.17 The free air bubble forces in water[23].

By assuming upward forces as positive and downward as negative, the balance on the free bubble is:

$$\sum F_B = F_{BB} - F_{DB}$$

$$= \frac{\pi}{6} d_B^3 (\rho_l - \rho_g) g - 0.06 \mu \pi d_B v_B - 0.01 \mu^{1/3} \pi d_B^{1\frac{2}{3}} v_B^2 - 1.9 \mu^{0.78} \pi d_B^{1.22} v_B \dots\dots\dots (3.32)$$

Where  $F_{BB}$  is bubble buoyancy force and  $F_{DB}$  is bubble drag force. After collision with any suspended particle the bubble-particle pair will move upward together, since suspended particle is floating in water.

### 3.4.2 The Forces Acting on a Bubble-particle Pair

The forces acting on the bubble and particle, when they are in contact, are shown in Figure 3.17 and upward movement of the suspended particle has been studied under the following 3 conditions:

1. When the particle diameter is similar with the bubble diameter.
2. When the particle diameter is smaller than the bubble diameter.
3. When the particle diameter is bigger than the bubble diameter.



The vortex inside the bubble due to air-water friction is shown in Figure 2.3 The vortex would help the smaller particle to remain attached to the bubble as long as they are in line of motion. Similar behavior is expected for larger particles; however, in case the line of motion is changed, then the bubble would be separated and would not force the particle upward. A next inline bubble would take the place and pushes the particle upward, unless, the particle reaches the top.

### 3.4.2.1 When Particle Diameter is Similar to Bubble Diameter

The passage of bubble-particle when they have similar diameter is shown in Figure 3.18. The upward force is buoyancy, whereas the downward force is drag. The drag is produced by the particle, while the buoyancy is produced by air bubble. The bubble and particle are assumed in a line moving upward. By assuming the surface area condition is similar, therefore the particle drag is similar with the bubble drag and formulated as:

$$F_{DP} = 0.06\mu\pi d_p v_p + 0.01\mu^{1/3}\pi d_p^{1/3} v_p + 1.9\mu^{0.78}\pi d_p^{1.22} v_p \dots\dots\dots (3.33)$$

The balance force is:

$$\sum F_{B1} = F_{BB} - F_{DP}$$

$$= \frac{\pi}{6} d_B^3 (\rho_l - \rho_g) g - 0.06\mu\pi d_p v_p - 0.01\mu^{1/3}\pi d_p^{1/3} v_p - 1.9\mu^{0.78}\pi d_p^{1.22} v_p \dots\dots (3.34)$$

$$\Delta F = \left[ \frac{\pi}{6} d_B^3 (\rho_l - \rho_g) g - 0.06\mu\pi d_B v_B - 0.01\mu^{1/3}\pi d_B^{1/3} v_B - 1.9\mu^{0.78}\pi d_B^{1.22} v_B \right] -$$

$$\left[ \frac{\pi}{6} d_p^3 (\rho_l - \rho_g) g - (0.06\mu\pi d_p v_C + 0.01\mu^{1/3}\pi d_p^{1/3} v_C + 1.9\mu^{0.78}\pi d_p^{1.22} v_C) \right]$$

$$= (0.06\mu\pi d_p + 0.01\mu^{1/3}\pi d_p^{1/3} + 1.9\mu^{0.78}\pi d_p^{1.22}) v_C - (0.06\mu\pi d_B + 0.01\mu^{1/3}\pi d_B^{1/3} + 1.9\mu^{0.78}\pi d_B^{1.22}) v_B$$

$$\dots\dots\dots (3.35)$$

The velocity ratio is:

$$\frac{v_{B(B)}}{v_{B(S)} + v_P} = \frac{v_{B(B)}}{v_C} = \frac{(0.06\mu_l .d_p + 0.01\mu_l^{1/3} d_p^{1/3} + 1.9\mu_l^{0.78} d_p^{1.22})}{(0.06\mu_l .d_b + 0.01\mu_l^{1/3} d_b^{1/3} + 1.9\mu_l^{0.78} d_b^{1.22})} \dots\dots\dots (3.36)$$

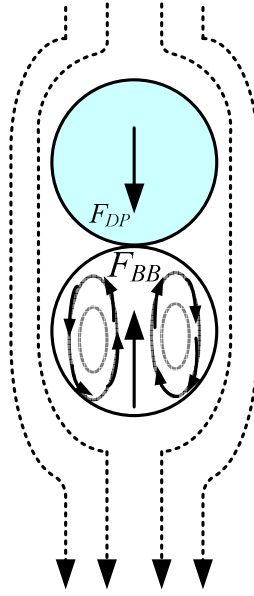


Figure 3.18. The bubble-particle pair, when their diameters are similar. Assuming the bubble and suspended particle are vertically in line.

### 3.4.2.2 When Particle Diameter is Smaller than Bubble Diameter

Figure 3.19 shows the bubble-particle pair when the bubble diameter is bigger than the particle diameter. The drag forces are produced by the movement of particle and bubble. The bubble drag force as described in equation (3.30) is :

$$F_{DB} = \left( \frac{0.484\mu}{\rho_l v_B d_B} + \frac{0.081\mu^{1/3}}{\rho_l v_B d_B^{1/3}} + \frac{14.6\mu^{0.78}}{\rho_l v_B d_B^{0.78}} \right) \frac{\pi}{4} d_B \left( d_B - 2d_p + \frac{d_p^2}{d_B} \right) \frac{\rho_l v_B^2}{2}$$

$$= (0.06\mu\pi v_B + 0.01\mu^{1/3}\pi v_B d_B^{2/3} + 1.9\mu^{0.78}\pi v_B d_B^{0.22}) \left( d_B - 2d_p + \frac{d_p^2}{d_B} \right) \dots\dots\dots(3.37)$$

The balance force is formulated:

$$\sum F_{B2} = F_{BB} - F_{DB} - F_{DP}$$

$$= \frac{\pi}{6} d_B^3 (\rho_l - \rho_g) g - (0.06\mu\pi v_B + 0.01\mu^{1/3}\pi v_B d_B^{2/3} + 1.9\mu^{0.78}\pi v_B d_B^{0.22}) \left( d_B - 2d_p + \frac{d_p^2}{d_B} \right) -$$

$$(0.06\mu\pi d_p v_p + 0.01\mu^{1/3}\pi d_p^{1/3} v_p + 1.9\mu^{0.78}\pi d_p^{1.22} v_p)$$

.....(3.38)

The force difference between the bubble-particle pair after and before is formulated:

$$\Delta F = \sum F_{before.merge} - \sum F_{after.merge}$$

$$\Delta F = \left[ \frac{\pi}{6} d_B^3 (\rho_l - \rho_g) g - 0.06 \mu \pi d_B v_B - 0.01 \mu^{1/3} \pi d_B^{1\frac{2}{3}} v_B - 1.9 \mu^{0.78} \pi d_B^{1.22} v_B \right] -$$

$$\left[ \frac{\pi}{6} d_B^3 (\rho_l - \rho_g) g - (0.06 \mu \pi v_B + 0.01 \mu^{1/3} \pi v_B d_B^{2/3} + 1.9 \mu^{0.78} v_B d_B^{0.22}) (d_B - 2d_p + \frac{d_p^2}{d_B}) - \right.$$

$$\left. (0.06 \mu \pi d_p v_C + 0.01 \mu^{1/3} \pi d_p^{1\frac{2}{3}} v_C + 1.9 \mu^{0.78} \pi d_p^{1.22} v_C) \right]$$

$$= \pi v_B (0.06 \mu + 0.01 \mu^{1/3} d_B^{2/3} + 1.9 \mu^{0.78} d_B^{0.22}) (\frac{d_p^2}{d_B} - 2d_p) +$$

$$\pi v_C (0.06 \mu d_p + 0.01 \mu^{1/3} d_p^{1\frac{2}{3}} + 1.9 \mu^{0.78} d_p^{1.22})$$

.....(3.39)

Assuming the bubble particle pair combines velocity ( $v_C$ ) is the same as that of bubble upward velocity ( $v_{B(S)}$ ) and particle upward velocity ( $v_p$ ), the velocity ratio becomes:

$$\frac{v_{B(B)}}{v_{B(S)} + v_p} = \frac{v_{B(B)}}{v_C} = \frac{(0.06 \mu_l d_p + 0.01 \mu_l^{1/3} d_p^{1\frac{2}{3}} + 1.9 \mu_l^{0.78} d_p^{1.22})}{(0.06 \mu_l + 0.01 \mu_l^{1/3} d_b^{2/3} + 1.9 \mu_l^{0.78} d_b^{0.22}) (2d_p - \frac{d_p^2}{d_b})} \dots\dots\dots(3.40)$$

Where  $v_{B(B)}$  is bubbles velocity before merge the particle and  $v_{B(S)}$  is the velocity of the system. It can be divided into three conditions as follow:

- If the  $v_{B(B)} > v_{B(S)}$  or  $v_{B(B)} > v_p$  Then, the velocity ratio would be very high, therefore the suspended particle separation rate would be quick.
- If the  $v_{B(B)} < v_{B(S)}$  or  $v_{B(B)} < v_p$  It is not possible, due to the bubble velocity should be greater than the bubble-particle velocity after merge.
- If the  $v_{B(B)} = v_{B(S)}$  or  $v_{B(B)} = v_p$  Then, the velocity ratio would be very low and it shows the very slow separation process.

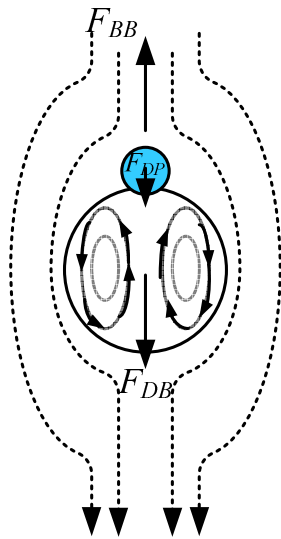


Figure 3.19 The bubble (○) is bigger than the particle (●). Assuming the bubble and suspended particle are vertically in line.

### 3.4.2.3 When Particle Diameter is Larger than Bubble Diameter

Figure 3.20 shows the bubble-particle pair when the particle diameter is bigger than the bubble diameter. The representing particle drag equation is:

$$F_{DP} = \left( \frac{0.484\mu_l}{\rho_l v_p d_p} + \frac{0.081\mu_l^{1/3}}{(\rho_l v_p d_p)^{1/3}} + \frac{14.6\mu_l^{0.78}}{(\rho_l v_p d_p)^{0.78}} \right) \left( \frac{\pi}{4} d_p^2 \right) \frac{\rho_l v_p^2}{2} \dots\dots\dots(3.41)$$

The force balance is:

$$\begin{aligned} \sum F_3 &= F_{BB} - F_{DP} \\ &= \frac{\pi}{6} d_b^3 (\rho_l - \rho_g) g - (0.06\mu_l \pi d_p v_p + 0.01\mu_l^{1/3} \pi d_p^{1/3} v_p^2 + 1.9\mu_l^{0.78} \pi d_p^{1.22} v_p) \dots\dots\dots(3.42) \end{aligned}$$

The deference force before and after bubble-particle merge is:

$$\Delta F = \sum F_{before.merge} - \sum F_{after.merge}$$

$$\begin{aligned}
\Delta F &= \left[ \frac{\pi}{6} d_B^3 (\rho_l - \rho_g) g - 0.06 \mu \pi d_B v_B - 0.01 \mu^{1/3} \pi d_B^{1.22} v_B - 1.9 \mu^{0.78} \pi d_B^{1.22} v_B \right] - \\
&\left[ \frac{\pi}{6} d_B^3 (\rho_l - \rho_g) g - (0.06 \mu \pi d_p v_C + 0.01 \mu^{1/3} \pi d_p^{1.22} v_C + 1.9 \mu^{0.78} \pi d_p^{1.22} v_C) \right] \\
&= (0.06 \mu \pi d_p + 0.01 \mu^{1/3} \pi d_p^{1.22} + 1.9 \mu^{0.78} \pi d_p^{1.22}) v_C - \\
&(0.06 \mu \pi d_B + 0.01 \mu^{1/3} \pi d_B^{1.22} + 1.9 \mu^{0.78} \pi d_B^{1.22}) v_B \\
&\dots\dots\dots(3.43)
\end{aligned}$$

The velocity ratio is:

$$\frac{v_{B(B)}}{v_{B(S)} + v_P} = \frac{v_{B(B)}}{v_C} = \frac{(0.06 \mu_l d_p + 0.01 \mu_l^{1/3} d_p^{1.22} + 1.9 \mu_l^{0.78} d_p^{1.22})}{(0.06 \mu_l d_b + 0.01 \mu_l^{1/3} d_b^{1.22} + 1.9 \mu_l^{0.78} d_b^{1.22})} \dots\dots\dots(3.44)$$

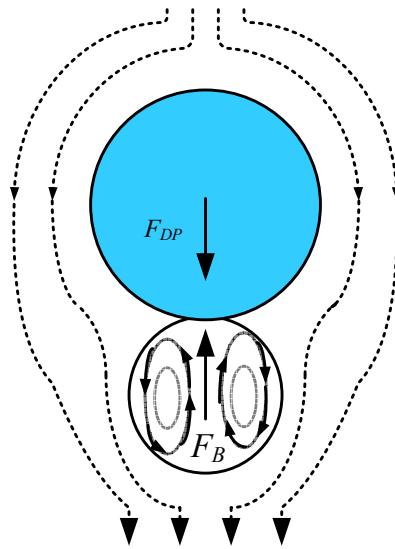


Figure 3.20 The bubble (○) is smaller than the particle (●). Assuming the bubble and suspended particle are vertically in line.

### 3.5 The Investigated Variables and Parameters

Five experiments were conducted in this study. The variables and parameters data that have been adjusted and taken in this research are listed in Table 3.3.

Table 3.3. The investigated variables and parameters

No.	Experiment	Variable	Parameter
1	Bubble dynamics in distilled and polluted water	Air inlet pressure	Bubble diameter, vertical and horizontal velocities
2	Suspended particle entrain	Air inlet flow	Turbidity level
3	Aeration process	Milli & micro bubble	DO level
4	Biodegradation	Milli & micro bubble	COD, COD removal rate, sCOD and sCOD removal rate
5	Nitrification	Milli & micro bubble	Amonia, Amonia removal rate, Nitrate and Nitrate removal rate

### 3.6 Summary

The millimeter size bubble can be generated by using perforated aluminium plate diffuser, while for micro size bubble can be generated using sintered porous glass diffuser. A regulated valve is mounted to adjust the inlet air pressure and flow simultaneously. Some transducers that monitor the properties of air inlet are mounted before the submerged diffuser. The submerged diffuser is located at the base of the water column. The PDA, the high speed camera and SEM (scanning electron microscope) can be used to monitor the bubbles and particles properties. The Hach Turbidity-meter and DO-meter are monitoring the turbidity level and DO level respectively.

The balance of the bubbles buoyancy force and the bubble-particle pair drag force shows the mechanism of the pushing up of suspended particles to the top of water column. The bubble-particle pair upward motion represents the particle lift-up process. Inline bubble-particle movement takes the separation action, whereas the rest of the particles would meet the next inline bubbles. Due to continuing bubbles generation, most of suspended particles would be separated and maintain on the top of water column.

The Biodegradation and Nitrification can be done in aeration process using the both millimeter and micro diffusers in the simultaneously periods of time.





## CHAPTER 4

### RESULTS AND DISCUSSION

#### **4.1 Dynamics of Bubbles**

This chapter deals with the high speed camera images and Particle Doppler Anemometry (PDA) measurement of bubble movement in distilled water and polluted water. The bubbles in both cases show difference in upward motion between millimeter bubble and micro bubble. Being the larger in size, millimeter bubble have high buoyancy and higher upward velocity. The bubbles velocities have two components, which are vertical and horizontal. The vertical velocity activates the counter force (drag) to resist the upward movement of the bubbles. Under the vertical and horizontal forces on the bubbles, they tend to change their shapes from spherical to ellipsoidal, which eventually changes the drag and buoyancy forces.

High speed camera images and PDA measurement are shown in this chapter. Size of the bubbles and velocities are the main parameter to be measured, whereas the air pressure, air flow and porosities of sintered glass are the variables. The generated bubbles are either the non uniform bubbles (polydispersed) or the uniform bubbles (monodispersed). The variation of porosity sintered glass diffusers generate both the forms of bubbles that are controlled by changing air pressure and air flow. The relationships between bubble velocities and diameter have been characterized and plotted using some dimensionless number like Reynolds number etc.

Due to the opaqueness of real wastewater, the light can not pass through it. Hence it can not be used in PDA measurement, Thus leaving the only possibility of imitated polluted water, This imitated polluted water have similar physiochemical characteristics (surface tension, density and viscosity) as that of real wastewater.

Glycerin in the range of 0.1% to 0.5% is used to prepare imitated water for further investigation. The graphs of relationships among the bubble diameter, bubble velocities and air pressure-flow using variety of sintered porous glass diffuser have been plotted.

The Carboxy Methyl Cellulose (CMC) pollutant produces turbidity (the cloudiness of solution) in the water. The CMC crystals represent the suspended particle in the range of 5 to 20 micron. The linear curve fit graph of turbidity level versus the PPM of the CMC pollutant has been observed and show the relationships between them. The decreasing level of turbidity of the solution shows that the suspended particles have been reduced in the artificial polluted water.

Biodegradation and Nitrification need the sufficient oxygen to fulfill their process. Compare to the millimeter bubble, micro bubble has a better in Biodegradation and Nitrification process, due to the significant of DO level increasing. The performance of micro bubble aeration is discussed in this chapter.

#### **4.1.1 The High Speed Camera Image Results**

Figure 4.1 shows the image of non spherical shape of millimeter bubbles. In general, the bubble has a sphere shape, whereas this non spherical shape is caused by the higher forces working on it. The millimeter bubbles have insufficient surface tension to maintain their shape. The main forces are buoyancy and drag. The higher forces produce higher vertical and horizontal velocity. The vertical velocity always acts in upward direction whereas, the horizontal velocity always acts at left or right, front or rear. Higher horizontal component of velocity of bubble indicate that bubble move in non-linear trajectory. Thus can be effect as water stirring. The non-linear trajectory also creates bubbles coalescence and bubbles merge more frequently. The coalescence is often in the vertical direction due to the higher vertical forces (buoyancy and drag), whereas the coalescence rarely in the horizontal direction.

The various measurements of diffuser holes diameter, air bubbles diameter and rise-up velocity, in case of the perforated Aluminium disc diffuser are listed in Table 4.1. The data is taken from 20 reading per samples. The air bubble diameters are found in the order of 10 to 20 times of the diffuser holes diameter. Most of the bubbles have non spherical shape and are continuously change their shape. They move upward in a non linear trajectory. The inlet pressure is in the range 5 to 7.5 kPa and the inlet flow in range 0.024 to 0.042 m<sup>3</sup>/s.

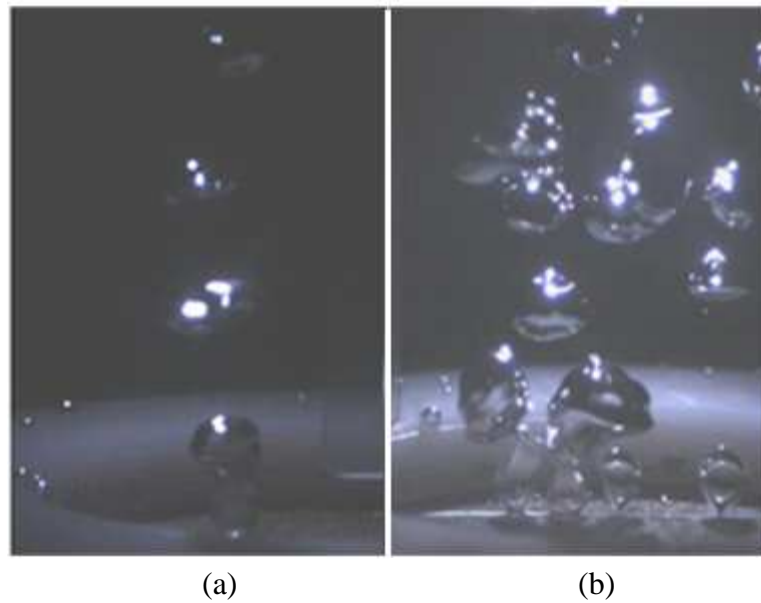


Figure 4.1 (a) monodispersed bubbles magnified 4 times (b) polydispersed bubbles magnified 2 times.

Table 4.1 Bubbles diameter and rise-up velocity for various diffuser holes.

No	Diffuserhole diameter (mm)	Bubble diameter (mm)	Vertically upward velocity (m/s)
1	0.247	3	0.332
2	0.271	3.7	0.283
3	0.285	4.09	0.287
4	0.312	3.54	0.296
5	0.321	3.72	0.289
6	0.327	2.82	0.475
7	0.339	6.36	0.409
8	0.404	5.46	0.412

Figure 4.2 shows the relationship between bubble diameter and upward velocity. Compare to Figure 2.1, the second order polynomial curve fit plotted to represent the relationship between bubble diameter and upward velocity is valid.

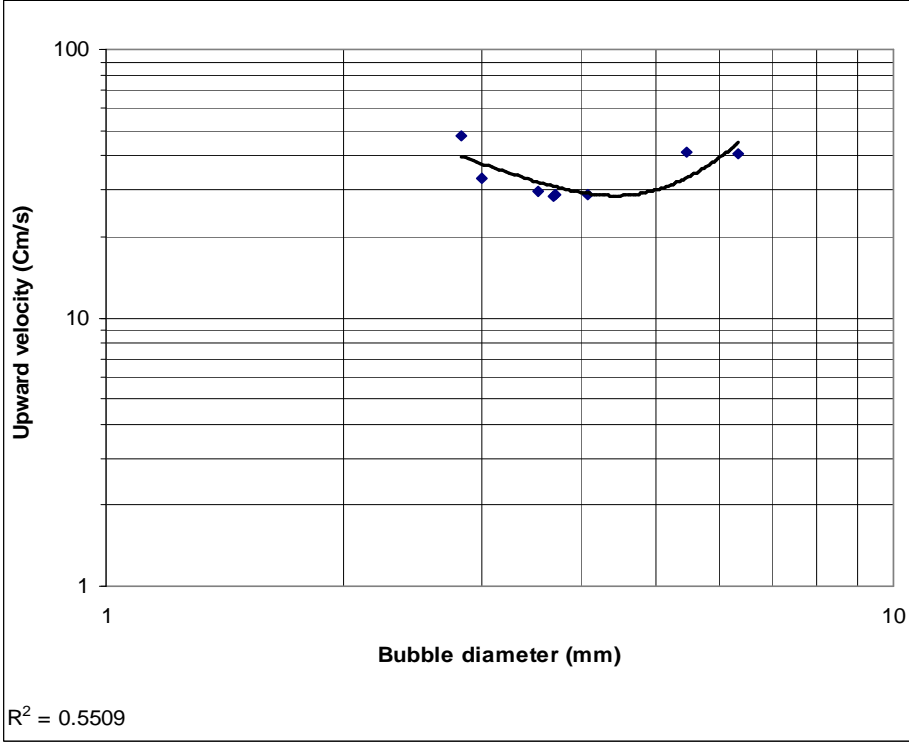


Figure 4.2 The relationship between bubble diameter and upward velocity of millimeter bubbles

Figure 4.3 shows the image of spherical micro bubbles. The shape is maintained during the upward motion of the bubble in the water column. Having spherical shape, the micro bubble accepts smaller buoyancy and smaller upward velocity. As the counter forces of bubbles upward motion, the drag forces appear in a lower scale. In consequences of smaller working forces, the micro bubble is maintained in sphere shape and moves linear upward. The lower horizontal velocity of micro bubble limited the non-linear trajectory in its flow, therefore the micro bubble upward motion is suitable for lifting-up the suspended particles. The linear motion to the top of water column keeps the lifting-up of suspended particle process last longer. The other suitable condition for lifting-up process is the micro bubbles population. Where the population of micro bubbles generated, are much more at the same air volume inlet than millimeter bubble.

The porous sintered glass diffuser holes are formed by the pores among the glass crystals, where the size is varied and the shape is irregular. Since the shape and the size are not uniform, it could therefore not generate uniform air bubbles. The uniformity of bubbles size can be achieved when the porous is made from uniform glass crystals, but it is very difficult to produce uniform glass crystal. Experimentally the porosity is always available in a randomly of size. Generally the size of bubble generated is bigger than the porous hole, where the bubbles up to 100  $\mu\text{m}$  are generated from less than 40  $\mu\text{m}$  porous hole. The inlet pressure is in range 21 to 33 kPa and inlet flow is in range 0.03 to 0.132  $\text{m}^3/\text{s}$ . The energy derive from air inlet pressure and flow is found at a range 2.2 to 3.5 time differences between micro and millimeter bubble

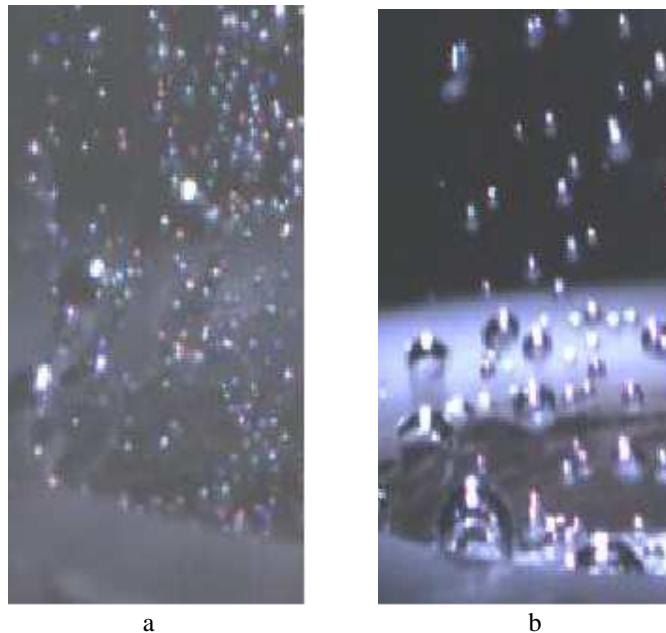


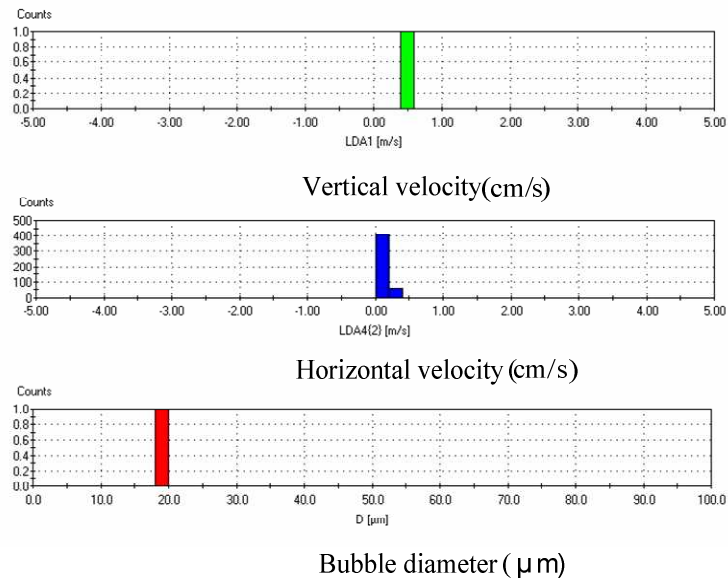
Figure 4.3 The air bubbles are formed by the porous sintered glass (a) the 10-16  $\mu\text{m}$  porosity generated bubble diameters in a range 30  $\mu\text{m}$  to 60  $\mu\text{m}$  with 20 times magnification (b) the 16-40  $\mu\text{m}$  porosity, the maximum bubble diameter was 100  $\mu\text{m}$  with 20 times magnification.

#### 4.1.2 PDA Graph Results

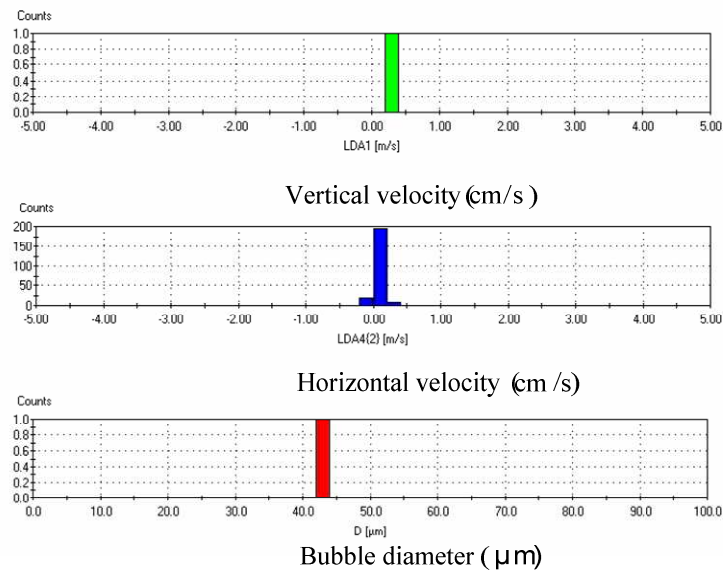
Figure 4.4 shows the PDA print out of the results in case of the ordinary tap water. At an inlet air pressure in the range of 22-24 kPa, the micro bubble produced, are

monodispersed whereas at higher pressure in the range of 24-27 kPa, the production of bubbles is polydispersed. The graph (print-out) shows the bubble diameter, horizontal velocity and vertical velocity of the bubble, when it crosses the point of intersection of the two laser beams. It is clear from Figures 4.4 and 4.5 that with a change of pressure from 22 kPa to 27 kPa, the production of bubbles changes from monodispersed (single bubble) to polydispersed (many bubbles at the same time).

The print-out of the PDA consists of three bar graphs. The upper is the vertical velocity, the middle is the horizontal velocity and the bottom is the diameter of particles. Figure 4.4.a represents a 19  $\mu\text{m}$  bubble diameter, with average bubble horizontal and vertical velocity of 0.1 and 0.5 cm/s respectively. Figure 4.4.b shows 43  $\mu\text{m}$  bubbles diameter, with sampling data detecting time was 30 seconds and detects one bubble represented in vertical axis. The bubbles have 0.1 cm/s horizontal velocity. The sampling data detecting were in level counts 200. The bubbles have randomly horizontal velocities. In the vertical direction, the bubbles have 0.3 cm/s velocity. The measurement result is listed in Table 4.2 and 4.3.



(a)



(b)

Figure 4.4 PDA print outs for Monodispersed bubble monitored at (a). 22 kPa. (b). 24 kPa. using 16-40 micro porosity sintered glass diffuser in the tap water.

Figure 4.5 shows that the PDA detects four different bubbles diameters (20, 25, 45, and 48  $\mu\text{m}$ ). The PDA also measures those bubbles having different vertical and horizontal velocities. Therefore, the velocity of each bubble can not be easily determined in the Polydisperse case compared to Monodispersed case. The problem had been solved by taking the average value of bubble diameters, horizontal velocities

and vertical velocities. The average values are used to correlate various parameters in the experiments.

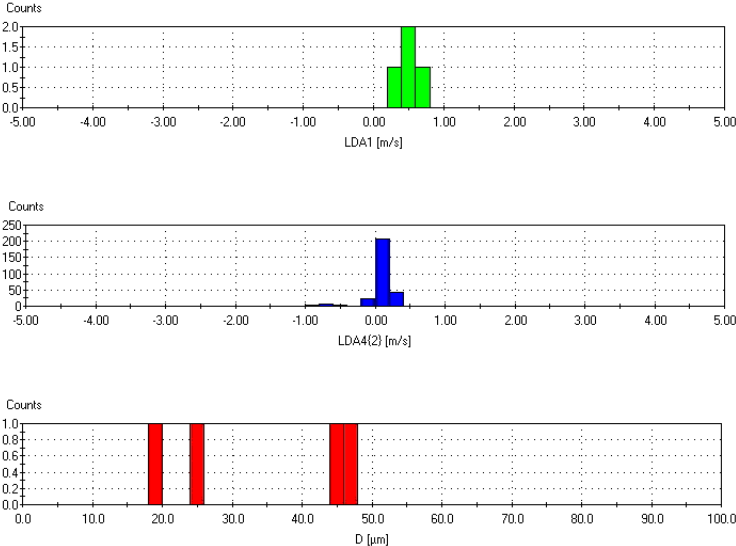


Figure 4.5 Polydispersed bubble was monitored at 27 kPa, used 16-40 micro porosity sintered glass diffuser in tap water medium.

**4.1.2.1 The Effect of Air Inlet Pressure on Bubble Characteristics.**

The air bubble diameter produced by the sintered glass diffuser depends mainly on the porosities and supplied air (pressure and flow). The capability of smaller porosity diffuser to produce uniform bubbles (monodisperse) is higher than that of the larger porosity, whereas the larger porosity diffuser has the higher possibility in producing non uniform bubbles (Polydisperse). The polydispersed bubbles upward movement has many horizontal velocity varieties (non-linear trajectory). A similar movement of bubbles has been reported by Kracht [30], Tomiyama [42], eventually, creating a stirring effect in the water. Micro bubbles have a smaller stirring effect due to small component of their velocities in the horizontal direction. A slower upward movement is obtained, and the turbulent effect is avoided, if the bubble is produced in micron size. By adjusting the air inlet pressure, the uniform bubble diameter is generated. The limiting air pressure and using small porosity sintered glass, the size and velocity of



bubbles can be controlled in a narrow pressure range. The pressure ranges used to produce monodispersed are is between 12 to 14 kPa, 14 to 16 kPa, and 21 and 26 kPa for porosity 1-10  $\mu\text{m}$ , 10-16  $\mu\text{m}$ , and 16-40  $\mu\text{m}$  respectively. Table 4.2 and 4.3 are listed the averaged of bubble diameter, horizontal and vertical velocities in different air inlet pressure-flow, using submerged sintered glass diffuser with porosity 1-16  $\mu\text{m}$ , 16-40  $\mu\text{m}$  respectively.

Table 4.2 Bubble diameter and velocity for various pressure and air flow of 1-16  $\mu\text{m}$  porosity sintered glass diffuser in tap water.

Pressure (kPa)	Air flow (l/min)	Bubble diameter ( $\mu\text{m}$ )	Hor. velocity (cm/s)	Ver. velocity (cm/s)
12	0.6	11	0.1	0.1
13	0.7	48	0.1	0.2
14	0.8	65	0.1	0.1
15	0.9	83	0.1	0.1
16	1	84	0.1	0.2
17	1.3	95	0.1	0.2
18	1.5	100	0.2	0.2
19	2	94	0.2	0.2

Table 4.3 Bubble diameter and velocity for various pressure and air flow of 16-40  $\mu\text{m}$  porosity sintered glass diffuser in tap water.

Pressure (kPa)	Air flow (l/min)	Bubble diameter ( $\mu\text{m}$ )	Hor. velocity (cm/s)	Ver. velocity (cm/s)
21	0.9	11	0.1	0.1
22	1	10	0.1	0.1
23	1.2	14	0.1	0.1
24	1.2	20	0.2	0.2
25	1.3	44	0.2	0.2
26	1.5	70	0.2	0.2
27	1.6	74	0.2	0.2
28	1.3	70	0.2	0.3
29	1.4	70	0.2	0.4
30	1.5	59	0.2	0.4

The second order polynomial curve fitting is implemented as shown in Figure 4.6, in which the correlation coefficient is 0.9. It has been used to establish the relationship between bubble diameter and inlet air pressure. The left curve fit represent 1-16  $\mu\text{m}$ , and the right represent 16-40  $\mu\text{m}$  porosity of sintered glass. The pressure ranges depend on the porosity of sintered glass and the water level in water column. The 1-16  $\mu\text{m}$  porous sintered glass, the pressure range is measured at 12 to 19 kPa, while 16-40  $\mu\text{m}$  is measured 21 to 30 kPa. In this case, the water level is measured at 30 cm high. To control the bubble diameter, first need to use lower porosity sintered glass and second very controlled low inlet air pressure. For using of 10-16  $\mu\text{m}$  sintered porous glass, each unit of pressure changing the approximate  $\Delta d_B$  on average would be 13.57 micron and this maximum value of bubble production is 100 micron. While the 16-40  $\mu\text{m}$  sintered porous glass, each unit of pressure changing the approximate  $\Delta d_B$  on average would be 9 micron and the maximum value of bubble production is 74 micron. In this case the tap water is used.

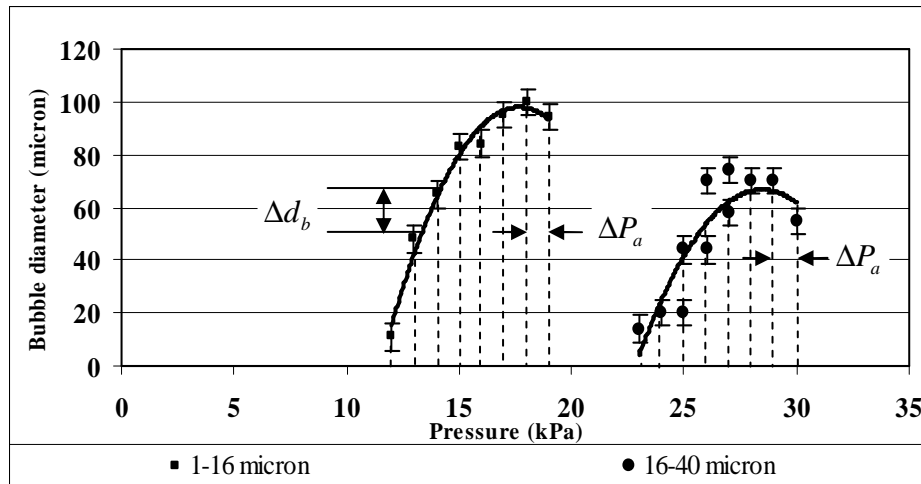


Figure 4.6 The effect of various inlet air pressures on the bubble size through different porosity diffusers. Error bar in y direction is  $\pm 5\%$ .

#### 4.1.2.2 The Effect of the Water Level on Air Inlet Pressure and Bubble Diameter

Figure 4.7 shows the relationship between bubble diameter, inlet air pressure and water level. Inlet air pressure to produce the bubble, depend on the water level, The higher water level the higher inlet air pressure to produce bubble at diffuser. Eventually, the increase inlet air pressure would produce the bigger bubble size.

At any position between 0 and 50 cm from the base side of water column, the varied bubble size would be produced. The increase or decrease in bubble size would start the phenomena of merging and breaking of bubble inside the water column. The Figure 4.7 shows almost a linear relationship between the inlet air pressure and water height in the column above diffuser and also it relates the bubble diameter to water level and pressure linearly.

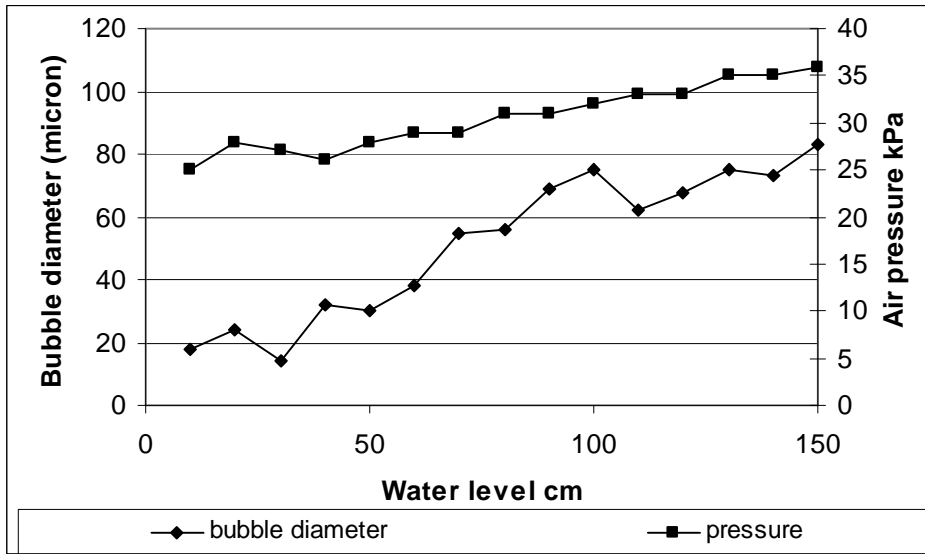


Figure 4.7 Relationship between bubble diameters, and air pressure versus altered water level are measured at air flow  $0.075 \text{ m}^3/\text{s}$ .

#### 4.1.2.3 The Effect of Buoyancy and Drag Force on Bubble Dynamics

As mention earlier all forces that have been worked on the bubbles would lead to the bubble production characteristics. Their characteristics (size and velocities) determine the flow, therefore the Reynolds number can be observed. The relationship between bubble diameter and vertical velocity is plotted and show in Figure 4.8. The bigger the bubble size, the higher the velocity would be.

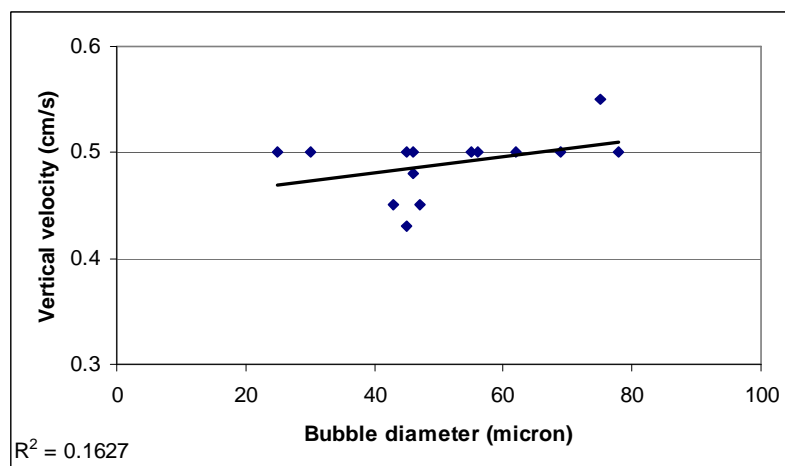


Figure 4.8. The relationship between bubble diameter and vertical velocity using 16-40  $\mu\text{m}$  porous sintered glass.

The Buoyancy force acting on the bubble is calculated using air and water properties, eg.  $\rho_{\text{air}} = 1.204 \text{ kg/m}^3$ ,  $g = 9.80665 \text{ m/s}^2$  and  $\rho_{\text{water}} = 998 \text{ kg/m}^3$ , etc. The bubble volume is taken from the data gathered during the experimentation. Thus, the calculated buoyancy force is shown in Figure 4.9, which is a function of bubble diameter. The result of third order polynomial curve fit as shown in Figure 4.9, show that the higher buoyancy the higher vertical velocity is generated.

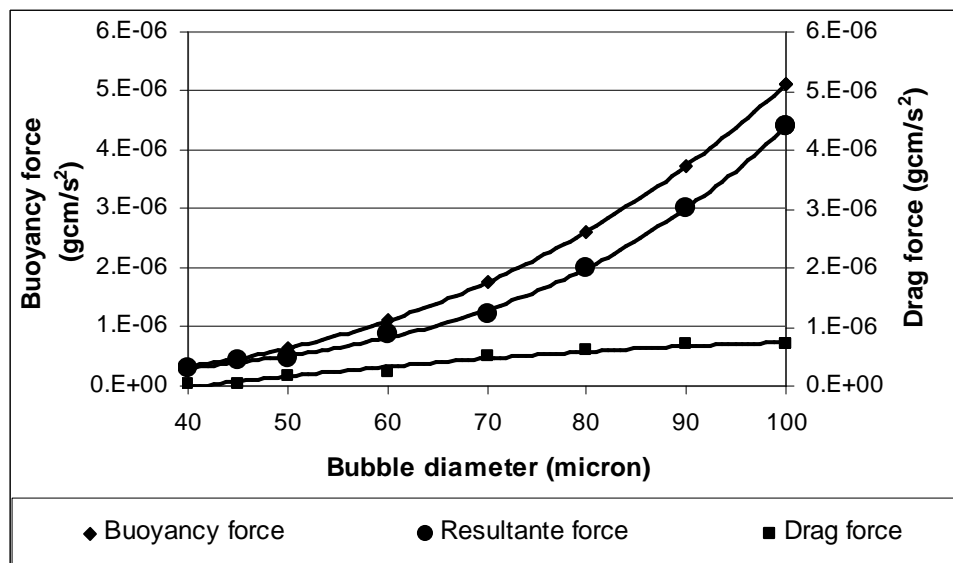


Figure 4.9 The relationship between Buoyancy, Drag force and Bubble diameter

The bigger the bubble is the higher buoyancy would be, and consequently bubble would expression higher velocities. The high upward velocity is the most suitable parameter to achieve the high energy to transfer or entrains suspended particles. But then higher upward velocity of bubble altered the acting drag force become high. The horizontal velocity of bubble would increase when the acting drag increase or the bubbles shape change. For lifting suspended particle ideally bubble sizes is produced in micron level to maintain their shape or to limit the drag force. For 90  $\mu\text{m}$  bubble size, the maximum buoyancy force is  $3.72 \cdot 10^{-6} \text{ gcm/s}^2$ , and the maximum vertical velocity and calculated drag force are found at 0.5 cm/s and  $2.27 \text{ E-7 gcm/s}^2$  respectively. The bubble shape is key factor to keep the higher energy to entrain suspended particles, as long as the bubble in spherical shape the lower drag is maintainable.

The velocity distribution in the cross section of water column is shown in Figure 4.10. The maximum velocity is 0.8 cm/s when the inlet air flow is adjusted at 0.132 m<sup>3</sup>/s. The lower inlet air flow is 0.03 m<sup>3</sup>/s and maximum velocity 0.3 cm/s.

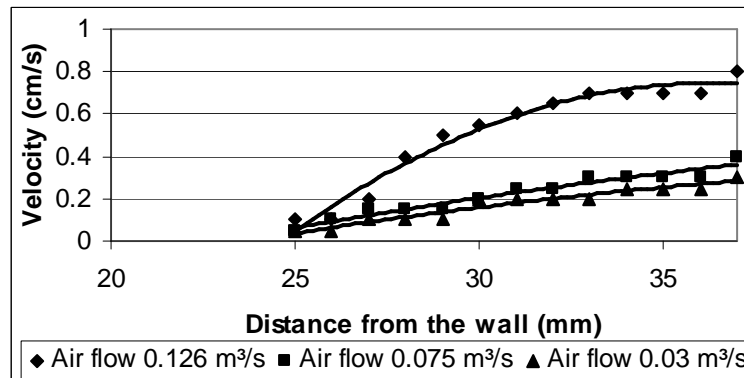


Figure 4.10 The vertical velocity distribution vs distance from the wall.

#### 4.1.3 Effect of Glycerin Water Solution on Bubble Dynamics.

The bubble dynamics in water are dependent on the physiochemical properties of the medium, where they are produced and are moving upward. The moment, the physical or chemical characteristics of the medium would change the size of bubbles and their movement i.e. their velocities would change altogether. One of the problems of using the actual wastewater in the experiment is that it is not transparent, that is why it does not allow measuring the bubble dynamics. Glycerin as a pollution is used to solve the problem, where it maintains similar physiochemical characteristics as that of polluted water and offer reasonable transparency. Table 4.4 shows the physiochemical properties of distilled and polluted water. The residential wastewater has liquid phase properties similar to the glycerin solution with a fraction between 0.1% until 0.5%.

Table 4.4 Physiochemical properties of distilled and polluted water.

Glycerin percentages (% by vol.)	Viscosity (centi-poise)	Density (1000 kg/m <sup>3</sup> )	Surface tension (mN/m)
0.0 (distilled water)	1.0	1.0000	73
0.1	1.1	0.9975	67
0.2	1.2	0.9979	63
0.3	1.2	0.9983	59
0.4	1.2	0.9986	55
0.5	1.5	0.9990	53
Residential wastewater	1.2	0.9982	55
Tap water	0.5	0.997	69.53

A volume fraction of glycerin in the percentage of 0.1 to 0.5 is used to pollute distilled water. The 0.4% volume fraction of glycerin exhibits the similar properties to that of wastewater, collected from UTP wastewater treatment plant.

The physical characteristics of distilled water and glycerine polluted water are shown in Figure 4.11. The volume percentages of 0.1, 0.2, 0.3, 0.4 and 0.5 of glycerin are added in distilled water, it would increase density and viscosity of water solution and decrease surface tension. The change of these parameters influence the bubbles dynamic like velocities, size, etc due to the change of working forces on the bubble. The main working forces on the bubble are buoyancy, drag and surface tension. The buoyancy and drag would increase as the density and viscosity increase. The surface tension force influences the decreasing of the detachment force (eq (3.22), (3.26)). Therefore the bigger bubbles are generated.

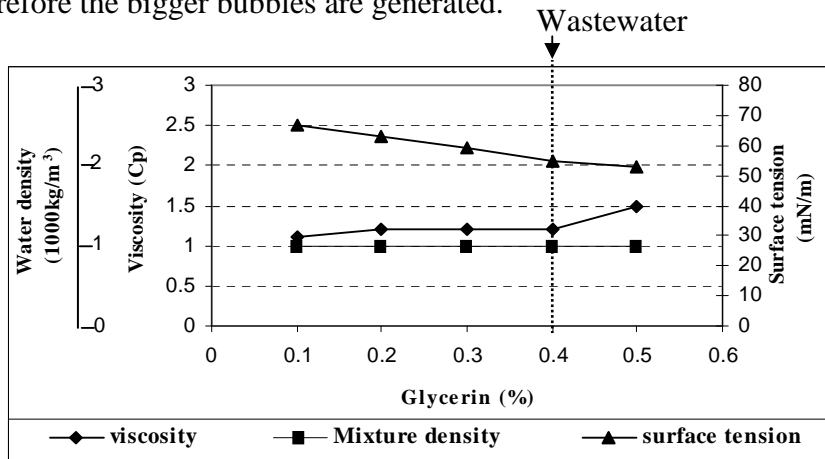


Figure 4.11 The relationship of Glycerin impurities in distilled water to viscosity, water density and surface tension.

#### **4.1.3.1** *The PDA Graph of Bubble Dynamics in Glycerin Polluted Water*

The condition where the collision, merging and breaking of the bubbles have been occurred, the polydispersed bubbles are produced. In general decreasing surface tension would increasing bubble size even using the smallest porosity of sintered glass diffuser and very fine control of air input pressure. The increasing bubble size would increase buoyancy force, velocity and drag force due to both forces depend upon the bubble diameter as listed in Table 3.1. The bigger bubbles production happens in the time of detachment of the bubble from the diffuser surface, where at that time the surface tension force work on the diffuser surface. However, after detachment where the free moving bubble take turn, the surface tension work only at the interface between air bubble and water. The bigger bubble has the weakness of the surface tension as compared to the smaller bubbles. Therefore, the bigger bubbles are easy to break into smaller bubbles. In the condition where the higher bubble breaks become smaller bubble, these smaller bubbles would remain at its size due to the higher surface tension (as mention earlier, at the free moving bubble, the surface tension work only at interface between air bubble and water, the smaller bubble the smaller interface area would be and higher surface tension acts). At the free moving bubble, the water viscosity takes over to control the bubble upward movement, the more viscous water (here 5% glycerin added) the more drag force worked would be. Since the Reynolds number is dependent on the water viscosity, the increase water viscosity would lead to decrease the Reynolds number (eq. (3.29)). Due to the decreasing of the Reynolds number, the coefficient of drag (CD) would increase (eq. (3.28)). Finally the increasing of CD gives impact to the increasing the drag force works on the bubble (eq (3.30)). This higher drag force would act on the smaller bubbles on free moving bubble regime.

The PDA bar graphs of adding glycerin with a fraction of 0.1% up to 0.5% in distilled water are plotted in Figures 4.12., 4.13, and 4.14. As listed in Table 4.4, the addition of glycerin would decrease the water surface tension. The distilled water surface tension is 73 mN/m, while the presence of glycerin decreased the surface tension to the level of 53 mN/m.



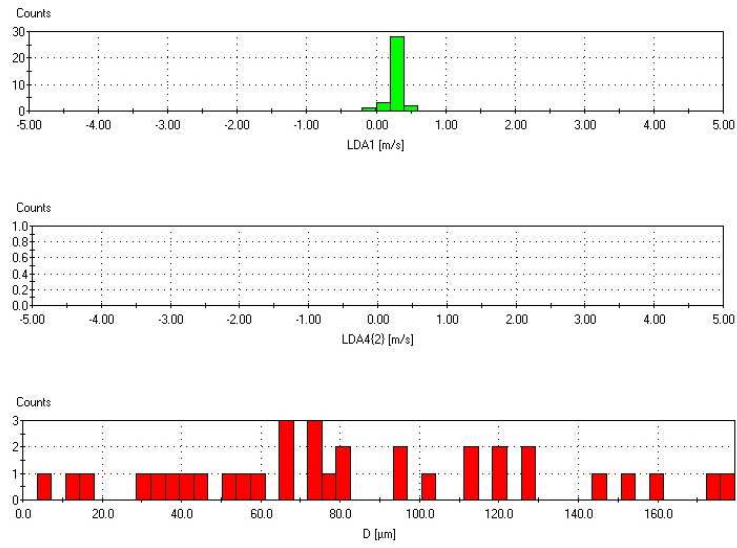


Figure 4.12 Polydispersed bubble from 1-10  $\mu\text{m}$  porosity sintered glass diffuser at air pressure 25 kPa and air flow 0.06  $\text{m}^3/\text{s}$  in 0.1% glycerin solution.

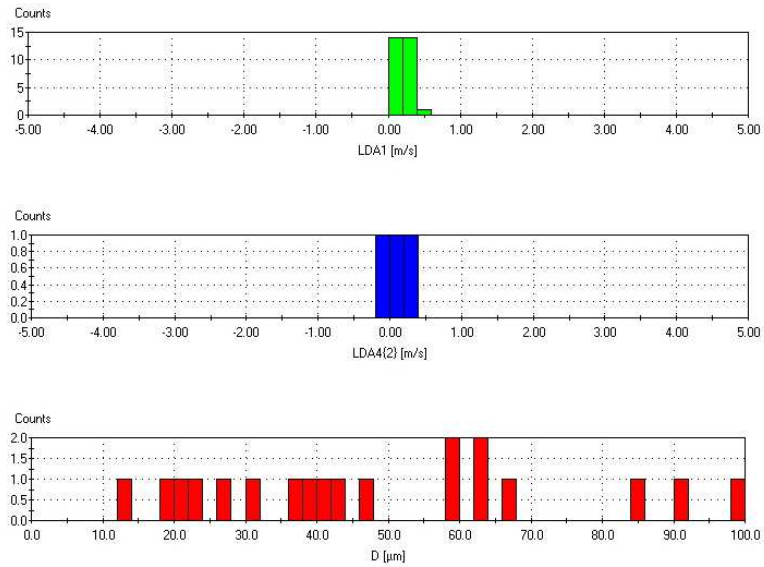


Figure 4.13. Polydispersed bubble from 1-10  $\mu\text{m}$  porosity sintered glass diffuser at air pressure 25 kPa and air flow 0.06  $\text{m}^3/\text{s}$  in 0.3% glycerin solution.

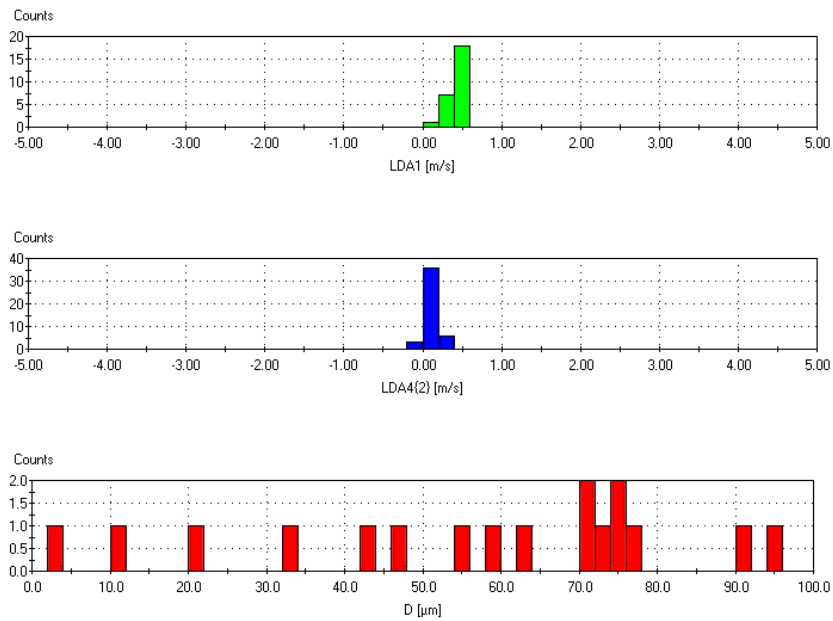


Figure 4.14. Polydispersed bubble from 1-10  $\mu\text{m}$  porosity sintered glass diffuser at air pressure 25 kPa and air flow 0.06  $\text{m}^3/\text{s}$  in 0.5% glycerin solution.

The higher buoyancy force acting on the bubble is the most wanted parameter to separate the suspended particles. Because of the density gap between air and water, is widening, therefore horizontal velocity of bubble is also increasing, this creating undesired turbulent flow. From these phenomena, the glycerine impurity does not only reduce the linearity of the bubble movement and create high horizontal velocities, but also adds the variation of bubble size, due to the bubble dispersion. The high divergence of bubble is due to the fact that the three liquid phase properties (density, viscosity, and surface tension) can not be manipulated independently. It is impossible to modify one property without changing the other two. Consequently, the realizable range of air pressure to achieve zero horizontal velocity is very limited.

When 0.5% by volume glycerin is added, the zero horizontal velocity condition is reached at inlet air pressure 23 kPa, as shown in Figure 4.15. This inlet air pressure is two kPa lower compare to the 0.1% volume of glycerin added.

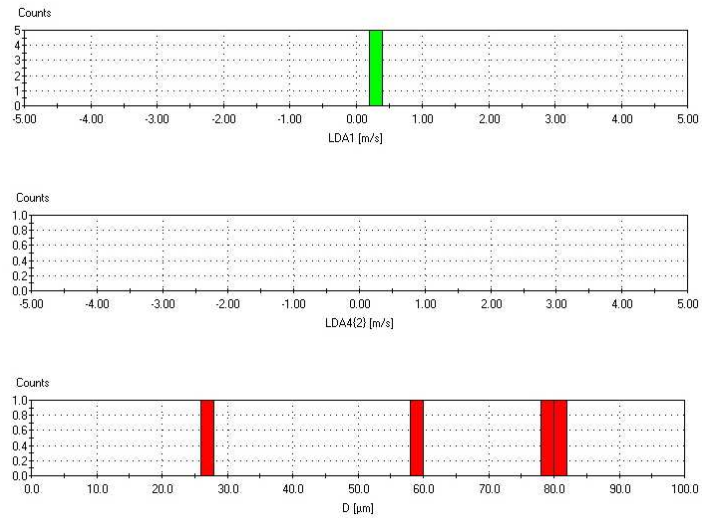


Figure 4.15 Polydispersed bubble from 1-10  $\mu\text{m}$  porosity sintered glass diffuser at air pressure 23 kPa and air flow  $0.048 \text{ m}^3/\text{s}$  in 0.5% glycerin solution.

Various volume fractions of glycerin effect the velocities of free floating bubbles. In some cases, the horizontal velocity reaches almost zero, i.e. the bubble is moving upward only and at this point, the bubble would exert maximum forces on the suspended particle to move it to the water level. The zero horizontal condition of micro bubble has been recorded when the inlet air pressure through diffuser is controlled at the range between 20 and 24 kPa, beyond 24 kPa air inlet pressure, the horizontal velocity exist. The different addition percentage volume of glycerin the different range of inlet air pressure applied to produce zero horizontal velocity bubble would be as listed at Table 4.5.

Table 4.5 Effect of pressure and air flow on the bubbles diameter and velocities in a glycerin solution, using 1-10  $\mu\text{m}$  sintered glass diffuser

Air inlet pressure (kPa)	20	21	22	23	24
Ai inlet flow (L/min)	0.8	0.8	0.9	0.9	0.9
0.1 % Glycerin					
Bubble diameter. ( $\mu\text{m}$ )	42	45	56	50	85
Horizontal velocity (cm/s)	0	0	0	0	0
Vertical vel. (cm/s)	0.1	0.1	0.3	0.3	0.3
0.2 % Glycerin					
Bubble diameter ( $\mu\text{m}$ )	40	45	50	60	70
Horizontal velocity (cm/s)	0	0	0.1	0.3	0.3
Vertical velocity (cm/s)	0.1	0.1	0.3	0.3	0.5
0.3 % Glycerin					
Bubble diameter ( $\mu\text{m}$ )	41	50	31	40	45
Horizontal velocity (cm/s)	0	0	0.1	0	0.3
Vertical velocity (cm/s)	0.3	0.3	0.1	0.1	0.3
0.4 % Glycerin					
Bubble diameter ( $\mu\text{m}$ )	25	27	29	30	40
Horizontal velocity (cm/s)	0	0	0	0.1	0.1
Vertical velocity (cm/s)	0.3	0.3	0.3	0.3	0.5
0.5 % Glycerin					
Bubble diameter ( $\mu\text{m}$ )	23	27	29	30	35
Horizontal velocity (cm/s)	0	0	0	0	0.1
Vertical velocity (cm/s)	0.3	0.3	0.3	0.3	0.3
Distilled Water (DW)					
Bubble diameter ( $\mu\text{m}$ )	20	23	35	40	45
Horizontal velocity (cm/s)	0	0	0	0	0
Vertical velocity (cm/s)	0.3	0.3	0.3	0.3	0.5

The addition of glycerin in distilled water effect on the bubble production, due to every increase percentage of the glycerin pollutant added in the water the lower line

curve fit would be. Therefore line curve fit of the 0.5% glycerin polluted water is lower than the 0.4% glycerin polluted water, the line curve fit of the 0.4% glycerin polluted water is lower than the 0.3% glycerin polluted water and so on until the line curve fit of the 0.1% glycerin polluted water is lower than distilled water. The bubble production is determined from air inlet pressure and the size of the diffuser, hence the higher air inlet pressure the bigger bubble would be. The line curve fit has been used to establish the relationship between the inlet air pressure and bubble diameter. The bubble diameter, before and after various percentage of glycerin added into distilled water is recorded as shown in Figure 4.16. The 0.4% glycerin added in distilled water has similar physiochemical characteristics as that of real waste water from UTP wastewater treatment plant.

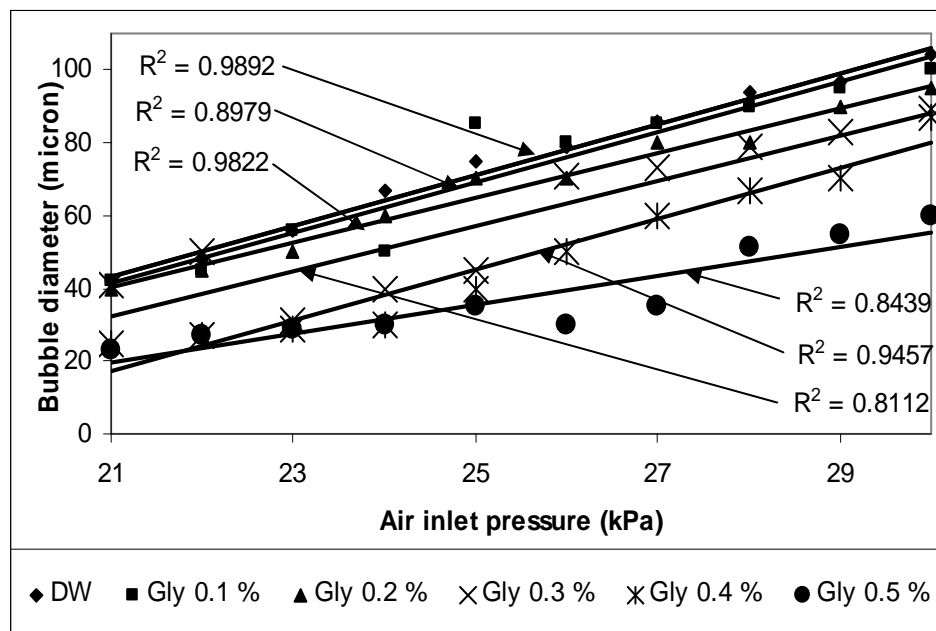


Figure 4.16 The relationship between inlet air pressure and bubbles diameter in varied percentage of glycerin in distilled water using 1-10  $\mu\text{m}$  sintered glass diffuser.

The addition of glycerin in distilled water would increase the bubble upward velocity due to the decreasing water surface tension. As stated in equations (3.22) and (3.25), the bubble generation forces would be increased when the surface tension decrease. The relationship between the vertical velocity and bubble diameter before and after various percentages of glycerin added into distilled water has been plotted in Figure 4.17.

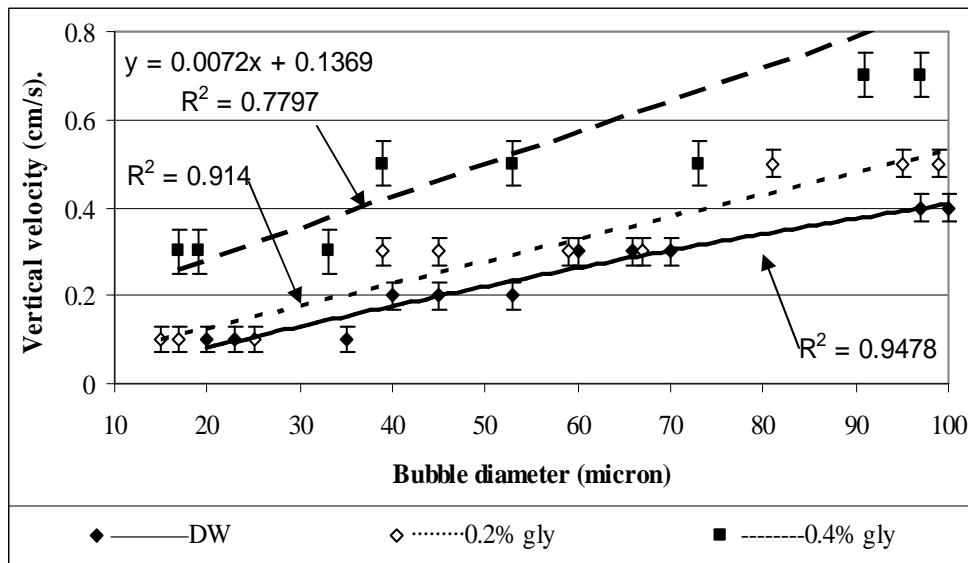


Figure 4.17 The relationship between bubble diameter vs bubble vertical velocity. The y error bars at distilled water, 0.2% and 0.4% glycerin are 0.03, 0.03, and 0.05 respectively.

The higher percentage of pollutant added into water the faster vertical velocity of the bubble would be, therefore in the same bubble size production would elevate the bubble upward motion. Hence the buoyancy and drag force acts on the bubble increase, due to the increase of water density and viscosity by increase the percentage of pollutant in the water. This phenomena leads to the reducing of correlation factor ( $R^2$ ) of the curve fit. The line curve fit of the 0.2 % glycerin pollutant water has correlation factor as high 0.914, whereas the 0.4 % glycerin polluted water has  $R^2$  as high as 0.7797. This relationship between bubble size and its velocity became weakness.

#### 4.1.3.2 The Dimensionless Number of Bubble Dynamics in Glycerin Polluted Water

Since the bubble movement is dependent on the dynamics as well as gravitational forces acting on it, and the relationship between these forces leads to Froude number, therefore the Froude number is presented and plotted in Figure 4.18. The upward velocity and bubble size are the dependent elements to establish the Froude number.

The presence of a pollutant in water would change the bubble diameter and its velocity; consequently Froude number would be shifted to a lower value. The lower Froude number is found less than one, therefore the bubble flow is in constant line named tranquil (sub critical) flow [16], which would assure the lifting-up of suspended particles process in water.

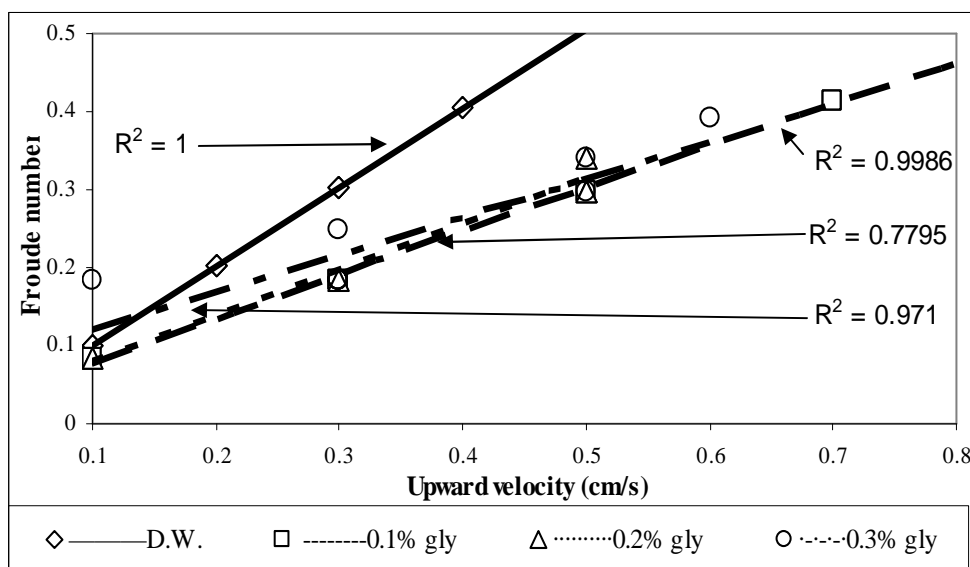


Figure 4.18 The relationship between velocity versus Froude number in glycerin polluted water.

Acknowledging the significance of air inlet flow as the main factor for determining Reynolds number, the relationship between Reynolds number and air inlet flow both before and after various percentages of glycerin added into distilled water is presented and plotted in Figure 4.19. It is observed that increasing percentage of pollutant would decrease the Reynolds number due to the increase of mixture viscosity. At any positions after 0.2 % glycerin added, a significant decrease of the Reynolds number is recorded.

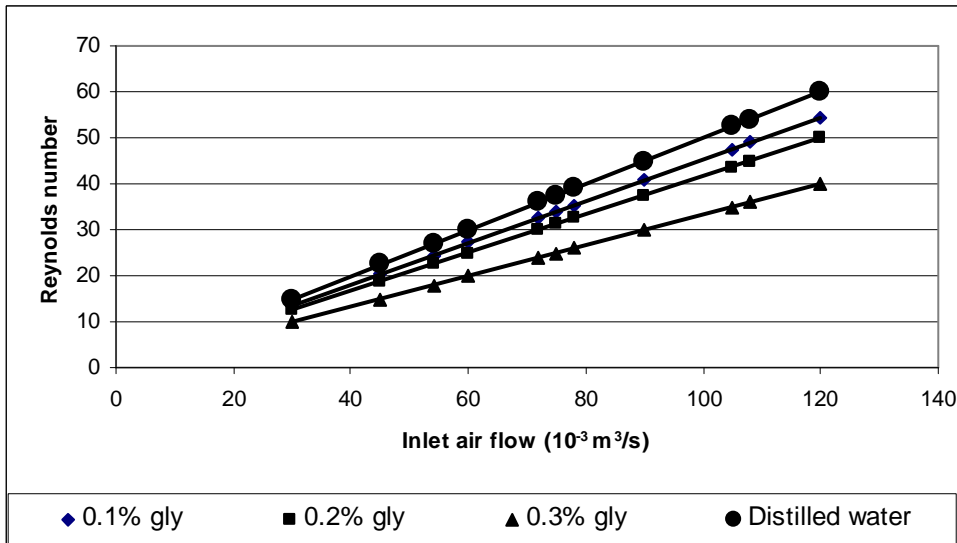


Figure 4.19 The relationship between Reynolds number versus bubble diameter  
The y error bar is in between 2 and 3. DW stands for distilled water.

Increasing the inlet air pressure tend to generate bigger bubble or shorter vertical distance between bubbles also higher vertical velocity. Consequently the merging between bubbles happens more frequently. The change in bubble diameter is controlled by the inlet air pressure. This can be observed in Figure 4.20, where a 9 kPa increment (from 21 to 30 kPa) produced a 5 fold increase in the average bubble size. The vertical velocity increased 4 fold (0.1 to 0.4 cm/s) (Figure 4.17), and the Reynolds number increased 4 times (from 15 to 60) as indicated in Figure 4.19. These show that in order to control the Reynolds number, one needs to control the air inlet flow and follow by the bubble size, due to the strong relationship between bubble diameter and air inlet flow also pressure.

By keeping the bubble size and its upward velocity constant, the lift-up of suspended particle process can be achieved at an optimum condition, which has been validated by the decrease of pollutant level (Figure 4.27 and 4.29).

#### 4.1.3.3 The Bubble Production in Variance Porosity Diffuser

Figure 4.20 shows the relationship between inlet air pressure and the bubble diameter for two different porosities sintered glass diffuser, when the volumetric range of



pollutant in water is 0.5%. Comparing with Figure 4.6, the 1-16 micron porous line is shifted to the right close to the 16-40 micron porous glass, its shows that increasing water viscosity by added glycerin would effect of increasing drag force (eq.(3.26)) and follow by increasing the inlet air pressure to produce same diameter bubble. By comparing Figure 4.6 and Figure 4.20, it is evident that air inlet pressure required to produce micron bubbles through 1-16  $\mu\text{m}$  porous sintered glass, in an increment to 20 ~ 30 kPa; one of the obvious reasons for this increased inlet air pressure is that of addition of glycerin into distilled water, that has increased the viscosity of water solution. Due to the increase viscosity, a slightly higher pressure is required to produce similar sized bubble, etc.

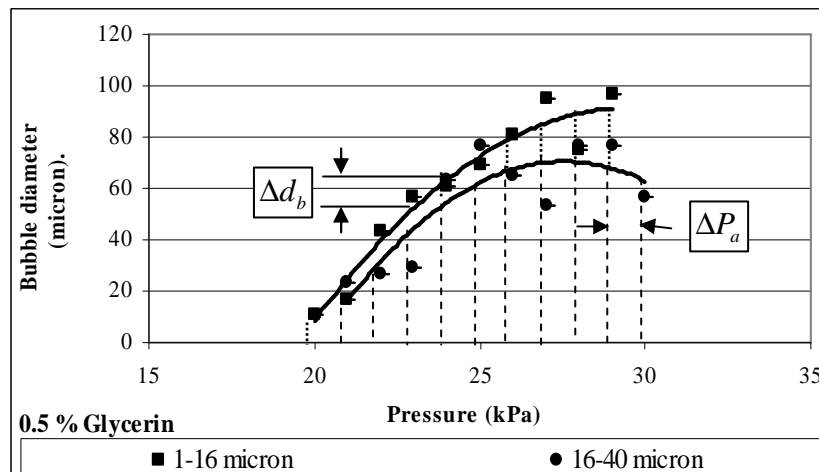


Figure 4.20 The effect of various inlet air pressures on the bubble size through different porosity diffusers in 0.5% glycerin pollutant.

Since the vertical component of velocity is produced by the buoyancy force acted on the bubble, while the buoyancy depend on bubble diameter, therefore vertical component of velocity is dependent on the bubble size, Figure 4.21 shows the relationship between the vertical velocity and the bubble size in distilled water. At any inlet air pressure between 20 and 30 kPa, three categories of bubbles diameter eg. fine, medium and large produced by 1-10, 10-16 and 16-40  $\mu\text{m}$  sintered porous glass diffusers respectively. The second polynomial curve fit is implemented to represent the strong relationship between bubble diameter and vertical velocity. The 1-10 and

10-16  $\mu\text{m}$  porosities give comparable results between vertical velocity and bubble size. On the other hand, the 16-40  $\mu\text{m}$  porosity produces different results, which do not show significant changes in vertical velocity with increasing bubble diameter as shown in Figure 4.21.

Usually, vertical component of velocity is dependent on the bubble size, whereas, bubble size is dependent on porosities and inlet air flow and pressure. Figure 4.21 shows the relationship of vertical velocity to the bubble size in distilled water. Generally, bubbles of larger size would have more vertical velocity.

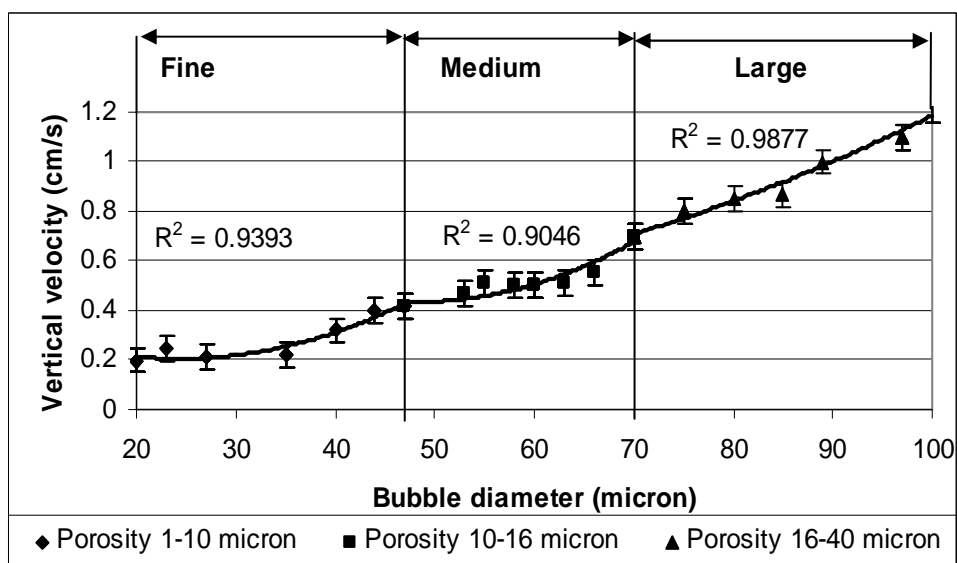


Figure 4.21 Relationship between bubble diameter and vertical velocity in distilled water. Maximum error bar in y direction is  $\pm 5\%$ .

The pollutant concentrations added in water effect on bubble diameter and vertical velocity of bubble production. The investigation show that the more pollutant added the higher vertical velocity would be. The results of any glycerine pollutant at concentration between 0.1% and 0.5% are plotted in Figure 4.22. The vertical velocity increase due to the increased viscosity, water density and decreased surface tension.

Using 16-40  $\mu\text{m}$  porosity sintered glass, a larger population of small bubbles and higher vertical velocity are achieved. The maximum vertical velocity was reached by adding 0.5% glycerin. The physiochemical characteristics bring the change to the bubble dynamic behaviour.

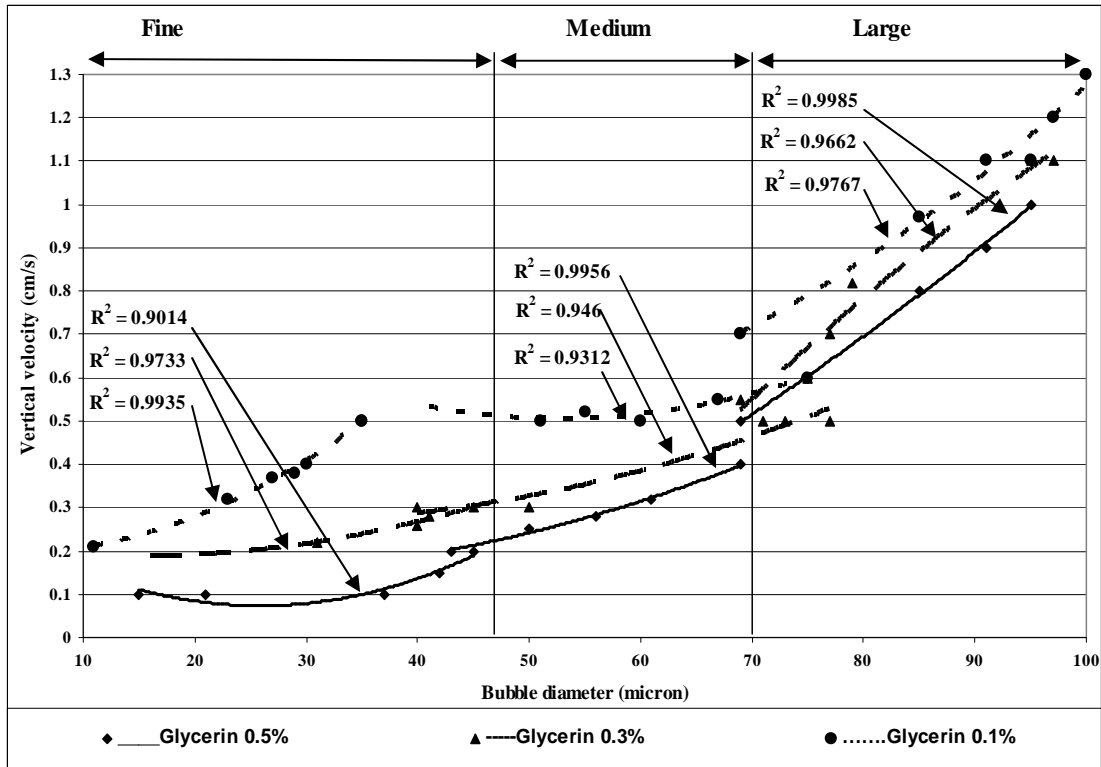


Figure 4.22 Relationship between bubble diameter and vertical velocity in polluted water.

#### 4.1.4 Effect of CMC Polluted on Water Turbidity

The pollutants present in water are categorized as suspended particle or colloid. In this research, the CMC pollutant represents a suspended particle pollutant in the range of 1 to 20 micron. As mentioned earlier, the suspended particles can be lifted-up by the buoyancy force of air bubble in the vertical water column. When the air bubble attaches a suspended particle, they would move together in line as a bubble-particle pair. One of the assumptions is that the bubble is pushing the particle upward vertically. If the bubble is not exerting the force vertically, then the bubble would detach from the particle and the next inline bubble would start pushing the particle. These steps continue until these bubble-particle pair reaches to the top surface of water column. Implementing equation (3.37) (for bubble bigger than the particle diameter) and equation (3.41) (for bubble smaller than the particle diameter), which

experimental bubble and interpretation particle size (1~220 micron), the relationships between diameter and velocity ratio ( $v_B/v_C$ , where  $v_C = v_{B(S)} + v_P$ ) is plotted in Figure 4.23. Assuming the diameter ratio (Rd) as the ratio between the bubble diameter (db) and the particle diameter (dp), The graph shows the different sets of Rd, one with  $Rd < 1$  and the other as  $Rd \geq 1$  (dot plotted). The first line in the graph legend is  $Rd < 1(40)$ , it means that dp smaller than db and the number in bracket is bubble diameter (db=40). The particle diameter (dp) is varied in the range between 0 to 40 micron. The first dot line in the graph legend is  $Rd \geq 1(40)$ , it means that dp is larger than db and the bubble diameter is 40 micron, whereas the particle diameter is in the range between 40 to 80 micron. The second line legend is  $Rd < 1(60)$ , it means that dp smaller than db, bubble diameter is 60 micron and the particle varied from 0 to 60 micron diameter. The second dot line legend is  $Rd \geq 1(60)$ , it means the particle is larger than bubble in diameter, the particles diameter is varied in the range in between 60 to 120 micron. The next legend is similar meaning with different value of bubble and particle diameter. The  $v_B/v_C \leq 1$  when dp is smaller than db, the  $v_B = v_C$  when dp is equal to db, and the  $v_B/v_C \geq 1$  where dp is bigger than db.

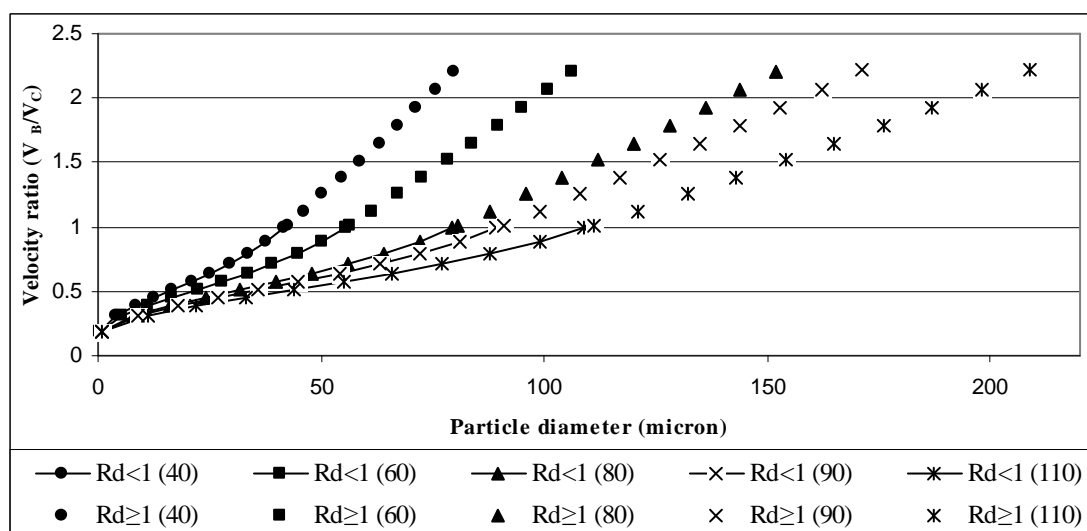


Figure 4.23 Velocity ratio( $v_B/v_C$ ) versus particle diameter.

To investigate the potential of the micro bubble to lift-up the suspended particle in the water column, it is necessary to imitate the suspended particle in the wastewater

using CMC polluted water. Because of the opaqueness of the CMC polluted water solution, the PDA can not be used to measure the micro bubble characteristics (bubble size and velocities) of that water. The one possible to study the bubble characteristic is used the transparent solution like glycerin polluted water. The physiochemical characteristics of glycerin solution should be similar with real wastewater, which are surface tension, viscosity and density. Those are the volume percentages of glycerin; 0.3, 0.4 and 0.5 are added in the distilled water. By taking the 40 microns bubble diameter and particle size varied in the range of 0 to 40 ( $Rd < 1$ ) and 40 to 80 ( $Rd \geq 1$ ), the relationship between combined upward velocity (bubble-particle pair velocity) and particle diameter is plotted in Figure 4.24 follow.

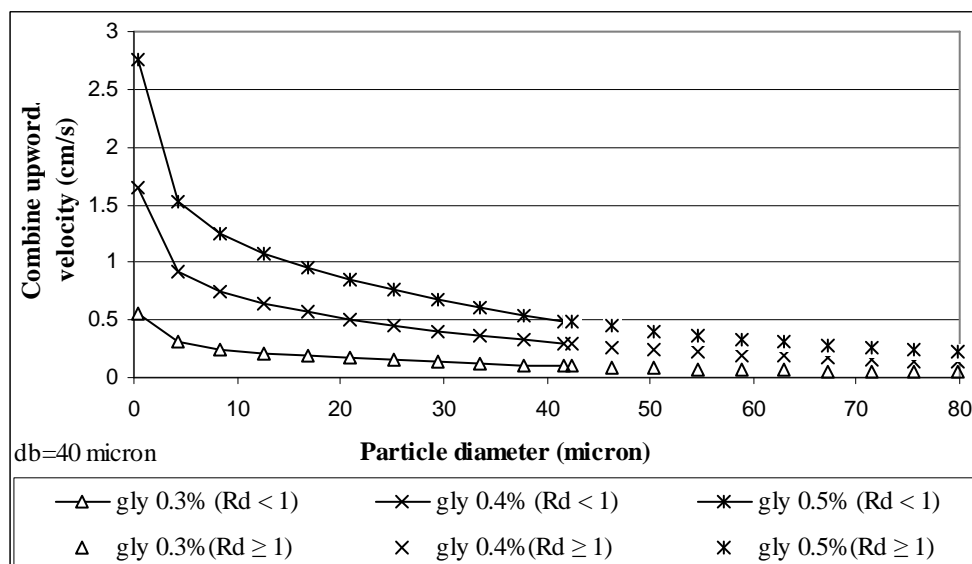


Figure 4.24 Relationship between the suspended particle diameter and combine velocity ( $v_c$ ).

The higher velocity ratio ( $v_B/v_C$ ), the larger particle can be lifted-up. To achieve the higher velocity ratio need to increase the bubble size, due to the bigger bubble size the higher buoyancy force and then the higher bubble velocity would be. After the bubble attach the particle, their velocity would be slower than the initial bubble velocity, therefore the larger particle the slower combine velocity ( $v_{B(S)} + v_p$ ) would be. Figure 4.24 shows the particle size in between 0 to 20 micron give the significant combine velocity, therefore CMC particles size in the range between 1 and 20 is used.

Some dosages of CMC have been added into distilled water, and their turbidity levels have been measured, the relationship between the turbidity level and the PPM of CMC water polluted solution is listed in Table 4.6 and is plotted in Figure 4.25. The graph shows that the higher CMC is added, the higher would be the Turbidity level

Table 4.6 The Comparison of PPM and Turbidity using CMC solution.

PPM	Turbidity
0	0.07
250	0.6
500	1.45
750	2.53
1000	2.54
1500	4.3
2000	5.92

The PPM equation is formulated in turbidity level follow:

$$PPM = 340.12 \times \text{Turbidity} + 21.91 \dots \dots \dots (4.1)$$

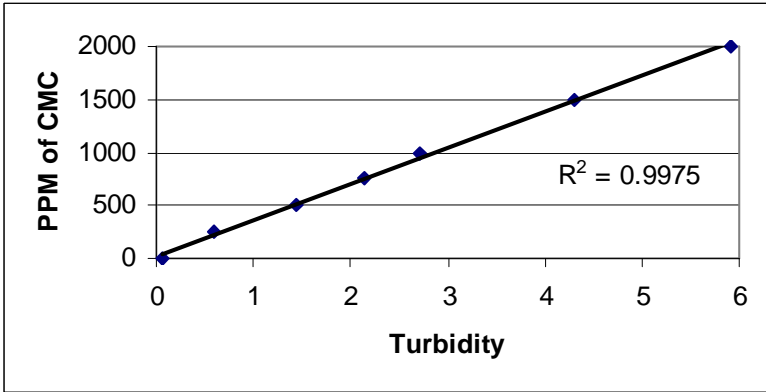


Figure 4.25 The linearity of PPM and Turbidity of CMC population in distilled water.

Tables 4.7, 4.8 and 4.9 list the decreasing of turbidity level of CMC polluted water after the aeration process has been applied using fine bubbles (10-45 micron), medium bubbles (45-70 micron) and larger bubbles (70-100 micron). Table 4.7 the turbidity level decreases from 6.767 to 3.569. after six hours aeration process. It is found that of

the aeration process continues beyond six hours, it does not change the Turbidity level. Therefore for further turbidity level decreasing, bubble size should be changed.

The maximum turbidity level decreasing per liter air of aeration process reach 0.153 NTU /liter using the 1-10  $\mu\text{m}$  porous sintered glass diffuser, while using the 10-16  $\mu\text{m}$  and the 16-40  $\mu\text{m}$  porous sintered glass diffuser reach 0.077 NTU/liter and 0.031NTU/liter respectively.

Table 4.7 The decreasing of turbidity level using 1-10  $\mu\text{m}$  porous sintered glass.

Aeration time (hour)	Air flow l/min	Aeration volume (liter)	Turbidity (NTU)	Turbidity decreasing
0	0.2	0	6.767	
1	0.2	12	4.937	1.83
2	0.2	24	4.321	0.616
3	0.2	36	3.94	0.381
4	0.2	48	3.747	0.193
5	0.2	60	3.586	0.161
6	0.2	72	3.569	0.017
10	0.2	120	3.549	0.02

Table 4.8 The decreasing of turbidity level using 10-16 $\mu\text{m}$  porous sintered glass.

Aeration time (hours)	Air flow l/min	Aeration volume (liter)	Turbidity (NTU)	Turbidity decreasing
0	0	0	7.138	
1	0.4	24	5.29	1.848
2	0.4	48	4.399	0.891
3	0.4	72	3.587	0.812
4	0.4	96	3.491	0.096
5	0.4	120	3.406	0.085
6	0.4	144	3.390	0.016
10	0.4	240	3.373	0.019

Table 4.9 The decreasing of turbidity level using 16-40 $\mu$ m porous sintered glass.

Aeration time (hour)	Air flow l/min	Aeration Volume (liter)	Turbidity (NTU)	Turbidity Decreasing
0	0	0	7.044	
1	0.8	48	5.556	1.489
2	0.8	96	4.519	1.037
3	0.8	144	4.031	0.488
4	0.8	192	3.847	0.184
5	0.7	210	3.846	0.001
6	0.7	252	3.566	0.280
10	0.7	420	3.500	0.066

Figure 4.26, shows the relationships between aeration volume and turbidity decreasing. The first line in the graph, the smallest air flow (0.012 m<sup>3</sup>/s) is used, The smallest air flow would be the smallest volume of air used in aeration process (0.072 litre). The second line in the graph represent turbidity decreasing in aeration process using air flow 0.4 litre/min. Compare among the three kind of air flow rate in aeration process, the minimum turbidity level decreasing is achieved when apply the 0.012 m<sup>3</sup>/s reduce Turbidity level from 6.7 NTU to the level 3.5 NTU.

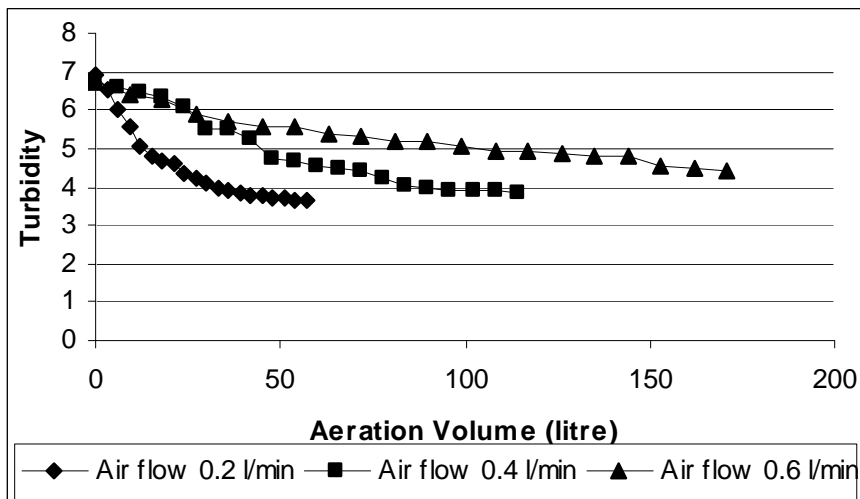


Figure 4.26. The turbidity of CMC solution in distilled water versus micron bubble aeration volume using 1-10 $\mu$ m porous sintered glass.



In this research the effectiveness of turbidity decreasing achieve in 5 hours aeration process. The 0.012 m<sup>3</sup>/s air flow is the better result of Turbidity decreasing as shown in Figure 4.27

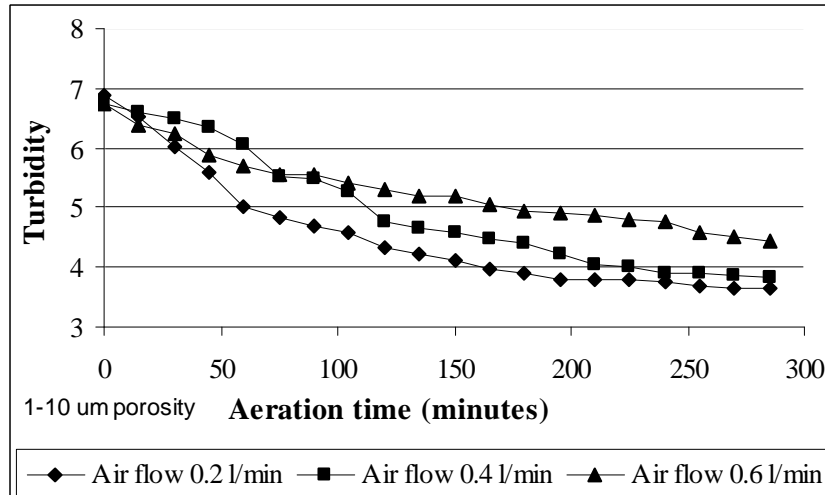


Figure 4.27 The turbidity of CMC solution in distilled water vs micron bubble aeration time using 1-10 µm porous sintered glass.

Figure 4.28 and 4.29 show the effectiveness of the micro bubble aeration in Turbidity decreasing achieves when 12 10<sup>-3</sup> m<sup>3</sup>/s air flow is applied. The suitable air flow rate and the time duration for reducing the Turbidity level in aeration process show the characteristic of the diffuser.

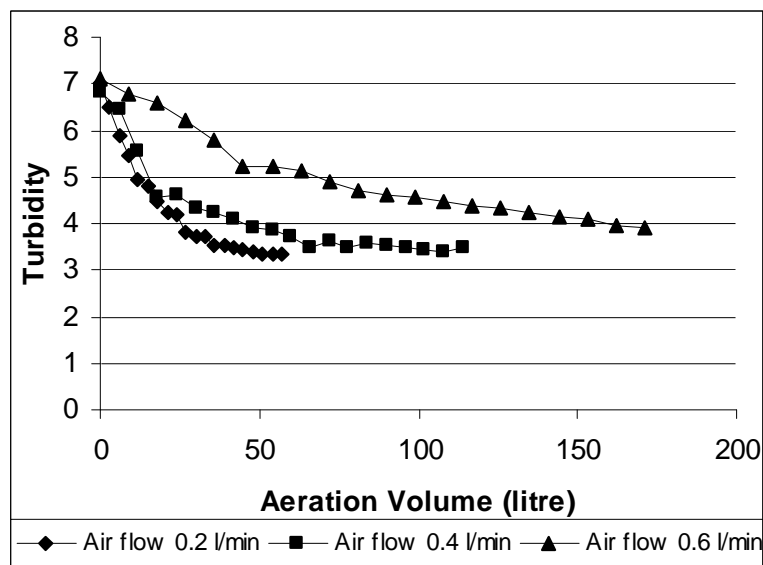


Figure 4.28 The turbidity of CMC solution in distilled water vs micron bubble aeration volume using 10-16µm porous sintered glass.

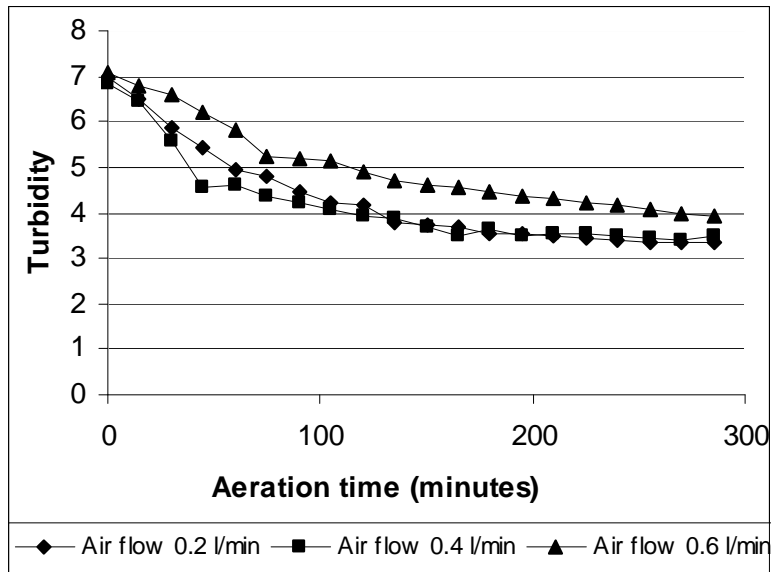


Figure 4.29 The turbidity of CMC solution in distilled water vs micron bubble aeration time using 10-16 $\mu$ m porous sintered glass.

The smaller porosity of sintered glass, producing fine bubbles (10-45 micron) shows a better performance of the turbidity level decreasing. The micro bubble upward movement would sweep the suspended particle off to the surface. Some of the immersed particles that move close to the wall of the container would move down with the passage of water and settle down around the diffuser. This continuous process would separate the suspended particles from the solution, whereas the suspended particles can not be totally separated. However a significant reduction of water turbidity level shows the effectiveness of aeration using micro bubbles.

The suspended particle has similar density with water since it floats in the water. Due to the density similarity, the suspended particle can be pushed upward by the micro bubble, as long as the micro bubble has suitable velocity that has been produced by buoyancy force. After the micro bubble attaches the particle, the bubble-particle pair moves with very low velocity. In the travelling up the drag force would be created and resist the bubble particle pair motion. At this time the diameter and velocity of bubble-particle pair play a role in travelling up, due to the drag force depend on skin friction area and velocity of bubble. The comparison between previous

bubble velocity and bubble-particle pair named velocity ratio that depend on particle diameter, is essential factor in upward motion. For that reason the graph of velocity ratio versus particle removal rate can be plotted in Figure 4.30. It represents the effectiveness of the bubbles in lift-up suspended particle in their travelling to the top of water column. The particle removal rate data is taken from PPM level decreasing that equivalence to turbidity decreasing in aeration process. The aeration is applied to the CMC pollutant water using three porous sintered glass diffusers i.e., 1-10, 10-16 and 16-40  $\mu\text{m}$ . The bubble production can be categorized in fine, medium and large bubble that can be produced by 1-10, 10-16 and 16-40  $\mu\text{m}$  sintered porous glass respectively. The first line in the graph is representing fine bubble to lift-up 20 micron particle size, second line is medium to lift-up 30 micron particle size and the last is large bubble to lift-up 40 micron particle size.

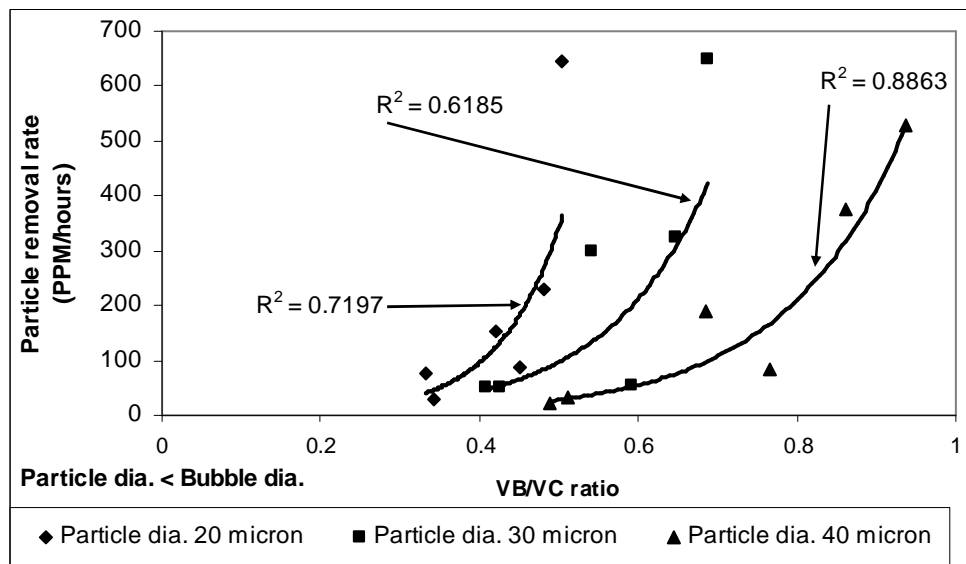


Figure 4.30. The relationship between velocity ratio and particle removal rate.

Figure 4.31 shows an enlarge photograph of micro air bubble using high speed camera. The dark dots are micro bubbles, while the grey background is suspended particles. The 90 to 100 micron diameter of bubble is captured, whereas the particle diameter can not be clearly captured due to the insufficient of the image magnification.

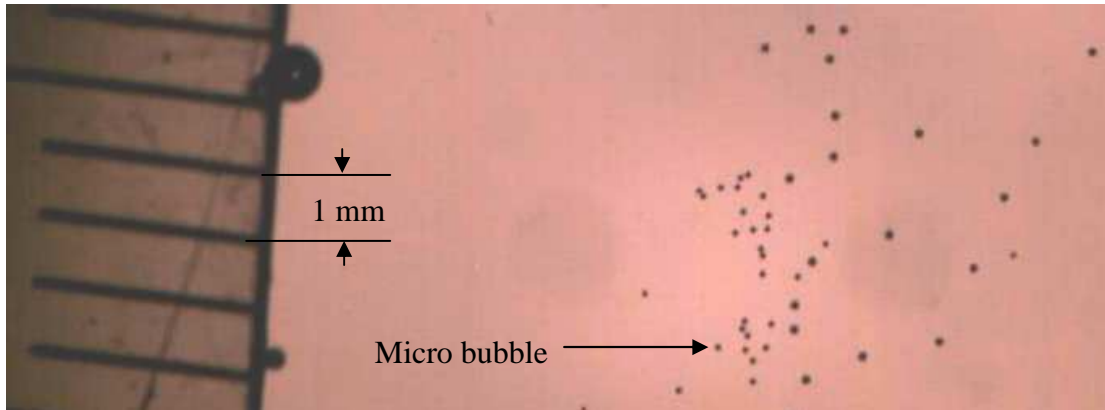


Figure 4.31 The micro air bubble image captured by high speed camera at 2000 fps.

#### 4.2. Biodegradation and Nitrification of Organic Mater

Micro air bubbles provide larger interfacial area for oxygen transfer as the air bubble provides large surface area to volume ratio. Decreasing the bubble diameter from 2.5 mm to 0.5 mm would increase the interfacial contact area between air and water twenty-five times for spherical bubbles. This helps to fulfill the goal of aeration which is to dissolve oxygen into water [6]. Oxygen diffusion is influenced by the interaction between air and the wastewater. Degradation of organic matter and nitrification also depend on the diffusion rate of oxygen into the water. By enhancing the oxygen diffusion rate, higher and faster organic matter removal can be achieved [96]. Therefore the oxidation of ammonia also increased. In the diffusion process, air in the atmosphere has a higher concentration of oxygen than water; hence oxygen diffuses or is pushed from the air into the water [1].

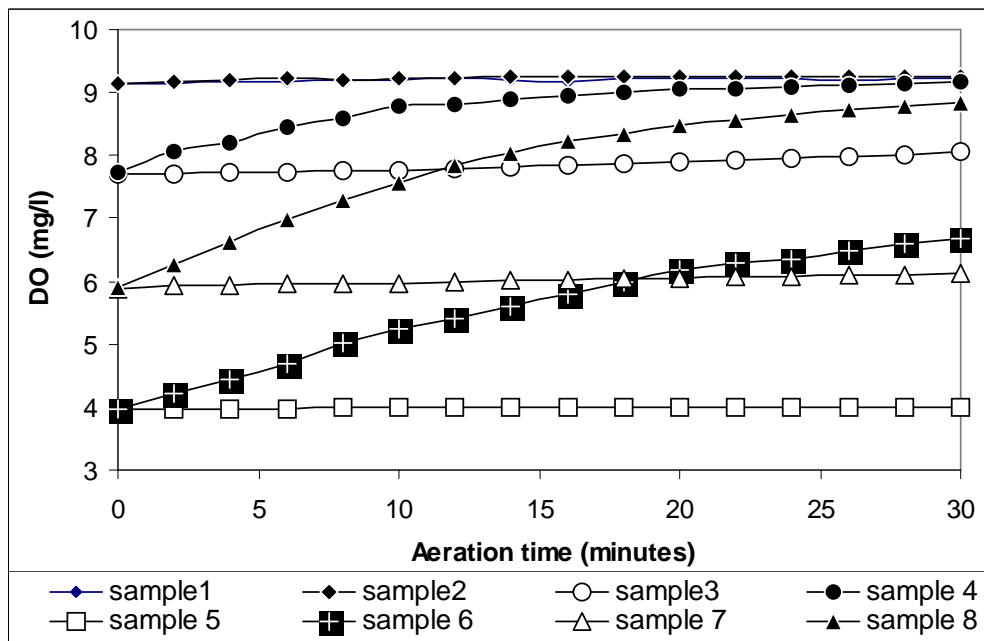
Submerged air diffusers are mostly used to increase dissolved oxygen (DO) levels and promote water circulation. Air or pure oxygen bubbles are released at depth, producing a free, turbulent bubble-plume that rises to the water surface through buoyant force [97]. As the bubble plume ascends, it entrains water, causing vertical circulation and lateral surface spreading. Oxygen is then transferred to the water across the bubble interfaces as the bubbles rise from the diffuser to the top water surface. There are two main interfaces over which oxygen transfer occurs; across the bubble interfaces as the bubbles rise through the water column and across the water

surface at the air-water interface [97]. However, the bubble-transfer rate involved some additional considerations. The liquid-phase equilibrium concentration of a given bubble is not only a function of temperature and atmospheric pressure, but also hydrostatic pressure and gas-phase oxygen composition. As the bubbles rise, bubble-water gas transfer of oxygen, nitrogen, argon, carbon dioxide, and trace gases occurs due to a concentration gradient between the equilibrium bubble concentration and the ambient water concentration. Over depth, the bubble-water transfer of all gases affects the gas-phase oxygen composition and the equilibrium oxygen concentration. The equilibrium oxygen concentration inside a bubble also depends on gas flow rate and the changing bubble-water transfer coefficient over depth [6, 96].

The effect of DO on nitrification is affected by the activated-sludge floc size and the density and total oxygen demand of the mixed liquor [1]. Nitrifying bacteria are mostly distributed within a floc containing heterotrophic bacteria and other solids, with the floc diameters ranging from 100 to 400  $\mu\text{m}$ . Oxygen from the bulk liquid diffuses into floc particles, however bacteria deeper within the floc are exposed to lower DO concentrations. Therefore, a higher bulk liquid DO concentration is required to maintain the same internal floc DO concentration and subsequent nitrification rate [1]. Biodegradation of organic matter is accelerated by increased temperature (20°C to 40°C), but the amount of stoichiometric oxygen needed has to be achieved at first. By using micro bubble aeration the diffused oxygen can be preserved [98]. Dissolved oxygen should also be adequate to support the biodegradation process. As micro bubbles' aeration increase the oxygen diffusion process. Studies have shown that sufficient aeration is required for significant biodegradation of various wastes, such as olive oil husks, Pentachlorophenol (PCP), diesel oil and gasoline contaminated water and petroleum waste [99-103]. Meanwhile, coarse bubbles were found to use more energy and sometimes oxygen absorption is inadequate because the bubbles were quickly raised to the top water surface. However, micro bubbles move slower and take more time to reach water top surface. This gives adequate time for the transfer of oxygen from the bubbles to water medium since there is a longer contact time. Oxygen transfer was also found to be enhanced with or without surfactants [16].

### 4.2.1 DO Level

Figure 4.32 shows the dissolved oxygen. It can be achieved by the micro air bubble aeration. Initially they have different DO level, due to the different capacity to absorb oxygen from the air. Because of the temperature difference of water and air, there would any heat flow from air into water, therefore the elevated temperature of water will reduce the DO. It is occurred until 15 to 20 minutes aeration, after that time the DO will be sloped slightly. It is influent by the saturated oxygen level and also the rising up of water temperature. The incline line curve of micro bubbles aeration shows the lower DO level the higher rate of DO increase, whereas the millimeter bubbles aeration process does not increase the DO level.



Sample	1	2	3	4	5	6	7	8
Water	disti- lled	distilled	tap	tap	influent waste	influent waste	effluent waste	effluent waste
aeration	milli	micro	milli	micro	milli	micro	milli	micro
Density (gr/cm <sup>3</sup> )	1	1	0.997	0.997	0.9976	0.9976	0.996	0.996
Viscosity (cp)	1	1	1	1	1.5	1.5	1.2	1.2

Figure 4.32 DO versus time in various water using millimeter bubble and micro bubble aeration.

Figure 4.33 shows the salinity of resident wastewater of UTP STP (Sewage Treatment Plant). The influent salinity levels' fluctuations show the resident activity in producing wastewater. During the day from 6 am to 18 pm, as showed in sample taking times' interval 0 to 12, the fluctuation is higher than in the night from 18 pm to 5 am. While in the effluent salinity levels show the stability of the treatment process. In the average, the salinity was very low therefore the influence of salinity on DO can be neglected. The Effluent wastewater has higher salinity compare to the Influent wastewater, the higher evaporation of this wastewater is the obvious reason. Therefore the further step to decrease the Effluent wastewater salinity should be applied before flowing to the river.

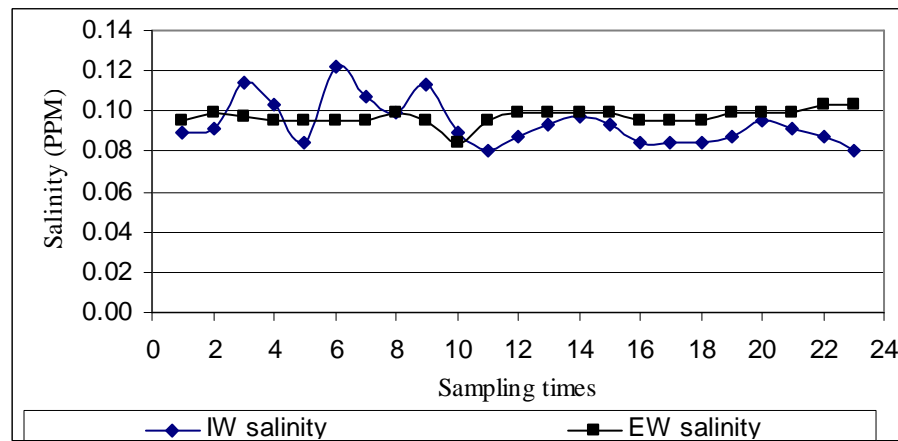


Figure 4.33 The salinity level of UTP wastewater in 24 hours measurement. IW is stand for influent wastewater and EW is effluent wastewater.

#### 4.2.2 COD Removal

The removal of COD throughout the study period was plotted in Figure 4.34 below. In Figure 4.34a, it can be observed that the COD of the wastewater dropped gradually throughout the study period. Samples taken from Reactor B which utilized the micro diffuser showed lower effluent COD concentrations than samples from Reactor A which utilized the millimeter diffuser. The experiment was done twice: first and second trial. It can be observed that the degradation of COD is higher after 12 hours of aeration. The experimental data was expressed in the form the first order kinetic

model with the coefficient rate,  $k$  or the rate of organic matter removal. After obtaining the coefficient rate,  $k$  value, the theoretical COD degradation was plotted for both COD as shown in Figure 4.34b. From the theoretical study, it was found that, the COD degradation kinetic parameter was found to be 0.041 and 0.028, for the micro and millimeter diffusers, respectively. Statistical t-tests conducted on both experimental and theoretical values indicated that there is a significant difference between effluent COD from micro- and millimeter diffuser reactors at 5% level of significance. On average, micro and millimeter diffusers removed COD at approximately 87% and 81%, respectively,

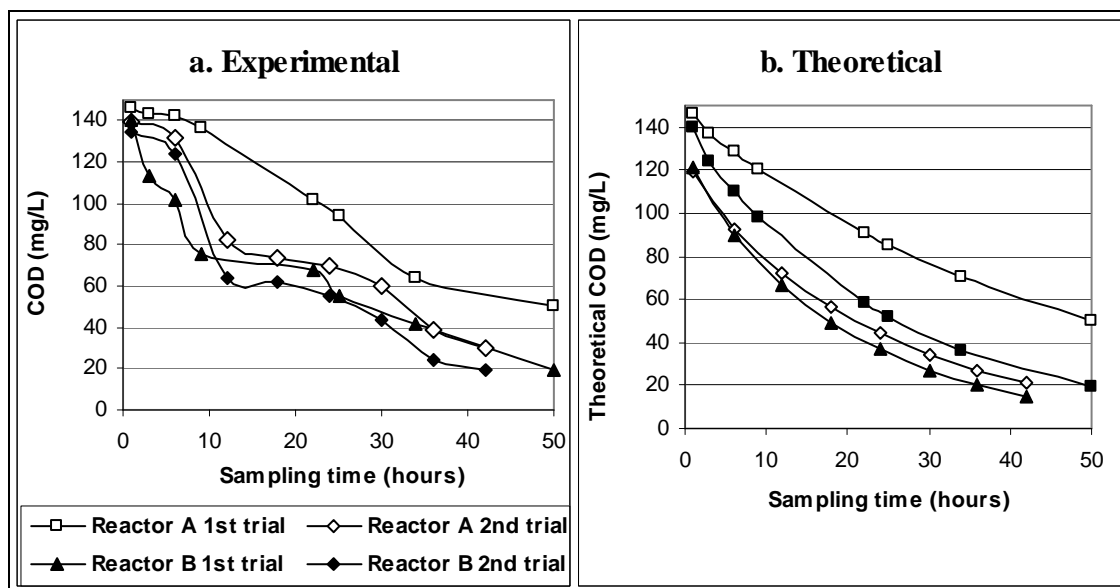


Figure 4.34 Graph of: COD value vs Sampling Time (hrs)

The experimental and theoretical COD degradation rate throughout the study period was plotted in Figure 4.35a and Figure 4.35b, respectively. It can also be observed that the degradation of COD was at a higher rate during the initial stage of the study for Reactor B which utilized micro diffuser compared to Reactor A which utilized millimeter diffuser. This indicates that faster COD degradation rate was achieved using the micro diffuser. The average degradation rate from 30-42 hr of aeration was found to be 3 mg/L.hr and 2.48 mg/L.hr, for micro and millimeter diffuser, respectively. Statistical analysis conducted indicated that both experimental



and theoretical COD degradation rates were significantly different at 10% level of significance for both diffusers.

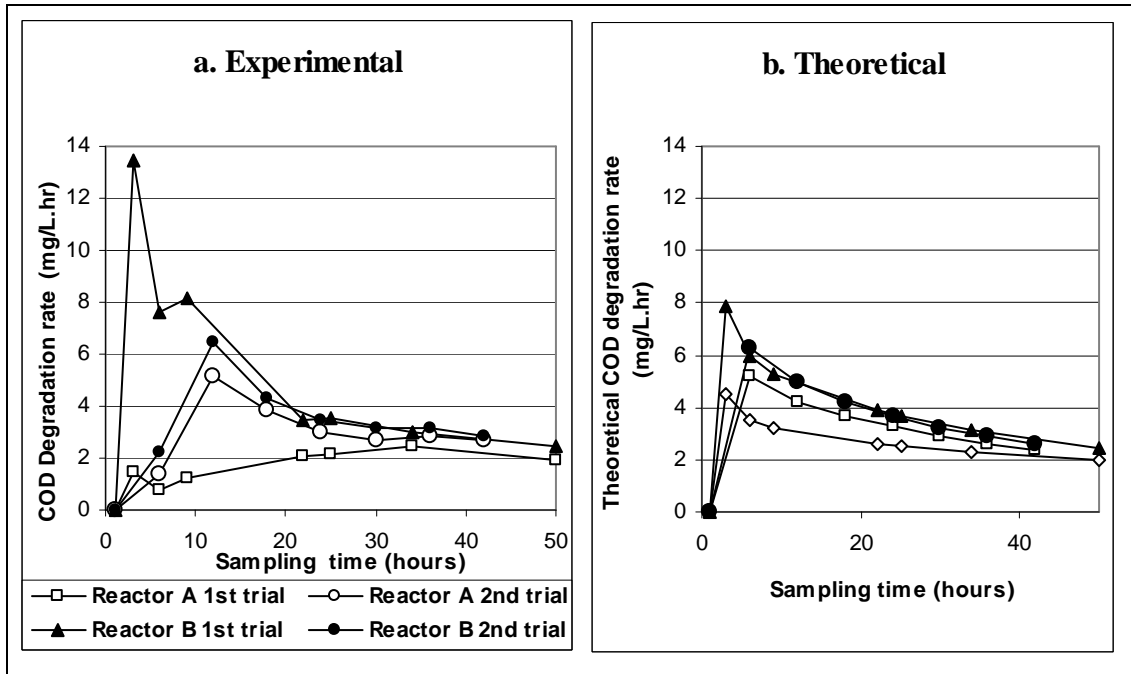


Figure 4.35 Degradation rate of COD.

#### 4.2.3 sCOD Removal

The experimental and theoretical sCOD degradation was plotted in Figure 4.36a and 4.36b respectively. It can be observed from Figure 4.36a that the degradation of sCOD is highest at approximately 10 hours of aeration. The final effluent sCOD for the reactors stabilized at approximately 20 mg/L and 6 mg/L, for millimeter and micro diffusers, respectively, at the end of the sampling period. It can be observed that effluent sCOD from the micro diffuser reactor (Reactor B) stabilized at approximately 24 hours of aeration. The experimental sCOD also closely follows the theoretical sCOD plotted in Figure 4.36b with sCOD degradation rate,  $k_s\text{COD}$  to be 0.060 and 0.044, for micro and millimeter diffuser, respectively. On average, micro and millimeter diffusers removed sCOD at approximately 91% and 75%, respectively.

Statistical t-tests conducted on both experimental and theoretical values indicated that there is a significant difference between effluent sCOD from micro- and millimeter diffuser reactors at 5% level of significance.

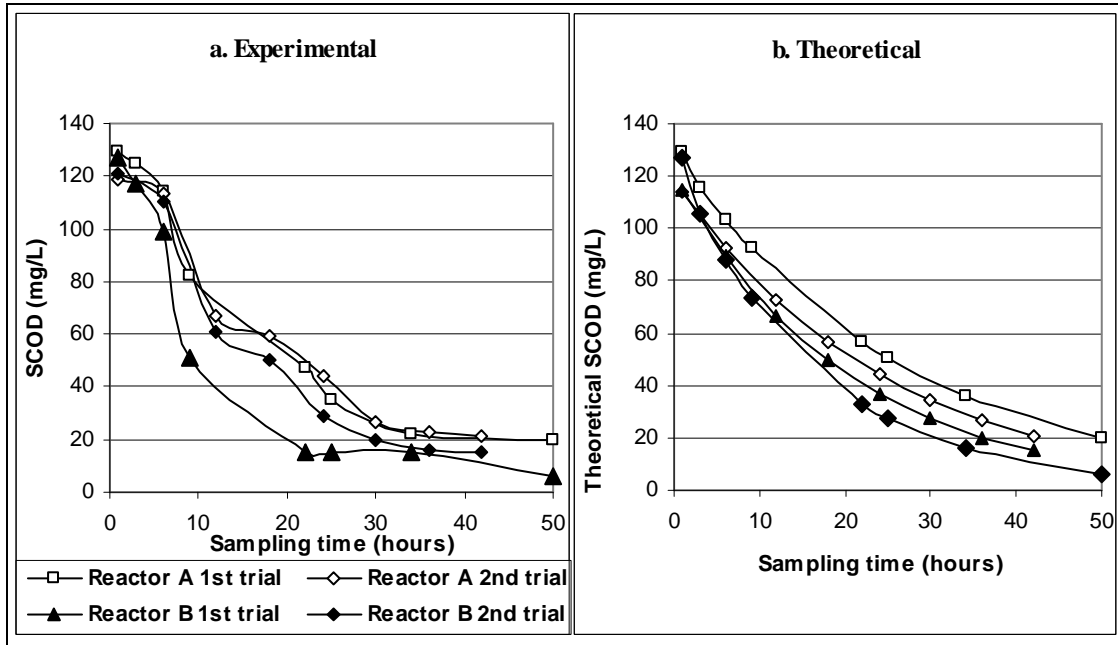


Figure 4.36 Graph of: sCOD vs Sampling time .

The experimental and theoretical sCOD degradation rate throughout the study period was plotted in Figure 4.37a and Figure 4.37b, respectively. It can also be observed that the degradation of sCOD was at a higher rate during the initial stage of the study for Reactor B which utilized micro diffuser compared to Reactor A which utilized millimeter diffuser. This indicates that faster sCOD degradation rate was achieved using the micro diffuser. The average degradation rate from 30-42 hr of aeration was found to be 3 mg/L.hr and 2.5 mg/L.hr, for micro and millimeter diffuser, respectively. The experimental degradation rate also closely follows the theoretical degradation rate with the theoretical degradation rate from 30-42 hr of aeration found to be 3.03 mg/L.hr. and 2.6 mg/L.hr. (average of the values) for micro and millimeter diffuser, respectively. Statistical analysis conducted indicated that both experimental and theoretical sCOD degradation rates were significantly different at 10% level of significance for both diffusers.

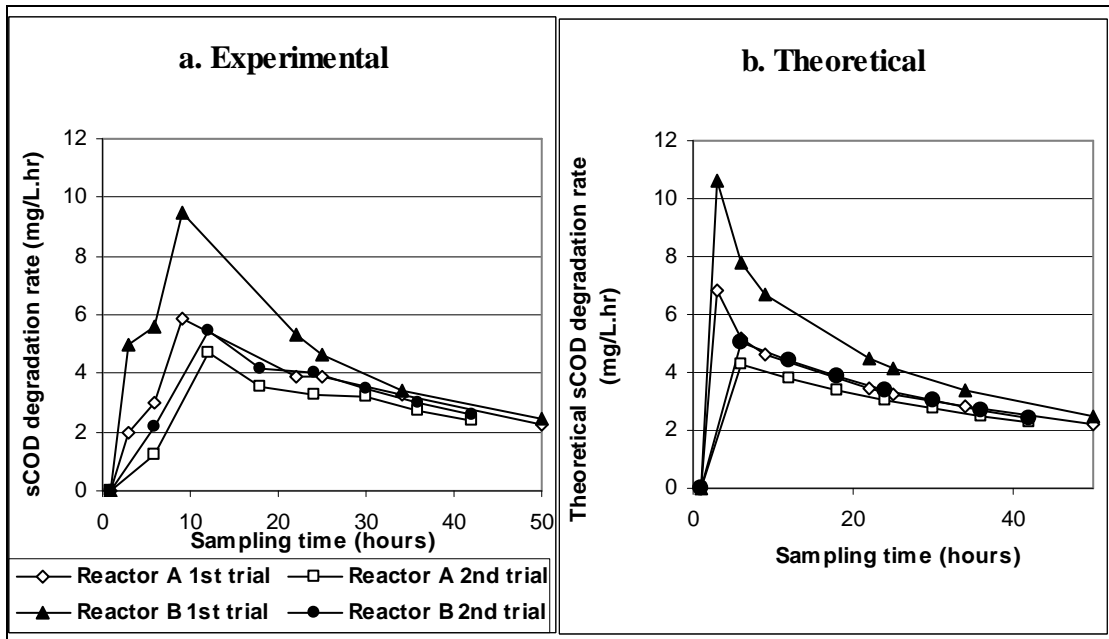


Figure 4.37 Degradation of sCOD

#### 4.2.4 Removal of Ammonia

The removal of ammonia throughout the study period was plotted in Figure 4.38a below. It can be observed that the ammonia removal of the wastewater dropped gradually throughout the study period. Samples taken from Reactor B which utilized the micro diffuser showed lower effluent ammonia concentrations than samples from Reactor A which utilized the millimeter diffuser throughout the study period. The experimental data was expressed in the form of the kinetic modeling so that the first order coefficient rate,  $k$  or the rate of ammonia removal can be calculated to determine the effectiveness of the micro diffuser. After obtaining the first order coefficient rate  $k$ , the kinetic modeling graph was plotted for both reactors in Figure 4.38b. From the theoretical study, it was found that, the ammonia removal kinetic parameter,  $kn$  was found to be 0.062 and 0.053, respectively, for the micro and millimeter diffusers. Statistical T-tests conducted on both experimental and theoretical values indicated that there is a significant difference between effluent of ammonia removal from micro- and milli- diffuser reactors at 5% level of significance. On average, micro and

millimeters diffusers removed ammonia-nitrogen at approximately 90% and 87%, respectively.

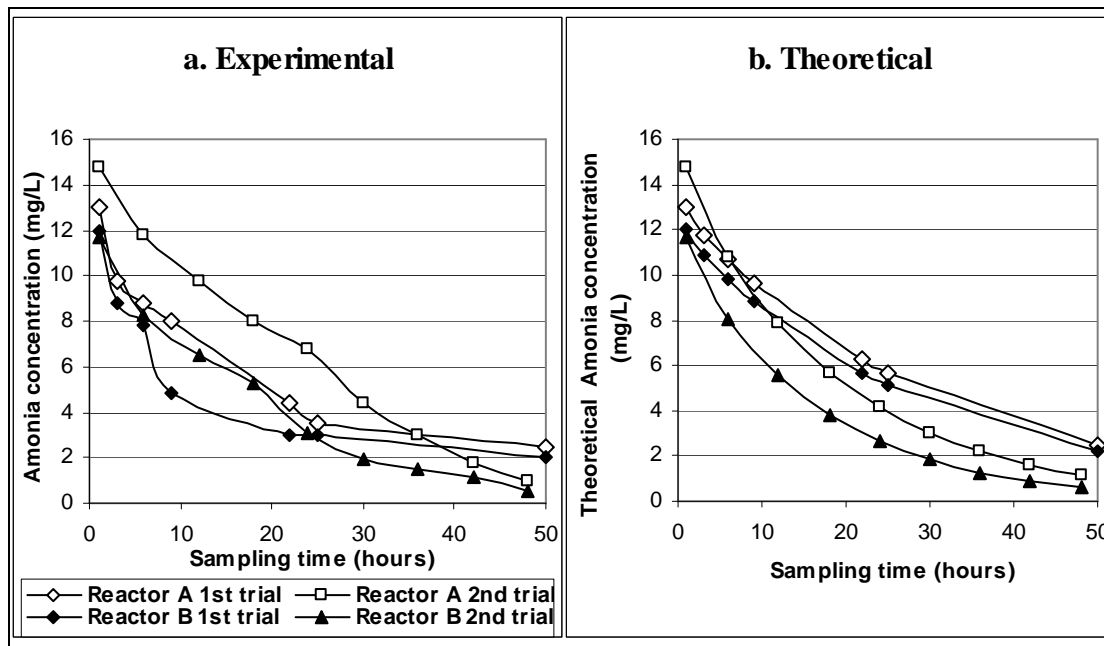


Figure 4.38 Ammonia removal vs sampling time

The experimental and theoretical ammonia removal rate throughout the study period was plotted in Figure 4.39a and Figure 4.39b, respectively. It can also be observed that the removal of ammonia for Reactor B which utilized micro diffuser was as comparable to the ammonia removal rate of Reactor A which utilized milli diffuser. This indicates that faster ammonia removal rate was achieved using the micro diffuser. The final average ammonia removal rate was found to be 0.26 mg/L.hr and 0.3 mg/L.hr, for micro and milli diffuser, respectively.

The experimental ammonia removal rate plotted in Figure 4.39a also closely follows the theoretical ammonia removal rate with the theoretical ammonia removal rate from 22-50 hrs. of aeration found to be 0.29 mg/L.hr and 0.32 mg/L.hr for micro and milli diffuser, respectively. However, statistical analysis conducted throughout the study period indicated that both experimental and theoretical ammonia removal rates were significantly different at 5% level of significance for both diffusers.

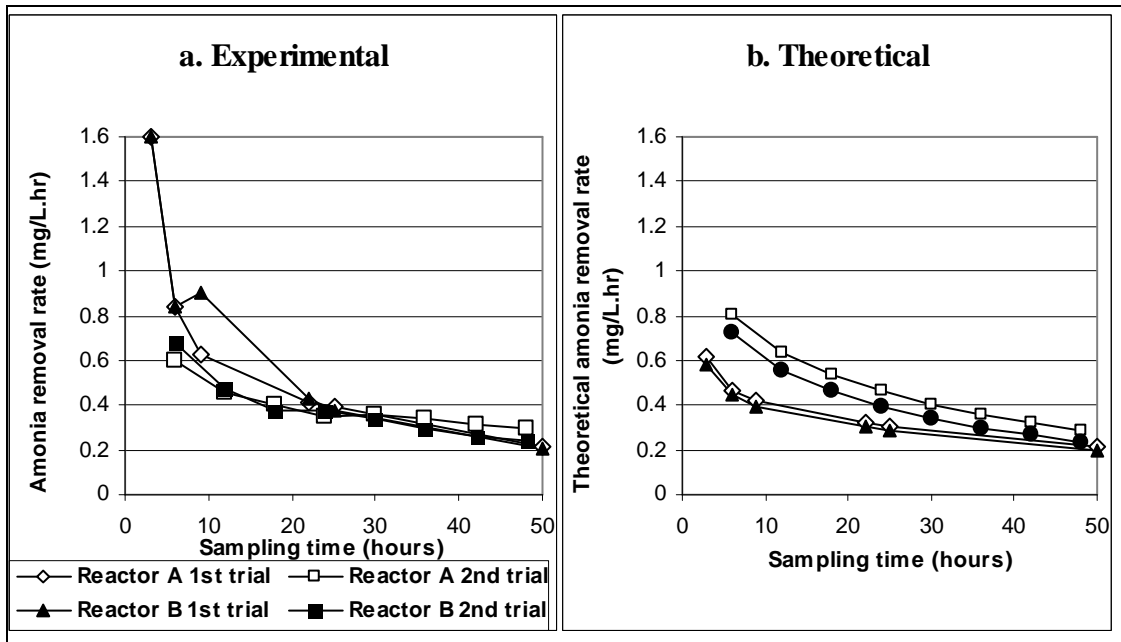


Figure 4.39 Ammonia removal vs sampling time

#### 4.2.5 Oxidation of Ammonia to Nitrate

The experimental and theoretical nitrate-nitrogen produced during nitrification was plotted in Figure 4.40 below. It can be observed from Figure 4.40 that the degradation of ammonia to nitrate essentially stopped at 34 hours for Reactor B in the first trial of the experiment. The final effluent nitrate concentration stabilized at approximately 26 mg/L and 22 mg/L, for milli and micro diffusers, respectively at the end of the sampling period.

Experimentally, the ammonia-nitrogen has been oxidized to nitrate-nitrogen at a faster rate for Reactor B which utilized the micro-diffusers. Effluent nitrate concentration from Reactor B can be seen to stabilize after 34 hours of aeration. Statistical T-tests conducted on experimental values indicated that there is a significant difference between effluent nitrate from micro- and submilli-diffuser reactors at 10% level of significance.

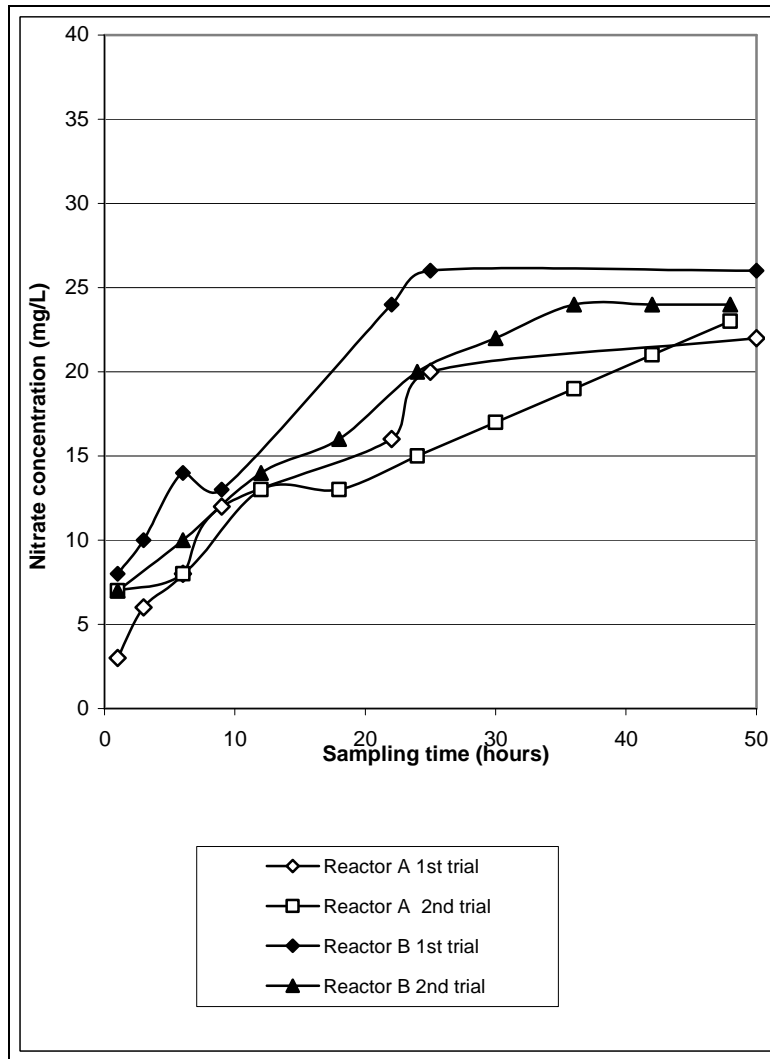


Figure 4.40 Nitrogen removal vs sampling time.

The experimental nitrate production rate throughout the study period was plotted in Figure 4.41. It can also be observed that the nitrate production rate was generally higher for Reactor B after 18 hours of aeration. This indicates that faster nitrate production was achieved using the micro diffuser. The average nitrate production rate from 30-40 hrs of aeration was found to be 0.44 mg/L.hr and 0.33 mg/L.hr, for micro and milli diffuser, respectively.

Statistical analysis conducted indicated that experimental nitrate production rate were significantly different at 10% level of significance for both diffusers from 34-40 hours of aeration.

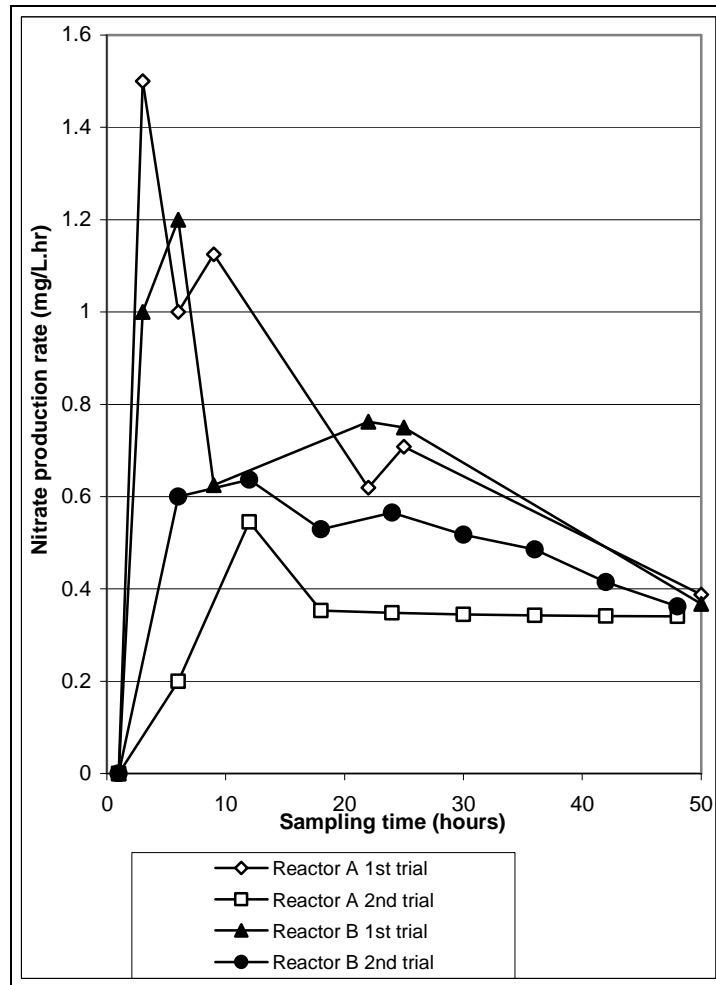


Figure 4.41 Nitrate Production vs sampling time

### 4.3 Summary

Size of the bubbles and velocities are the main parameters to be measured, whereas the inlet air pressure, air flow and porosities are the variables. Millimeter and micro size bubbles show altogether different dynamic behaviour in a vertical water column. Millimeter size bubbles add turbulence and acts as water stirrer, due to high velocity components (vertical and horizontal) and low surface tension (at the air-water surface contact), therefore they exhibit frequent shape change. These parameters add an influence of high buoyancy force and low surface tension. A reduction in the bubble size (millimeter to micro) tends to change the upward velocity, buoyancy force, drag

force and eventually a little or no turbulent effect. The changing of surface tension influence the bubble size generation, therefore the bubble shape changing is less frequent and bubble maintain its spherical shape during its upward motion. Generally, the spherical shape has high vertical velocity, therefore have more force to push the suspended particle upward. In the same air inlet volume through the diffuser, the micro bubbles have much more population compare to millimeter bubble, therefore the micro bubble have high possibility to attach the suspended particle. To produce millimeter bubble need sub- millimeter diffuser, whereas to produce micro bubble size need less than 40 micron porosity of sintered glass diffuser.

Monodispersed air bubbles are released at an inlet air pressure of 22 kPa or below, whereas, a combination of monodispersed and polydispersed bubbles are produced at a pressure range of 22 kPa to 27 kPa. However, when the inlet air pressure is increased beyond 27 kPa, only polydispersed bubbles are produced, and horizontal velocity increase. The phenomena of collision and emerging of bubble start with increased horizontal velocity component. These dynamic behaviours of air bubbles show that air pressure is a significant variable in controlling the generation of micro air bubble. A number of forces are acting on the air bubble at the time of its generation and detachment from diffuser surface into the water. The physical behaviors (size and velocities) of air bubble are controlled by the depth of column and physiochemical characteristics of water like surface tension, density, viscosity, etc. The depth of water column would determine the level of air inlet pressure adjusted.

Adding the glycerin pollutant to distilled water would increase the viscosity and density and decrease surface tension which consequently influence the bubbles generation. The bubble size determines its velocities, both horizontally and vertically, which generate their motion in the water column. Two conditions of bubble flow are laminar and turbulent. The smaller bubbles have laminar upward movement and the bigger bubbles have turbulent movement. The deformation of bigger bubble shape is one reason the turbulent flow exist.



The micro bubbles can entrain the suspended particles that remain in the water. The proposed method has been investigated the effectiveness to lift-up suspended particles from polluted water. Even though the scope of this study only covers CMC (carboxy methyl cellulose) suspended particles, the proposed method has potentials to be applied to other types of suspended particles. This claim is validated by experimental results, which show that the turbidity level in CMC polluted water decreased from 6.9 to 3.1 after five hours aeration using micro bubbles. The micro bubbles have smaller buoyancy and drag force. Applied small buoyancy and drag force, the lifting process is stronger than the stirring process.

From the study it was found that the reactor with micro- diffuser achieved higher percentage removals of COD, sCOD, and ammonia-nitrogen compared to the reactor with millimeter diffuser. Similarly, slightly higher degradation rates of COD, sCOD and ammonia-nitrogen were achieved for the reactor using the micro diffuser. This shows that there is a potential use of the micro diffuser in wastewater treatment as higher rate of oxygen diffusion into the water. Even the energy needed in producing micro bubbles is higher than milli bubbles, but in the certain condition like, the degree of suspended particle removal, the DO level, and or the quality Biodegradation and Nitrification, this system is reasonable and affordable to apply.



## CHAPTER 5

### CONCLUSIONS AND RECOMMENDATIONS

#### 5.1 Conclusions

The size of micro bubble production by the porous sintered glass diffuser depends mainly on the porosities and air inlet pressure. The capability of smaller porosity diffuser to produce uniform bubble (monodispersed) is higher than that of the larger porosity, whereas the larger porosity diffuser has the higher possibility in producing sets of various sized bubbles (polydispersed). Inlet air pressure to the diffuser is directly proportional to the size of bubbles. The size of bubble generation is influenced by the water level in the water column and is discussed in section 4.1.2.2 Generally, the higher water level requires more inlet air pressure to generate bubble, thus increasing the size of bubble. The effect of the buoyancy force is discussed in section 4.1.2.3, and it is found that the larger bubble diameter, would produce more buoyancy force, because of higher vertical velocity component. On the other hand, as the diameter of the rising bubble increases it would increase the Reynolds number that mainly depends upon bubble size, vertical velocity and viscosity of the liquid.

The dynamics of micro bubble in upward motion is influenced by the physiochemical characteristic of water medium like surface tension, density and viscosity. The bubble size and its velocity have been measured using PDA and is discussed in section 4.1.3.1. The relationship between bubble diameter and its velocities has been achieved in a linear curve fit with correlation factor ( $R^2$ ) of 0.9. By the addition of pollutant to water, upward velocity of the bubbles increase because of decreased surface tension. By increase of percentage pollutant to water, bubble size production decrease because of increase water density and viscosity. The physiochemical characteristics of water is discussed in section 4.1.3 and found that the resident wastewater has physiochemical characteristics close to those of 0.4% by

volume glycerin added in distilled water. The relationship between the inlet air flow and Reynolds number has been plotted in the line curve fit with correlation factor ( $R^2$ ) of 0.9, as discussed in section 4.1.3.2. The pollutant added into water, the Reynolds number decrease from 60 to 40 at  $12 \text{ E-3 m}^3/\text{s}$  inlet air flow. The relationship between bubbles' upward velocity and Froude number is achieved to be linear, thus the Froude number is less than one.

The effectiveness of micro bubble in removing suspended particles is fully dependent on the micro bubble dynamics and the suspended particle size. The bubble dynamics are controlled by the forces acting on a single moving bubble and/or a bubble-particle pair. These forces acting on the moving bubbles are detailed in section 3.8.1 and section 3.8.2. The evaluation is discussed in section 4.1.4 The bubble characteristics (diameter and velocities) are taken from the experimental data, while the particle size is assumed to be 1 to 220 micron, the relationship between the particle size and vertical velocity ratio (single bubble/bubble-particle pair velocity) is plotted. For entrain the larger particle size the higher velocity ratio is needed. The relationship between the particle size and bubble-particle pair velocity (combine velocity) shows the bigger particle the slower combined velocity. The optimum capability of micro bubble for entrain suspended particle is achieved when the particle size is in a range of 1 to 20 micron. The faster velocity of bubble upward motion is the most wanted parameter for the suspended particles entrains. The removals of pollutants from the water are characterized by the Turbidity level. Generally, the higher the turbidity, the more pollutant in the water is. The maximum turbidity removal rate is 0.153 /liter (using 1-10  $\mu\text{m}$  porous sintered glass) that has been achieved in Six hours micro bubbles aeration.

The effectiveness of micro bubble in enhancing the DO level has been achieved due to the higher surface area/volume interface between air and water and sufficient time to dissolve oxygen from air to water along their slower upward motion in the water column. The two types of diffuser made from perforated aluminium disk and porous sintered glass has been used in aeration process for the degradation of organic matter, however, they differ in terms of the efficiency and oxygen transferred. The removal of COD and sCOD are discussed in section 4.2.2 and 4.2.3 Generally, COD

and sCOD value reduces over time as the organic matter is removed from the wastewater by metabolizing microorganisms. The oxygen transfer rate using micro bubble aeration is greater than the millimeter bubble. The higher oxygen diffusion result in the higher COD and sCOD removal. Based on the calculated kinetics coefficient rate,  $k$ , it is calculated that the micro bubbles have higher effectiveness with average  $k$  value for COD and sCOD with 0.041 and 0.0595 respectively. While  $k$  value for millimeter bubbles have 0.0275 and 0.044 for COD and sCOD removals. On average the micro bubble aeration process removed 86.77 percent of COD and 90.86 percent of sCOD, while millimeter bubble aeration process remove 80.39 percent of COD and 75.13 percent of sCOD. As its efficiency of micro bubble aeration, the micro porous sintered glass diffuser has been used as another alternative type of more efficient in Sewage Treatment Plant aerators. Even though the energy needed is 2.2 to 3.5 time compare to milli bubble, but in the higher degree result of biodegradation level this micro bubble could be applied.

The higher nitrification rate has been achieved using the micro air bubbles aeration. The removal of ammonia and the oxidation of ammonia-nitrogen to nitrate-nitrogen are discussed in section 4.2.4 and 4.2.5 respectively. The mixing process between the organic matter and the substance is properly occurred in micro bubble aeration process. The micro bubble can enhance the rate of ammonia removal as well as the oxidation of ammonia-nitrogen to nitrate-nitrogen in wastewater treatment. The 90% efficiency of ammonia removal can be achieved.

## **5.2. Research Contributions**

Based on these results, it is concluded that the micro bubble aeration represent a new capability in wastewater treatment. The contributions of the research include:

- Developing a new system of wastewater treatment where the proper and the effective process should be fulfilled.
- Developing a new system of increasing quality and quantity of water treatment.

Previous aeration process in wastewater treatment using millimeter bubble has insufficient DO level and need more time for biodegradation of organic matters, thus

in the millimeter bubble aeration, further process is needed. While using the micro bubble aeration the DO level is achieved at proper time and the lower turbidity of treatment water is resulted.

### **5.3. Research Recommendations**

In the future, the propose method has many potential possibility application of micro bubble aeration in:

- Various other types and sizes of suspended particle in the water should be studied.
- Elimination the pathogen microorganism using elevated air inlet temperature.

## REFERENCES

- [1] E. Metcalf, *Wastewater Engineering Treatment and Reuse*, McGraw-Hill: international edition, 2004.
- [2] T. G. Susan, T. F. Edward, W. K. Dana, B. B. Larry, *Evaluation of wastewater chemicals as indicators of human fecal contamination*. Cincinnati, OH: U.S. Environmental Protection Agency (U.S. EPA), 2005.
- [3] American Public Health Association, American Water Works Association, Water Environment Federation, "Standard Methods for the Examination of Water and Wastewater," 1999.
- [4] I. S. Chang, J. Simon, Judd, "Air sparging of a submerged MBR for municipal wastewater treatment," *Process Biochemistry*, vol. 37, pp. 915–920, 2002.
- [5] E. Li, Z. X. Ying, Y. Fan, "Air–water ratio as a characteristic criterion for fine bubble diffused aeration systems," *Chemical Engineering Journal* 2007, submitted for publication
- [6] W. A. Burris, "Discovery of factors affecting bubble size in water," *Water technology*, pp. 54-57, 1999.
- [7] United\_States\_Environmental\_Protection\_Agency, "Wastewater Technology Fact Sheet Fine Bubble Aeration," *EPA 832-F-99-065 September* , 1999.
- [8] S. I. U Gilani., F. E. W. Winarto, Rangkuti C., Aziz A.R., "Dynamic behaviour of air bubbles generated by a submerged micro hole diffuser in a water purification system," *Icper*, 2008.
- [9] F.E.W. Winarto, S. I. U Gilani, "Study of dynamic behaviour of micro bubbles in distilled water and polluted water," *Icper*, 2010.
- [10] R. Pohorecki, W. I. Maniuk, P. Bielski, Artur Dabrowiecki, "Modeling of the coalescence-redispersion processes in bubble columns," *Chemical Engineering Science*, vol. 56, pp. 6157-6164, 2001.
- [11] R. Pohorecki, W. I. Maniuk, P. Bielski, P. Sobieszuk, G. Dabrowiecki, "Bubble diameter correlation via numerical experiment," *Chemical Engineering Journal*, vol. 113 , pp. 35–39, 2005.
- [12] A. C. Yunus, M. C. John, *Fluid Mechanics Fundamentals and Applications*. Singapore: Mc Graw Hill, 2006.

- [13] G.Q.Yang, Bing Du, and L. S. Fan, "Bubble formation and dynamics in gas–liquid–solid fluidization a review," *Chemical Engineering Science*, vol. 62 , pp. 2 - 27, 2006.
- [14] H. Xu C. Gustari, "Numerical simulations of a train of air bubbles rising through stagnant water," *International ANSYS conference proceedings*, 2004.
- [15] A. A. Kulkarni, B. Jyeshtharaj "Bubble formation and bubble rise velocity in gas-liquid system: a review," *India Engineering Chemical*, vol. 44, pp. 5873-5931, 2005.
- [16] C. Liu, L. Chang, Jing Liang Yang, Jian Bo Guo, Zai Xing Lin, "Effect of surfactants on oxygen transfer in microbubble aeration," *Energy and environment Technology*, vol. 2, pp. 531-534, 2009.
- [17] L Cheng a, D. Mewes, A. Luke, "Boiling phenomena with surfactants and polymeric additives: A state-of-the-art review," *International Journal of Heat and Mass Transfer*, vol. 50 , pp. 2744–2771, 2006.
- [18] J. W. M. Bush, (2006, March),"Surface tension module," *lecture note Departement of Mathematics, MIT, Taken from <http://web.mit.edu/alexmil/Macdata/afs.course /1/1.63/www/lec-notes/surfacetension Lecture1.pdf>, date 1 march 2011*, vol. lecture module 4, pp. 1-4.
- [19] J. Z. Yang, J. Tong, Jing-Bin Li, Ji-Guan Li, Jian Tong, "Surface tension of pure and water-containing ionic liquid C5MIBF4 (1-methyl-3-pentylimidazolium tetrafluoroborate)," *Journal of Colloid and Interface Science*, vol. s0021-9797(07)00376-1, pp. 1-7, 2007.
- [20] T.-S. Sheu and J.-C. Shyu, "Study on bubble formation at a submerged micro-hole by a two-stage model," *Journal of the Chinese Institute of Engineers*, vol. 28, No. 5, pp. 849-858 , 2005.
- [21] A. Zaruba, Dirk Lucas, Horst-Michael Prasser, and T. Höhne, "Bubble-wall interactions in a vertical gas–liquid flow: Bouncing, sliding and bubble deformations," *Chemical Engineering Science*, vol. 62 , pp. 1591 - 1605, 2007.
- [22] L.-S. Fan, G. Q. Yang, D. J. Lee, K. Tsuchiya, and X. Luo, "Some aspects of high-pressure phenomena of bubbles in liquids and liquid}solid suspensions," *Chemical Engineering Science*, vol. 54 , pp. 4681-4709, 1999.



- [23] I. Leifer, (2003, February) "Bubble rise velocity and Bubble measurement system," Available in [www.bubbleology.com/hydrodinamycs.html](http://www.bubbleology.com/hydrodinamycs.html)
- [24] A. A Kulkarni., "Lift force on bubbles in a bubble column reactor: Experimental analysis," *Chemical Engineering Science.*, vol. 63, pp. 1710-1723, 2008.
- [25] J. Soubiran, J. D. Sherwood,"Bubble motion in a potential flow within a Venturi," *International Journal of Multiphase Flow*, vol. 26, pp. 1771-1796, 2000.
- [26] W. Dijkhuizen, E. I. V. v. d. Hengel, N. G. Deen, M. v. S. Annaland, and J. A. M. Kuipers, "Numerical investigation of closures for interface forces acting on single air-bubbles in water using Volume of Fluid and Front Tracking models," *Chemical Engineering Science*, vol. 60 , pp. 6169 - 6175, 2005.
- [27] R. Pohorecki , P. Bielski, P. Sobieszuk, G. D. abrowiecki, "Bubble diameter correlation via numerical experiment," *Chemical Engineering Journal*, vol. 113 , pp. 35–39, 2005.
- [28] R. Pohorecki, P. Bielski, Artur Zdrojkowski, "Modelling of the coalescence-redispersion processes in bubble columns," *Chemical Engineering Science*, vol. 56, pp. 6157-6164, 2001.
- [29] M. Tange, (2004) "Dynamical Models of Bubble-bubble Interactions in Isothermal and Boiling Systems," *an University of Tokyo Thesis*.
- [30] W. Kracht, J. A. Finch,"Effect of frother on initial bubble shape and velocity," *International journal of Mineral processing*, vol. 94, pp. 115-120, 2010.
- [31] J. Katz, C. Meneveau, "Wake-induced relative motion of bubbles rising in line," *International journal multiphase flow*, vol. 22, pp. 239-258, 1996.
- [32] M. C. Ruzicka, "On bubble rising in line," *International Journal of Multiphase Flow*, vol. 26, pp. pp 1141-1181, 2000.
- [33] R. Scafer, C Merten, R., Eigenberger G., "Bubble size distributions in a bubble column reactor under industrial conditions," *Experimental Thermal and Fluid Science*, vol. 26, pp. 595-604, 2002.
- [34] K. Idogawa, K. Ikeda, Fukuda F., Morooka S., "Effect of gas and liquid properties on the behavior of bubbles in a column under high pressure," *International Chemical Engineering*, vol. 27, pp. 93-99, 1987.

- [35] P. M. Wilkinson, (1991, March) "Physical aspects and scale-up of high pressure bubble columns," *an University of Groningen thesis, taken from <http://dissertations.ub.rug.nl/faculties/science/1991/p.m.wilkinson>*,
- [36] T. Hong , L. S. Fan, Lee D.J., "Force variations on particle induced by bubble-particle collision," *International Journal of Multiphase Flow*, vol. 25, pp. 477-500, 1998.
- [37] P. Paimanakul, P. Sastaravet, Lersjintanakarn S., Khaodhiar S., "Effect of bubble hydrodynamic and chemical dosage on treatment of oily wastewater by induced Air Floatation (IAF) process," *Chemical Engineering Research and design*, vol. 396, pp. 10, 2009.
- [38] K. Vamsi, K. Paruchuri, Dinesh O. Shah, Jan D. Miller, "The effect of consurfactants on sodium dodecyl sulfate micellar structures at a graphite surface," *Colloids and Surfaces A: Physicochem. Eng. Aspects*, vol. 272, pp. 157-163, 2006.
- [39] M.E. Shawkat, Y. C. Chang, M. Shoukri, "Bubble and liquid turbulence characteristics of bubbly flow in a large diameter vertical pipe," *International Journal of Multiphase Flow*, vol. 34, pp. 767-785, 2008.
- [40] J. Zahradnik, M Fiolova, Ruzicka M., Drhos J., Kastanek F., Thomas N. H., "Duality of the gas-liquid flow regimes in bubble column reactors," *Chemical Engineering Science.*, vol. 52, pp. 3811-3826, 1997.
- [41] C. J. Yang, J. Chen, W. Ge, J. Li, "A conceptual model for analyzing the stability condition and regime transition in bubble columns," *Chemical Engineering Science*, vol. 65, pp. 517-526, 2010.
- [42] A. Tomiyama, G. P Celata, Hosokawa S., Yoshida S., "Terminal velocity of single bubbles in surface tension force dominant regime," *International Journal of Multiphase Flow*, vol. 28, pp. 1497-1519, 2002.
- [43] Z. Dongjian, G. Liejin, Lin Changzhi, Zhang Ximin, "An experimental study on local interfacial area concentration using a double-sensor probe," *International Journal of Heat and Mass Transfer*, vol. 48 , pp. 1926–1935, 2005.

- [44] S. Assemi, A. V. Nguyen, Jan D. Miller, "Direct measurement of particle-bubble interaction forces using atomic force microscopy," *International journal mineral process*, vol. 89, pp. 65-70, 2008.
- [45] A. V. Nguyen, G. M. Evans, J. Nalaskowski, J. D. Miller, "Hydrodynamic interaction between an air bubble and a particle: atomic force microscopy measurements," *Experimental Thermal and Fluid Science*, vol. 28, pp. 387-394, 2004.
- [46] A V. Nguyen, J. Nalaskowski, Jan D. Miller, "The dynamic nature of contact angles as measured by atomic force microscopy," *Journal of Colloid and Interface Science*, vol. 262, pp. 303-306, 2003.
- [47] R. A. Pushkarova, R. G. Horn "Surface forces measured between an air bubble and a solid surface in water," *Colloids and Surfaces A: Physicochem. Eng. Aspects*, vol. 261, pp. 147–152, 2005.
- [48] J. Ralston, D. Fornasiero, Robert Hayes, "Bubble-particle attachment and detachment in flotation," *International journal mineral process*, vol. 56, pp. 133-164, 1999.
- [49] A.V. Nguyen, J. Nalaskowski, J.D. Miller, "A study of bubble-particle interaction using atomic force microscopy," *Minerals Engineering*, vol. 16, pp. 1173-1181, 2003.
- [50] A. V. Nguyen, J. Nalaskowski, Jan D. Miller Hans-Jurgen Butt, "Attraction between hydrophobic surfaces studied by atomic force microscopy," *International journal mineral process*, vol. 73, pp. 215-225, 2003.
- [51] F. Omata, A. C. Dimian, Alfred Bliet, "Adhesion of solid particles to gas bubbles. Part I: Modelling," *Chemical Engineering Science*, vol. 62, pp. 823-834, 2006.
- [52] A. V. Nguyen, G. M. Evans, "Movement of fine particles on an air bubble surface studied using high-speed video microscopy," *Journal of Colloid and Interface Science*, vol. 273, pp. 271-277, 2004.
- [53] C. M. Phan, A. V. Nguyen. Jan D. Miller, Geoffrey M. Evans, Graeme J. Jameson, "Investigations of bubble-particle interactions," *International journal mineral process*, vol. 72, pp. 239-254, 2003.

- [54] W. Zhang, R. B. H. Tan. "A model for bubble formation and weeping at a submerged orifice with liquid cross-flow," *Chemical Engineering Science*, vol. 58, pp. 287-295, 2003.
- [55] N. Yang, J. Chen, Hui Zhao, Wei Ge, Jinghai Li, "A conceptual model for analyzing the stability condition and regime transition in bubble columns," *Chemical Engineering Science*, vol. 65, pp. 517-526, 2010.
- [56] J. Michael, W. B. Harvey, J. Prince, "Bubble Coalescence and Break-Up in Air-Sparged Bubble Columns," *AIChE Journal*, vol. 36, pp. 1485-1500, 1990.
- [57] L. Huilin, S. Zhiheng, J. Ding, L. Xiang, and L. Huanpeng, "Numerical simulation of bubble and particles motions in a bubbling fluidized bed using direct simulation Monte-Carlo method," *Powder Technology*, vol. 169, pp. 159-171, 2006.
- [58] W. Shuyan, L. Huanpeng, L. Huilin, L. Wentie, J. Ding, and L. Wei, "Flow behavior of clusters in a riser simulated by direct simulation Monte Carlo method," *Chemical Engineering Journal*, vol. 106, pp. 197-211, 2005.
- [59] J. Hua and J. Lou, "Numerical simulation of bubble rising in viscous liquid," *Journal of Computational Physics*, submitted for publication, 2006.
- [60] M.S. Politano, P. M. Carrica, J. Converti, "A model for turbulent polydisperse two-phase flow in vertical channels," *International Journal of Multiphase Flow*, vol. 29, pp. 1153-1182, 2003.
- [61] Berthier, (2011, March) "Dimensionless numbers in microfluidics," taken from [www.artechhouse.co.getblob.aspxstr](http://www.artechhouse.co.getblob.aspxstr).
- [62] M. Michaud, Teresa, L., Kelvin, F., Steve C., "Choosing the right Aeration System," *Lagoon Systems in Maine, Water Quality-our Maine Concern, Department of Environmental Protection, State of Maine*, 2003.
- [63] R. Nielsen, *The little green handbook*. New York: Picador, 2006.
- [64] J A Dean, "'Lange's Handbook of Chemistry, McGraw-Hill", New York," 1992.
- [65] H. Enwald, E. Peirano, A. E. Almstedt, and B. Leckner, "Simulation of the fluid dynamics of a bubbling fluidized bed. Experimental validation of the two-fluid model and evaluation of a parallel multiblock solver," *Chemical Engineering Science*, vol. 54, pp. 311-328, 1999.

- [66] C.C.Pain, S Mansoorzadeh, C.R.E.D. Oliveira, "A study of bubbling and slugging fluidized beds using the two-fluid granular temperature model," *International Journal of Multiphase Flow* 27, 527-551, 2001.
- [67] A.V Nguyen, P George, Jameson G.J., "Demonstration of a minimum in the recovery of nanoparticles by floatation: Theory and experiment," *Chemical Engineering Science* 61, 2494-2509, vol. 61, pp. 2494-2509, 2006.
- [68] M.J. Betancur, F. Martinez, C. Ocampo, J.A. Marino, G Buitron, I. Mareno-Andrade, "Acclimation model of an aerobic bioreactor for the treatment of toxic wastewater," *Simulation Modeling Practice and theory* 17 pp 680-691, 2009.
- [69] A Blastakova., I. Bodik, Dancova L., Jakubcova Z., "Domestic wastewater treatment with membrane filtration-two years experience," *Desalination* 240 pp 160-169, 2009.
- [70] W. Zhichau, W. Xinhua, W Zhiwei, Du Xingzhi, "Identification of sustainable flux in the process of using flat-sheet membrane for simultaneous thickening and digestion of waste activated slugde," *Journal of Hazardous Materials* 162 pp 1397-1403, 2009.
- [71] E. Smidt , V. Parravicini, "Effect of sewage sludge treatment and additional aerobic post-stabilisation revealed by infrared spectroscopy and multivariate data analysis," *Bioresource Technology* 100, pp 1775-1780, 2009.
- [72] J.-M. Chern, S. R. Chou, and C.-S. Shang, "Effects of impurities on oxygen transfer rates in diffused aeration systems," *Wat. Res.*, vol. 35, No. 13, pp. 3041–3048, 2000.
- [73] V. Mavrov, A. Fihnrich, and H. Chmiel, "Treatment of low-contaminated waste water from the food industry to produce water of drinking quality for reuse," *Desalination*, vol. 113, pp. 197-203, 1997.
- [74] R. Kumar, "Application of environmental Biotechnology in wastewater," *Institute of Genomics & Integrative Biology*, vol. 110007, 2006.
- [75] K. Amit, Argaval, Anand yethiraj, "Low-Density Ordered Phase in Brownian Dipolar Colloidal Suspensions," *PHYSICAL REVIEW LETTERS*, vol. PRL 102, pp. 198301.1-19883.4, 2009.

- [76] F. C-Escobar, J. P. Marin, P. Álvarez-Mateos, F. Romero-Guzmán, M.M. Durán-Barrantes, F. Barriga-Mateos, "Aerobic purification of dairy wastewater in batch reactors: kinetic study of the influence of a pre-storage stage without aeration in the degradation of organic matter and ammonium consumption by nitrification," *Process Biochemistry*, vol. 40, pp. 549-556, 2005.
- [77] E. Emmanuel, Y Perrodin, Gérard Keck , Jean-Marie Blanchard , Paul Vermande, "Effects of hospital wastewater on urban wastewater systems and ecological risk Bibliography," *Congreso Interamericano de Ingeniería Sanitaria Y Ambiental*, vol. XXVIII, 2001.
- [78] New\_Jersey\_Departement\_of\_Health\_and\_Senior\_Services, *Hazardous Substance Fact Sheet*. Trenton, NJ 08625-0360: Occupational Health Service, PO Box 360, 2003.
- [79] Holt, David, Rory D. Tood, Anaick Delanoue, and J. S. Colbourne, "A study of nitrite formation and control in chloraminated distribution systems," *In Proc. 1995 AWWA Water Quality Technology Conference*, vol. Part II, 1995.
- [80] C Antileo, A. Werner. Ciudad G, Munos C, Bornhardt C, Jeison D, Urrutia H., "Novel operational strategy for partial nitrification to nitrite in a sequencing batch rotating disk reactor," *Biochemical Engineering Journal*, vol. 32, pp. 69-78, 2006.
- [81] K. Okuyama, "Formation of a strong, high-porosity spinodal silica and its impregnation with a perfluoro ionomer to obtain a high performance solid acid catalyst composite," *J. Mater. Chem*, vol. 10, pp. 973-980, 2000.
- [82] M. Kukizaki and M. Goto, "Spontaneous formation behavior of uniform-sized microbubbles from Shirasu porous glass (SPG) membranes in the absence of water-phase flow," *Colloids and Surfaces A: Physicochem. Eng. Aspects*, vol. 296 , pp. 174–181, 2006.
- [83] M. Kukizaki and M. Goto, "Size control of nanobubbles generated from Shirasu-porous-glass (SPG) membranes," *Journal of Membrane Science*, vol. 281 , pp. 386–396, 2006.
- [84] Elena Diaz, F. J. M. M. Miguel, A. Galan, "Influence of the lift force closures on the numerical simulation of bubble plumes in a rectangular bubble column," *Chemical Engineering Science*, vol. 64, pp. 930-944, 2009.

- [85] G. Shen and J. A. Finch, "Bubble swarm velocity in a column:a two-dimensional approach," *Chemical Engineering Science.*, vol. 52, pp. 3287-3293, 1997.
- [86] Dantec, (February 2011)."Dantec dynamics A/S 2002 manual book," *retrieve from [www.dantecdynamics.com](http://www.dantecdynamics.com)*.
- [87] FASTCAM, "Fastcam-x 1280pci hardware manual," *PHOTRON LIMITED*, 2002.
- [88] C. Parmer (2011), "Oakton waterproof EW -35641-00 DO meter product detail," in *Available:www.coleparmer.com/catalog/product\_view.asp?sku - 3564100*. Illinois 60061,.
- [89] Hach\_Company, "Portable Turbidimeter model 2100P Instrument and Procedure Manual," *Catalog number 46500-88*, 2004.
- [90] Vinci\_Tecnologies\_FRANCE, "IFT 700 for inter-face tension determination Operating Manual," *OpMan IFT700*, 2007.
- [91] Anton\_Paar, "DMA 35N Portable density meter Instruction manual," *Firmware Version V2.014*, 2007.
- [92] Expotech USA, (2011, February) "Model 35 Viscometer Instruction Manual," *taken from [www.ExpotechUSA.com](http://www.ExpotechUSA.com)*.
- [93] Multi-kem,(2010, November) "corporation Food Grade CMC Gum Selection Chart," *retrieve from [www.multikem.com/cellulose\\_food.html](http://www.multikem.com/cellulose_food.html)*
- [94] A Vazquez., I. Liefer Sanchez R.M., "Consideration of the dynamic forces during bubble growth in a capillary tube," *Chemical Engineering Science*, vol. 65, pp. 4046-4054, 2010.
- [95] G.H Yeoh., J. Y Tu. "A unified model considering force balances for departing vapour bubbles and population balance in subcooled boiling flow," *Nuclear Engineering and Design*, vol. 235, pp. 1251-1265, 2005.
- [96] A. N. Anuar, Z. Ujang,, van Loosdrecht M.C.M., Olsson G., "Effects of aerated-mixing condition to the settling characteristics of aerobic granular sludge," *water resource*, 2008.
- [97] H. B. Fisher,J. E. List, Koh R.C.Y.,Imberger J., Brooks N.H., "Mixing in inland and coastal water," *San diego Academic press*, 1979.

- [98] L. Bizzukojc, Liwarska "Stoichiometry of the aerobic biodegradation of the organic fraction of municipal solid waste (MSW)," *Biodegradation*, vol. 14, pp. 51-56, 2003.
- [99] A.F.P Ururahy. M. D. M.Marin, Vital R.L., Gabardo I.T., Nie Pereira Jr., "Effect of aeration on biodegradation of petroleum waste," *Revista de Microbiologia*, pp. 1-13, 1998.
- [100] M. A. Lopez Zavala, "Onsite wastewater differentiable treatment system (OWDTS), an ecological sanitation alternative for developing countries," *XXVIII congreso interamericano de ingenieria sanitaria Y ambiental cancon*, 2002.
- [101] L. Baeta-Hall, S. M. Ceu Bartolomeu M.L., Anselmo A.M.,Rosa M.F., "Biodegradation of olive oil husks in composting aerated piles," *Bioresource Technology*, vol. 96, pp. 69-78, 2005.
- [102] M.N Miller., G. W.Stranton, Murray G., "Effects of soil moisture and aeration on the biodegradation of pentachlorophenol cantaminated soil," *Bull. Environ. Contam. Toxicol*, vol. 72, pp. 101-108, 2004.
- [103] P.A Vieira., R. B Viera.. Faria S., Rebeiro E.J., Cardoso V. L., "Biodegradation of diesel oil and gasoline cantaminated effluent employing intermittent aeration," *Journal of Hazardous Materials*, vol. 168, pp. 1366-1372, 2009.



### List of Journal Publications

1. Kutty, S.R.M. and **Winarto, F.E.W.** and Gilani, S.I.U. and Anizam, A.A. and Karimah, W.W.Z. and Isa, M.H. (2010) Degradation of organic matter using submerged micro bubble diffuser in a biological wastewater treatment system In: Waste Management and the Environment V. WIT Press, pp. 415-423. ISBN 978-1-84564-460-4
2. **Winarto F. E. W.** , Gilani S. I. U., Study The dynamic Behaviour of Micro Bubbles in Distilled and Polluted Water accepted in Journal of Applied Science 2011.

### List of Conferences

1. S. I. U. Gilani, **F. E. W. Winarto.**, Rangkuti C., Aziz A.R., "Dynamic behaviour of air bubbles generated by a submerged micro hole diffuser in a water purification system," *Icper*, Kuala Lumpur, 2008.
2. **F.E.W. Winarto**, S. I. U. Gilani. "Study of dynamic behaviour of micro bubbles in distilled water and polluted water," *Icper*, Kuala Lumpur 2010.
3. **F.E.W. Winarto**, S. I. U. Gilani, "Studying the effect on micro bubbles in removing the suspended particles in CMC polluted water". NPC, Tronoh, Ipoh 2009.
4. S.R.M. Kutty, and **F.E.W. Winarto**, and S.I.U. Gilani, and A.A. Anizam, and W.W.Z. Karimah, and M.H. Isa, "Degradation of organic matter using submerged micro bubble diffuser in a biological wastewater treatment system" WIC (Wessex Institute Conference) Waste management and the environment V conference, Tallinn Estonia Europe, 2010:.
5. **F.E.W. Winarto** and, S.R.M. Kutty, and S.I.U. Gilani, and A.A. Anizam, and W.W.Z. Karimah, and M.H. Isa, " Nitrification using submerged micro bubbles diffuser in an aeration system".Green Technologies for the benefits of Bottom Billions ICNV 2010 (International Conference on Environment 2010) USM Pulau Pinang 2010:

## APPENDICES

### A: Figures of Experimental Set-ups

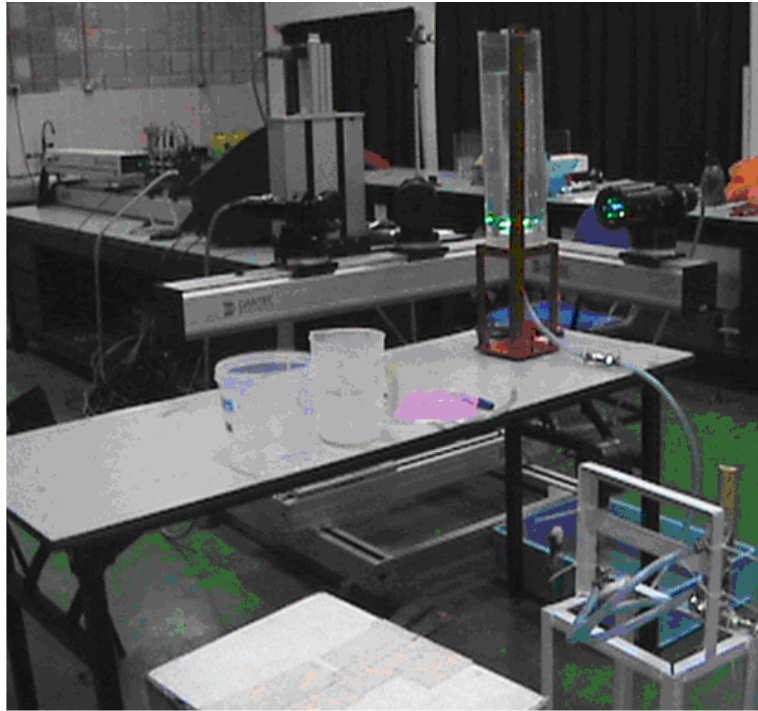


Figure A.1: The Laboratory scale stagnant water column (100 mm W x 100 mm L x 500 mm H)



Figure A.2: The experimental set-up water column (120 mm W x 120 mm L x 2 m H).

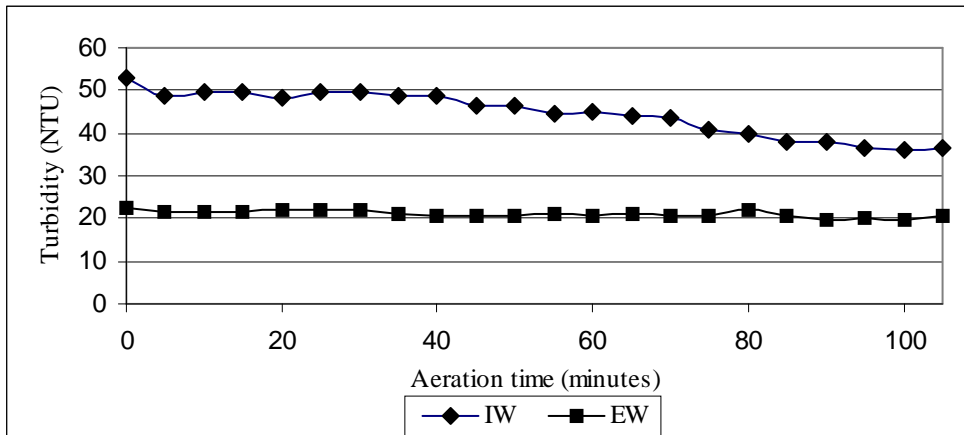
## B: Tables and Figure of Measurement

Table B.1: Comparison of DO (dissolve oxygen) in various water using millimeter air bubble and micro bubble.

Sam- Pling Time (min)	Distilled water		Tap water		influent wastewater		Effluent wastewater	
	sample1	sample 2	sample 3	sample 4	sample5	sample 6	Sample7	sample 8
	Tair=28 milli bubb DO (mg/l)	T <sub>w</sub> =23.4C micro bubb DO (mg/l)	Tair=27C milli bubb DO (mg/l)	T <sub>w</sub> =24.4C micro bubb DO (mg/l)	Tair=27C milli bubb DO (mg/l)	T <sub>w</sub> =23.9C micro bubb DO (mg/l)	Tair=26C milli bubb DO (mg/l)	T <sub>w</sub> =24.4C micro bubb DO (mg/l)
0	9.14	9.13	7.7	7.73	3.97	3.97	5.89	5.9
2	9.15	9.18	7.71	8.05	3.97	4.22	5.92	6.26
4	9.18	9.2	7.72	8.2	3.98	4.45	5.93	6.63
6	9.17	9.23	7.74	8.45	3.98	4.7	5.95	6.99
8	9.21	9.21	7.75	8.6	3.99	5.01	5.96	7.29
10	9.2	9.22	7.77	8.77	3.99	5.24	5.97	7.56
12	9.22	9.23	7.78	8.82	3.99	5.4	5.98	7.83
14	9.19	9.25	7.81	8.9	3.99	5.61	6.01	8.03
16	9.16	9.24	7.83	8.94	4	5.79	6.02	8.23
18	9.23	9.24	7.86	9	4	6	6.03	8.35
20	9.23	9.25	7.89	9.06	4	6.18	6.04	8.49
22	9.23	9.25	7.93	9.05	4	6.28	6.06	8.56
24	9.22	9.25	7.96	9.1	4	6.36	6.08	8.65
26	9.21	9.25	7.99	9.11	4	6.49	6.09	8.74
28	9.23	9.25	8.01	9.14	4	6.6	6.11	8.79
30	9.23	9.25	8.05	9.17	4	6.67	6.12	8.85

Table B.2: Turbidity decreasing of wastewater using micro bubble aeration

Time minutes	Influent wastewater turbidity NTU	Effluent wastewater turbidity NTU
0	53	22.3
5	48.8	21.7
10	49.7	21.6
15	49.7	21.7
20	48.4	22.1
25	49.5	21.8
30	49.6	21.9
35	48.9	20.9
40	48.7	20.4
45	46.4	20.4
50	46.3	20.5
55	44.5	21.1
60	44.9	20.8
65	44.1	21.1
70	43.8	20.5
75	40.7	20.6
80	39.9	21.9
85	38.1	20.8
90	38	19.6
95	36.4	20.2
100	36.3	19.9
105	36.4	20.6



Sample 1 Using Raw wastewater (density 0.9976 gr/cm<sup>3</sup>, viscosity 1.5 cp)

Sample 2 Using Effluent wastewater (density 0.996 gr/cm<sup>3</sup>, viscosity 1 cp)

Figure B.1 Turbidity decreasing of wastewater using micro bubble aeration

**C. Measurement Apparatus (Figures and Specification Tables).**

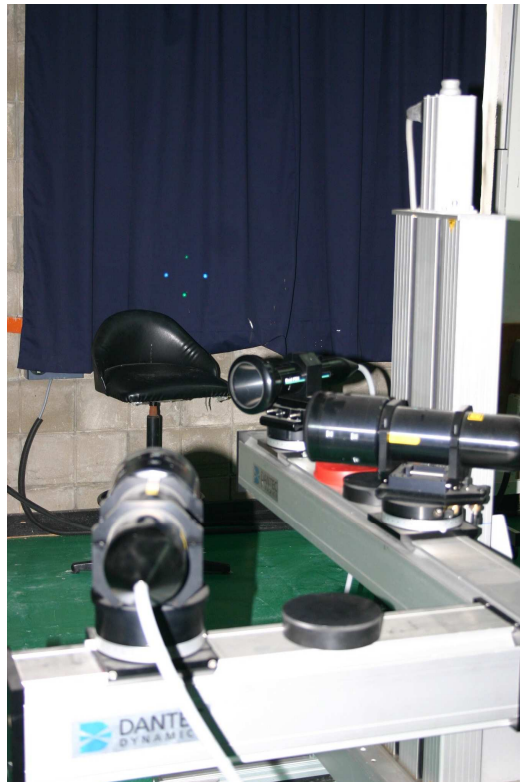


Figure C.1 The Laser Doppler Anemometry (PDA) used to measure the bubble size and velocities.



Figure C.2 The Fastcam-x1280pci camera head [87].



Figure C.3 The DO meter.[88]



Figure C.4 The Hach 2100P portable Turbidimeter



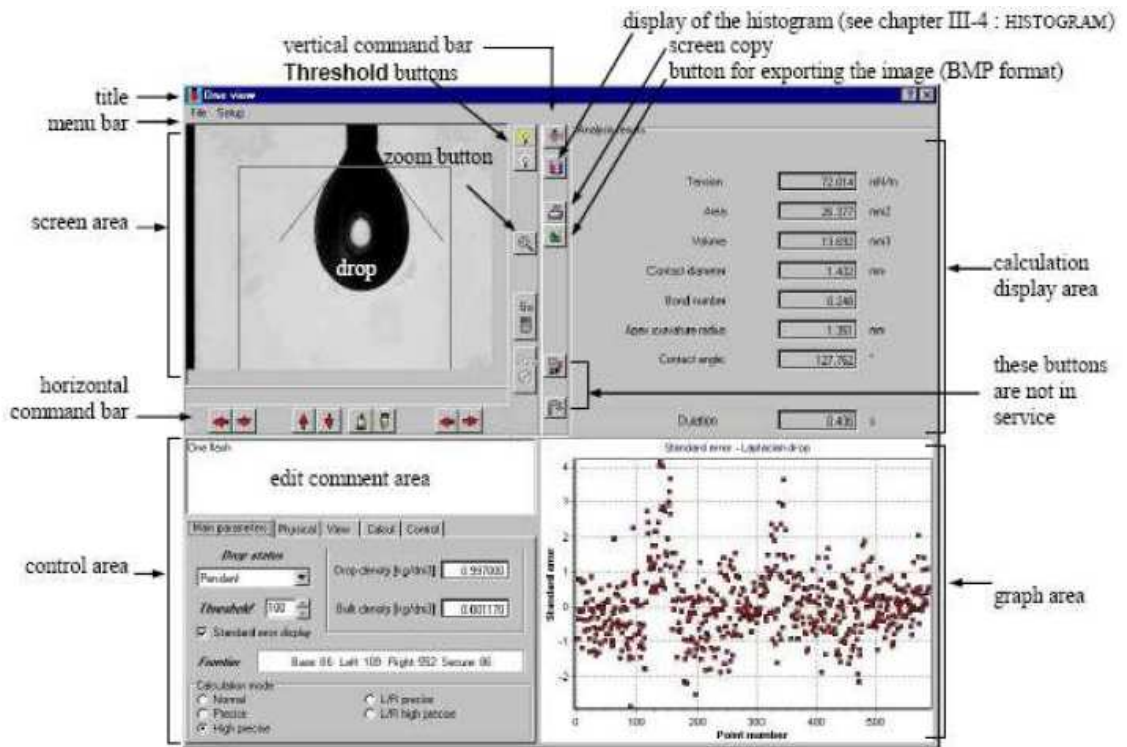


Figure C.5 The interface angle and the surface tension calculation display [90].

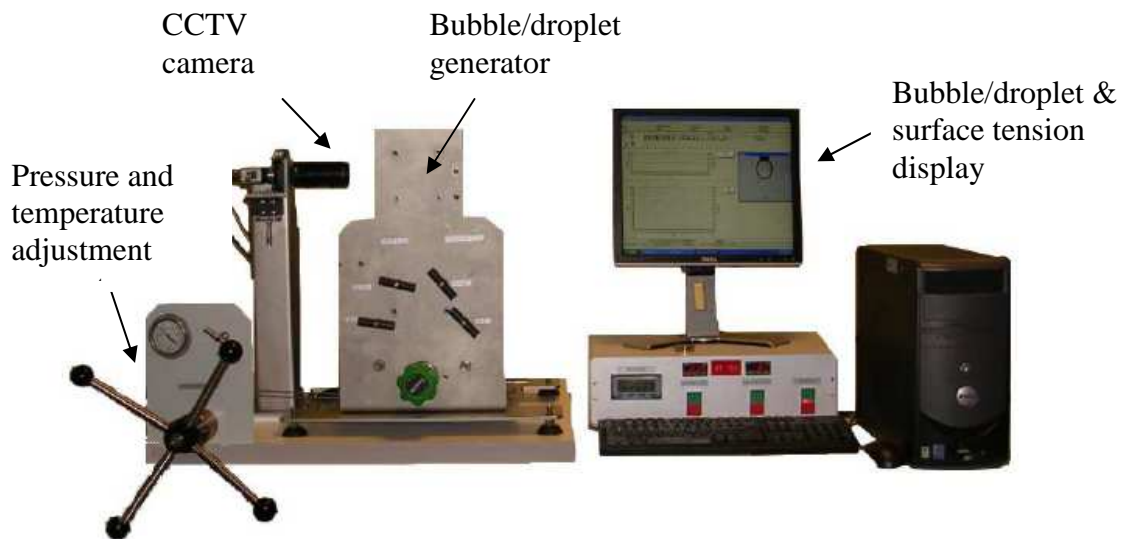
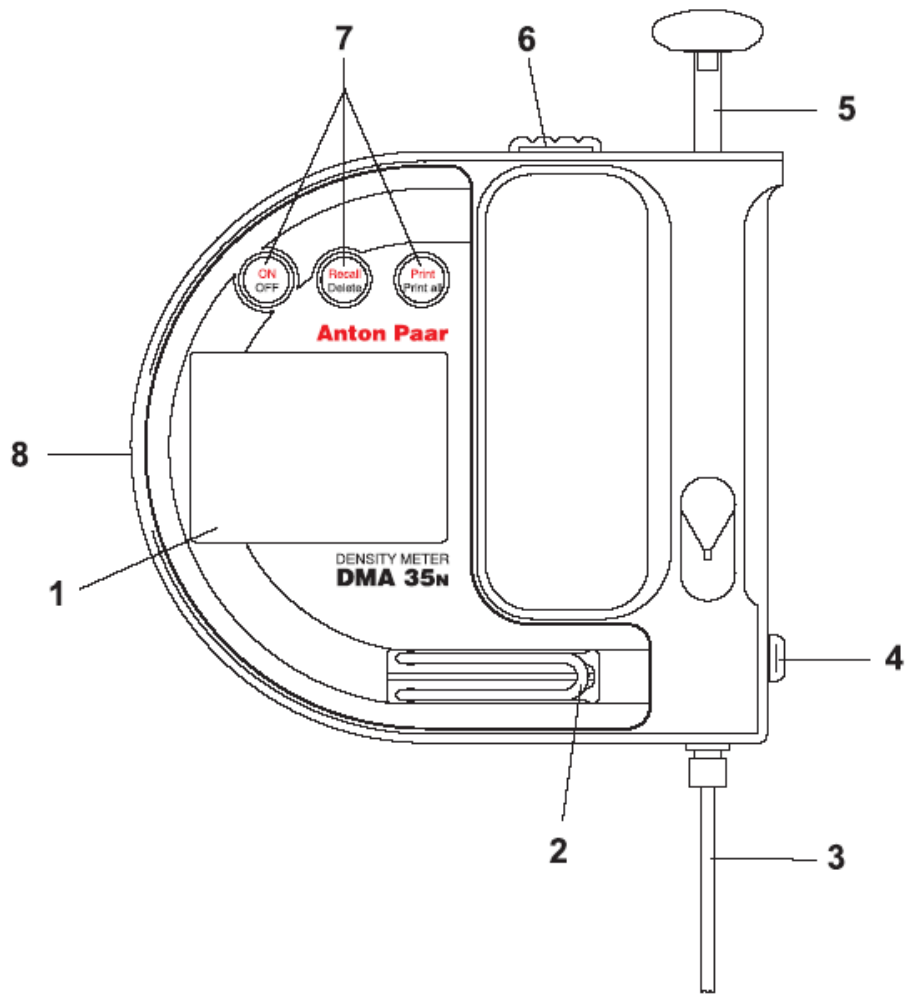


Figure C.6 The IFT 700 surface tension meter[90].



- 1 Display
- 2 Measuring cell
- 3 Filling tube
- 4 Screw plug
- 5 Built-in pump
- 6 Pump lock
- 7 Operating keys
- 8 Infrared interface connection

Figure C.7 The DMA 35 N portable density meter[91].

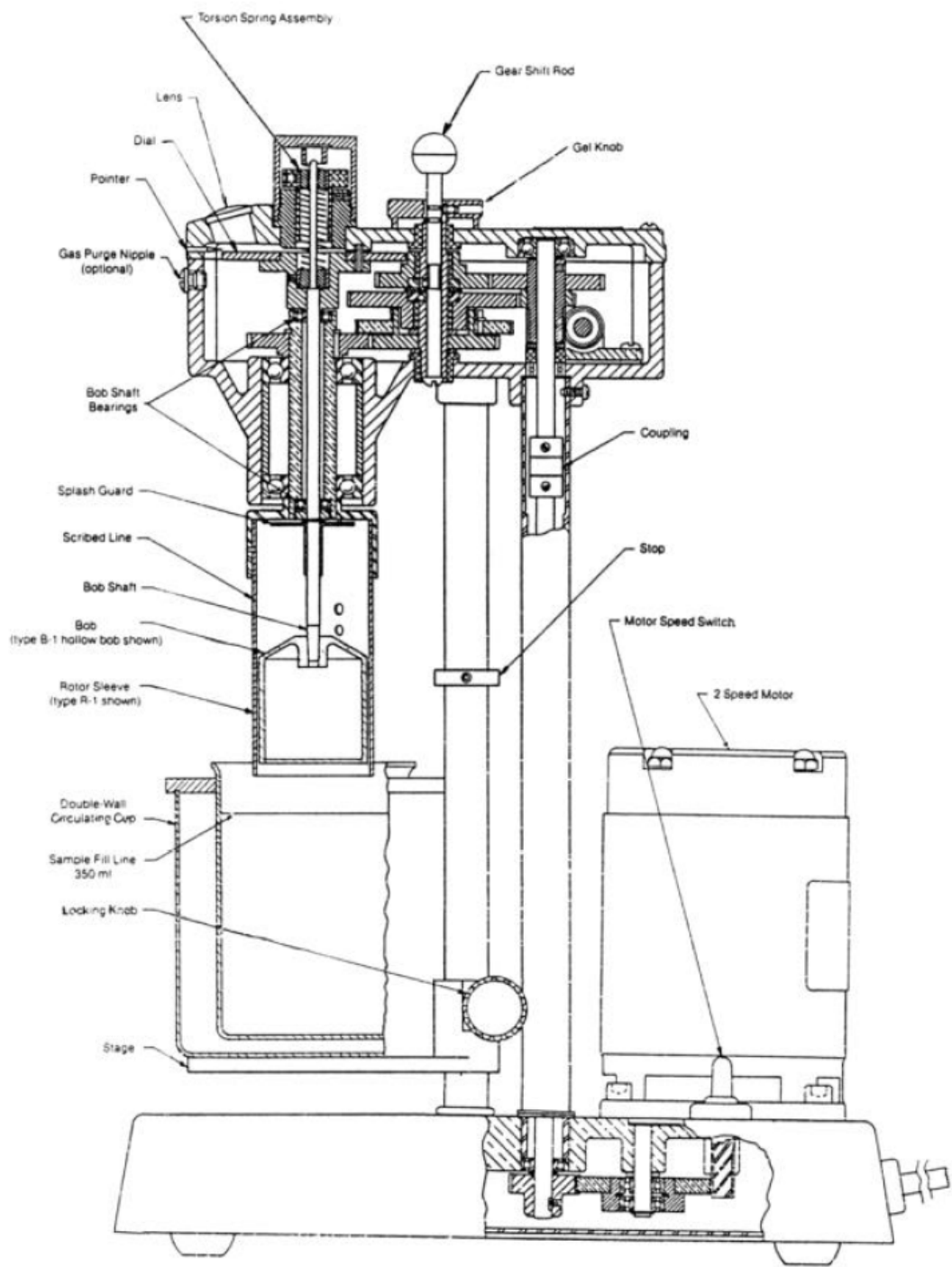


Figure C.8 The model 35 viscometer[92]

Table C.1 The Fastcam-x1280pci Framing rate vs image resolution [87].

Resolution (pixels)	Framing rate (FPS)								
	60	125	250	500	1000	2000	4000	8000	1600
1280x1024	O	O	O	O	-	-	-	-	-
1280x512	O	O	O	O	O	-	-	-	-
640x512	O	O	O	O	O	-	-	-	-
1280x256	O	O	O	O	O	O	-	-	-
640x256	O	O	O	O	O	O	-	-	-
320x256	O	O	O	O	O	O	-	-	-
640x128	O	O	O	O	O	O	O	-	-
320x128	O	O	O	O	O	O	O	-	-
160x128	O	O	O	O	O	O	O	-	-
640x64	O	O	O	O	O	O	O	O	-
320x64	O	O	O	O	O	O	O	O	-
160x 64	O	O	O	O	O	O	O	O	-
320x32	O	O	O	O	O	O	O	O	O
160x32	O	O	O	O	O	O	O	O	O

(O) is available and (-) is unavailable

Table C.2 The Fastcam-x1280pci Camera head specification [87].

Sensor resolution	1280 x 1024 pixels	
Grayscale	Mono	8 bits
	Color	8 bits each RGB (bayer color filter)
Lens mount	F mount (Nikon)	
Dimensions	85.4 (W) x 85.4 (H) x 56.0 (L) mm (exl. Lens mount, camera mount plate)	
Camera cable	5 meters (not expandable)	
Data bus I/F	Panel Link Standard (photron-modified)	
Power	5V DC power fed by grabber board via camera cable Never remove camera cable while PC is powered on.	
High gain feature 1 (Analog gain selection)	Gain selectable between Standard and High Gain Switch on camera back plate	
Sensor output range selection	Selectable by control software from Upper 8 bits (default)/Middle 8 bits/Lower 8 bits	

Table C.3 The EW-35641-00 specifications [88].

DO range	0.00 to 20.00
DO resolution	0.01
DO accuracy	± 1.5% full scale
Percent saturation accuracy	± 1.5% full scale
Percent saturation range	0.0 to 199.9%
Percent saturation resolution	0.1%
Temperature compensation	Automatic from 0 to 50° C
Temperature resolution	0.1° F, 0.1°C
Temperature accuracy	±0.5° F, ±0.3°C
Salinity compensation	Manual from 0.0 to 50.0 ppt, 0.1 ppt resolution
Barometric pressure compensation	Manual from 500 to 1499 mm Hg/ 66.6 to 199.9 kPa; 1 mm Hg/0.1 kPa resolution
Power	Four 1.5 V AAA batteries (included)
Temperature range	32.0° to 122.0° F, 0° to 50° C
Brand	Oakton
Operating temperature range	0° to 50° C
Memory	Up to 50 sets
Probe type	Galvanic probe
Probe length	10 ft
Clock	Stamps calibration data and stored data with time and date (month and day)
Battery life	100 hours continuous
Dimension	7-1/2" L x 3-1/2" W x 1-3/4" H

Table C.4 The specification of Turbidimeter model 2100P [89].

Principle of operation	Nephelometric Ratio
Operating Modes	Manual or Auto Range Selection
Measurement Mode	NTU
Range	0-1000 NTU in automatic range mode Manual range selection of 0-9.99, 0-99.9 and 0-1000NTU
Accuracy	$\pm 2\%$ of reading or $\pm 1$ least significant digit from 0-500NTU $\pm 3\%$ of reading between 500-1000NTU
Resolution	0.01 on lowest range
Repeatability	$\pm 1\%$ of reading, or 0.01 NTU, whichever is greater
Response time	6 seconds for full step change without signal averaging in constant reading mode
Stray light	<0.02 NTU
Standardization	Stabilized formazin primary standards
Light source	Tungsten lamp. Typical lamp life is >100,000 readings
Detectors	Silicon photovoltaic
Signal Averaging	Selectable on/off
Sample cells	60.0 H x 25 mm D borosilicate glass with screw caps
Sample required	15 ml
Operating temperature	0 to 50° C
Operating humidity range	0 to 90% RH noncondensing at 30° C 0 to 80% RH noncondensing at 40 C 0 to 70% RH noncondensing at 50 C
Power requirements	Four AA alkaline cells or optional battery eliminator
Shipping Weight	3.1 kg (6 lb 8.5 oz)

Table C.5 Specification of DMA 35 N portable density meter [91].

Measuring range	Density 0 to 1.999 g/cm <sup>3</sup> Temperature 0 to 40° C, 32 to 104° F Viscosity 0 to approx. 1000 mPa.s
Uncertainty of measurement	Density ±0.001 g/cm <sup>3</sup> Temperature ±0.2° C
Repeatability	Density ±0.0005 g/cm <sup>3</sup> Temperature ±0.1° C
Resolution	Density 0.0001 g/cm <sup>3</sup> Temperature 0.1° C or 0.1° F
Sample volume	Approx. 2 ml
Sample temperature	0 to 100° C
Ambient temperature	0 to +40° C
Air humidity	5 to 90% relative humidity, non condensing
Protection class	IP 54 (use in light rainfall/snowfall possible)
Memory	1024 values
Interface	Infrared/Rs 232
Power supply	2 x 1.5 V Alkaline batteries Micro LR03 (use only batteries of the same type and same level of charge)
Dimensions	140 x 30 x 25 mm
Weight	275 g (9.7 oz)